Monthly Notices of the ROYAL ASTRONOMICAL SOCIETY
MNRAS **493,** 871–898 (2020) doi:10.1093/mnras/staa126

# MEGARA-GTC stellar spectral library: I

M. L. García-Vargas [1]★ E. Carrasco,[2]★ M. Mollá [3]★ A. Gil de Paz,[4,5] S. R. Berlanas,[6,7] N. Cardiel,[4,5] P. Gómez-Alvarez,[1] J. Gallego,[4,5] J. Iglesias-Páramo,[8,9] R. Cedazo,[10] S. Pascual,[4,5] A. Castillo-Morales,[4,5] A. Pérez-Calpena [1] and I. Martínez-Delgado[1]

[1]*FRACTAL S.L.N.E., Calle Tulipán 2, portal 13, 1A, E-28231 Las Rozas de Madrid, Spain*
[2]*Instituto Nacional de Astrofísica, Óptica y Electrónica, INAOE, Calle Luis Enrique Erro 1, CP 72840 Santa María Tonantzintla, Puebla, Mexico*
[3]*Dpto de Investigación Básica, CIEMAT, Avda. Complutense 40, E-28040 Madrid, Spain*
[4]*Dpto de Física de la Tierra y Astrofísica, Fac. CC. Físicas, Universidad Complutense de Madrid, Plaza de las Ciencias, 1, E-28040 Madrid, Spain*
[5]*Instituto de Física de Partículas y del Cosmos, IPARCOS, Fac. CC. Físicas, Universidad Complutense de Madrid, Plaza de las Ciencias 1, E-28040 Madrid, Spain*
[6]*Instituto de Astrofísica de Canarias, Calle Vía Láctea s/n, E-38205 San Cristóbal de la Laguna, Santa Cruz de Tenerife, Spain*
[7]*Dpto de Astrofísica, Universidad de La Laguna, E-38205 San Cristóbal de la Laguna, Santa Cruz de Tenerife, Spain*
[8]*Instituto de Astrofísica de Andalucía, IAA-CSIC, Glorieta de la Astronomía s/n, E-18008 Granada, Spain*
[9]*Estación Experimental de Zonas Áridas, CSIC, Carretera de Sacramento s/n, E-04120 Almería, Spain*
[10]*Dpto de Ingeniería Eléctrica, Electrónica, Automática y Física Aplicada, ETS de Ingeniería y Diseño Industrial, UPM, Ronda de Valencia 3, E-28012 Madrid, Spain*

Accepted 2020 January 13. Received 2020 January 13; in original form 2019 January 30

## ABSTRACT

MEGARA (Multi Espectrógrafo en GTC de Alta Resolución para Astronomía) is an optical (3650–9750 Å), fibre-fed, medium-high spectral resolution ($R$ = 6000, 12 000 and 20 000) instrument for the Gran Telescopio CANARIAS (GTC) 10.4-m telescope, commissioned in the summer of 2017, and currently in operation. The scientific exploitation of MEGARA requires a stellar spectra library to interpret galaxy data and to estimate the contribution of the stellar populations. In this paper, we introduce the MEGARA-GTC spectral library, detailing the rationale behind the building of this catalogue. We present the spectra of 97 stars (21 individual stars and 56 members of the globular cluster M15, which are both subsamples taken during the commissioning runs, and 20 stars from our ongoing GTC Open-Time programme). The spectra have $R$ = 20 000 in the HR-R and HR-I set-ups, centred at 6563 and 8633 Å, respectively. We describe the procedures to reduce and analyse the data. Then, we determine the best-fitting theoretical models to each spectrum through a $\chi^2$ minimization technique, to derive the stellar physical parameters, and we discuss the results. We have also measured some absorption lines and indices. Finally, we introduce our project to complete the library and the data base in order to make the spectra available to the community.

**Key words:** atlases – catalogues – stars: abundances – stars: fundamental parameters – globular clusters: individual: M15.

## 1 INTRODUCTION

MEGARA (Multi Espectrógrafo en GTC de Alta Resolución para Astronomía) is a new mid-resolution optical fibre-fed multi-object spectrograph for the Gran Telescopio CANARIAS (GTC; see http://www.gtc.iac.es), a 10.4-m telescope in La Palma (Canary Islands, Spain). The main characteristics of the instrument are summarized in Table 1.

The instrument offers two spectroscopy modes: bi-dimensional, with an integral field unit (IFU); and multi-object (MOS). The IFU, called the large compact bundle (LCB), provides a field of view (FOV) of 12.5 × 11.3 arcsec$^2$, plus eight additional mini-bundles, located at the edge of the FOV, to provide simultaneous sky subtraction. The MOS assembly can place up to 92 mini-bundles covering a target area per minibundle of 1.6 arcsec and a total coverage area on the sky of 3.5 × 3.5 arcmin$^2$. The spatial sampling in both modes is 0.62 arcsec per fibre,[1] with each spaxel

★ E-mail: marisa.garcia@fractal-es.com (MLG-V); bec@inaoep.mx (EC); mercedes.molla@ciemat.es (MM)

[1]This size corresponds to the diameter of the circle on which the hexagonal spaxel is inscribed.

**Table 1.** Main characteristics of the MEGARA in LCB IFU and MOS modes.

| | | | |
|---|---|---|---|
| Telescope | | GTC | |
| Plate scale | | 0.824 mm arcsec$^{-1}$ | |
| | Observing mode | LCB | MOS |
| | Number of fibres | 623 | 644 |
| | Spaxel | 0.62″ | 0.62″ |
| | FOV | 12.5 × 11.3 arcsec$^2$ | 3.5 × 3.5 arcmin$^2$ |
| | $\Delta\lambda$ (EED$_{80}$) | 4.0 pix | 4.0 pix |
| | $\Delta\lambda$ (FWHM) | 3.6 pix | 3.6 pix |
| | LR | 6000 | 6000 |
| Resolving power | MR | 12000 | 12000 |
| | HR | 20000 | 20000 |
| Gratings (VPH) | | 6 LR, 10 MR and 2 HR | |
| Wavelength coverage | | 3650 – 9750 Å | |
| Detector | | e2V 1 × 4k × 4k, 15-μm pixel size, AR coated | |

**Table 2.** MEGARA spectral configurations as measured at the GTC. See the text for a description of the columns.

| VPH | $\lambda_{min,1}$ (Å) | $\lambda_{min}$ (Å) | $\lambda_c$ (Å) | $\lambda_{max}$ (Å) | $\lambda_{max,1}$ (Å) | Å pix$^{-1}$ |
|---|---|---|---|---|---|---|
| LR-U | 3640.0 | 3654.3 | 4035.8 | 4391.9 | 4417.3 | 0.195 |
| LR-B | 4278.4 | 4332.1 | 4802.1 | 5200.0 | 5232.0 | 0.230 |
| LR-V | 5101.1 | 5143.7 | 5698.5 | 6168.2 | 6206.0 | 0.271 |
| LR-R | 6047.6 | 6096.5 | 6753.5 | 7303.2 | 7379.9 | 0.321 |
| LR-I | 7166.5 | 7224.1 | 8007.3 | 8640.4 | 8822.3 | 0.380 |
| LR-Z | 7978.4 | 8042.7 | 8903.4 | 9634.9 | 9692.6 | 0.421 |
| MR-U | 3912.0 | 3919.8 | 4107.6 | 4282.2 | 4289.1 | 0.092 |
| MR-UB | 4217.4 | 4226.4 | 4433.7 | 4625.8 | 4633.7 | 0.103 |
| MR-B | 4575.8 | 4585.7 | 4814.1 | 5025.1 | 5033.7 | 0.112 |
| MR-G | 4952.2 | 4963.2 | 5214.0 | 5445.0 | 5454.6 | 0.126 |
| MR-V | 5369.0 | 5413.1 | 5670.4 | 5923.9 | 5659.6 | 0.135 |
| MR-VR | 5850.2 | 5894.2 | 6171.7 | 6448.5 | 6468.5 | 0.148 |
| MR-R | 6228.2 | 6243.1 | 6567.3 | 6865.3 | 6878.3 | 0.163 |
| MR-RI | 6748.9 | 6764.6 | 7117.1 | 7440.9 | 7454.5 | 0.172 |
| MR-I | 7369.4 | 7386.5 | 7773.1 | 8128.0 | 8142.8 | 0.189 |
| MR-Z | 8787.9 | 8810.5 | 9274.8 | 9699.0 | 9740.2 | 0.220 |
| HR-R | 6397.6 | 6405.6 | 6606.5 | 6797.1 | 6804.9 | 0.098 |
| HR-I | 8358.6 | 8380.2 | 8633.0 | 8882.4 | 8984.9 | 0.130 |

being projected because of the combination of a 100-μm core fibre coupled to a microlens that converts the *f*/17 entrance telescope beam to *f*/3, for maximum efficiency. The spaxel projection is oversized relative to the fibre core to allow for a precise fibre-to-fibre flux uniformity. A fibre link 44.5 m long drives the science light, coming from the folded Cassegrain F focal plane, into the spectrograph, hosted at the Nasmyth A platform.

The spectrograph is an all-refractive system (with *f*/3 and *f*/1.5 focal ratios for collimator and camera, respectively) and includes a set of 18 volume phase holographic (VPH) gratings placed at the pupil in the collimated beam. These gratings offer three spectral modes with different resolving power, $R$, labelled as low resolution (LR), $R$(FWHM) = 6000; medium resolution (MR), $R$(FWHM) = 12 000; and high resolution (HR), $R$(FWHM) = 20 000.

The different MEGARA set-ups in terms of wavelength coverage and linear reciprocal dispersion are shown in Table 2. The columns indicate: (1) set-up or name of the VPH; (2) the shortest wavelength (Å) of the central fibre spectrum; (3) the shortest wavelength (Å) common to all spectra; (4) the central wavelength (Å); (5) the longest wavelength (Å) for all spectra; (6) the longest wavelength (Å) of the central fibre spectrum; (7) constant linear reciprocal dispersion (Å pix$^{-1}$). The range between $\lambda_{min}$ and $\lambda_{max}$ is common to all fibres while the wavelengths $\lambda_{min,1}$ and $\lambda_{max,1}$ are not reachable in the fibres located at the centre and edges of the pseudo-slit, respectively.

A subset of 11 VPHs are simultaneously mounted on the instrument wheel so that they are available on the same observing night. We emphasize that the whole optical wavelength range is covered at $R$ = 6000 and 12 000 (FWHM) while $R$ = 20 000 is only available around two specific ranges defined by HR-R and HR-I. The scientific data are recorded by means of a deep-depleted e2V 4096 pix × 4096 pix detector with 15-μm pixel pitch. MEGARA is completed with the instrument control, fully integrated in the GTC control system (GCS), and a set of standalone software tools to allow the user to prepare, visualize and fully reduce the observations. Complete information and details of the final instrument performance on the GTC based on commissioning results can be found in Carrasco et al. (2018), Gil de Paz et al. (2018), Dullo et al. (2019) and Gil de Paz et al. (in preparation).

Population synthesis models have proven to be key to deriving the star formation histories of galaxies when used to interpret observations. The integrated properties of a galaxy can be modelled through a technique such as the ones used in the STARLIGHT (Cid Fernandes et al. 2005) and FADO (Gomes & Papaderos 2018) codes, as a combination of single stellar populations (SSPs), the building blocks of the population synthesis technique. There have been many studies devoted to the computation of SSP integrated properties (e.g. Mas-Hesse & Kuntz 1991; García-Vargas & Díaz 1994; García-Vargas, Bressan & Díaz 1995; Leitherer et al. 1999; Bruzual & Charlot 2003; González-Delgado et al. 2005; Fritze-v. Alvensleben & Bicker 2006; Eldridge & Stanway 2009; Maraston & Strömbäck 2011; Vazdekis et al. 2016; Vidal-García et al. 2017; Maraston et al. 2019), and our own POPSTAR models (Mollá, García-Vargas & Bressan 2009; Martín-Manjón et al. 2010; García-Vargas, Mollá & Martín-Manjón 2013).

There are important differences among the available SSP models because of the use of different stellar tracks (i.e. the isochrones), different input physics and computational algorithms, the inclusion of nebular emission and/or dust and, overall, different stellar atmosphere libraries with their particular wavelength coverage and spectral resolution. Stellar libraries are a key piece in the SSP code building. A spectral library is a collection of star spectra sharing the same wavelength range and resolution. The stars comprising these libraries are classified according to the main stellar atmospheric parameters governing their spectral energy distribution, namely effective temperature ($T_{eff}$), surface gravity (log $g$) and metallicity, usually given in terms of iron, [Fe/H], or all-metal, log ($Z/Z_\odot$), abundance (hereafter, we use [M/H] for metallicity). In order to reproduce the synthetic spectra as accurately as possible, the spectral star library should cover a wide range for all three parameters.

The stellar libraries can be classified empirically and theoretically, with the former based on observed data while the latter are built with models of stellar atmospheres and radiative-transfer processes computed as a function of physical parameters.The theoretical libraries have the advantages of covering a very wide range of selectable stellar parameters, in particular abundance, and providing noise-free spectra. However, these libraries require a wide and reliable data base of both atomic and molecular line opacity – not always complete or available – and they suffer from systematic potential uncertainties coming from the limitations of the atmosphere models, such as convection properties, line-blanketing, expansion, non-radiative heating, effects of non-local thermodynamic equilibrium (non-LTE), etc. Examples of theoretical libraries used for SSP models can be found in Kurucz (1993),

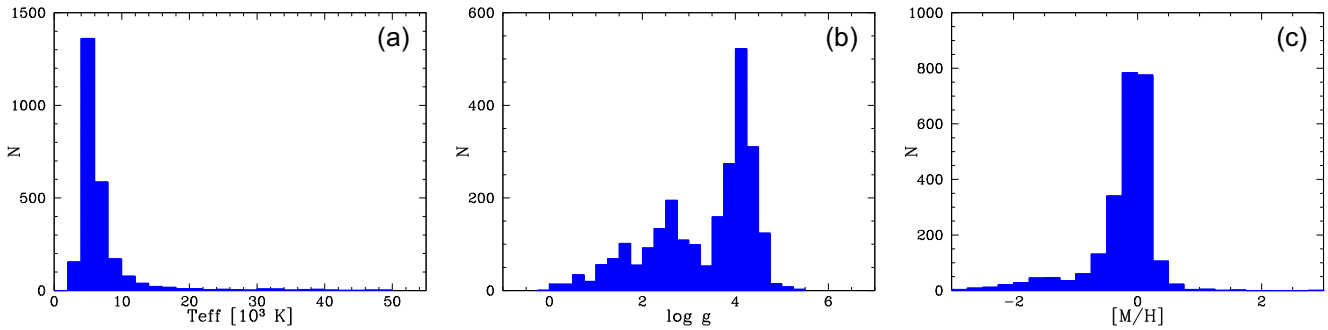


**Figure 1.** Histograms representing the number of stars in the current baseline library – without including the extension of hot stars – as a function of $T_{\rm eff}$ (a), log $g$ (b) and [M/H] (c).

Coelho et al. (2005), Martins et al. (2005), Munari et al. (2005, hereafter MUN05), Rodríguez-Merino et al. (2005), Frémaux et al. (2006), Coelho et al. (2007), Gustafsson et al. (2008), Leitherer et al. (2010), Palacios et al. (2010), Sordo et al. (2010), Kirby (2011), de Laverny et al. (2012), Coelho (2014) and Bohlin et al. (2017), among others.

The empirical stellar libraries have the advantage of being composed of real observed stars. A very good review of empirical libraries has been recently compiled by Yan (2019) and Yan et al. (2019), presenting the MaStar library (MaNGA project). However, there are some shortcomings and limitations. The existing libraries have relatively low resolution and a limited coverage in terms of the parameter space. They are also constrained to the ranges of $T_{\rm eff}$, log $g$ and [M/H] spanned by the stars in the Milky Way galaxy and its satellites. Moreover, these existing libraries are often biased to the brightest stars (to save observing time) and/or the most frequent types (associated with the length of the evolutionary stage of each star type). For these reasons, the empirical libraries are short in low-metallicity stars, in general, and also deficient in cool dwarfs, and other types of stars that are not so numerous. This can make a big difference in the composed synthetic spectrum. This is the case of Wolf–Rayet (WR), luminous blue variable (LBV) and thermally pulsing asynthotic giant branch (AGB) stars, whose high luminosity in certain wavelength intervals could even completely dominate the spectrum. For these reasons, few SSP codes include an empirical stellar library to model the atmospheres.

There is a final consideration in the use of libraries when the resulting synthetic spectra are intended to be compared with observations. That is, in both theoretical- and empirical-based spectra, the instrument characteristics (noise, instrumental specific effects, spectral resolution and even data reduction) introduce another level of uncertainty in the observed spectra. The exception is an empirical library obtained from star observations with the same instrument. This is the case of the MEGARA-GTC spectral library, a total instrument-oriented catalogue, crucial for creating the necessary synthetic templates to interpret the observations taken with MEGARA at the same instrumental set-up.

We describe the construction of our catalogue in Section 2. In Section 3, we summarize the observations of the sample presented in this work. Sections 3.1, 3.2 and 3.3 concern the subsamples of commissioning single stars (COMs hereafter), M15 members and Open-Time (OT hereafter) stars, respectively, while Section 3.4 is devoted to the data-reduction process. The spectra analysis is described in Section 4, with Sections 4.1–4.3 dedicated to the derivation of the stellar parameters and their analysis, and Sections 4.4 and 4.5 dedicated to the description of the absorption-line spectra in the HR-R and HR-I set-ups, respectively. Section 5 contains an overview of the MEGARA-GTC data base tool. Our conclusions are summarized in Section 6.

## 2 MEGARA STELLAR LIBRARY

The MEGARA-GTC basic stellar library currently contains 2983 stars covering wide ranges in $T_{\rm eff}$, log $g$ and abundance [M/H], whose histograms are shown in Fig. 1. To define the catalogue, we made a compilation of observed stars from different libraries whose main characteristics and references are summarized in Table 3. We selected libraries whose spectral resolution was comparable to that of MEGARA at LR, MR and HR modes, with resolving power of 6000, 12 000 and 20 000 respectively. For this search, we used data bases from SAO/NASA ADS and ArXiv. The INDO-US library (Valdes et al. 2004) and ELODIE low-resolution (Prugniel & Soubiran 2001, 2004) fit the MEGARA-LR spectral set-ups well; X-SHOOTER (Chen et al. 2012, 2014) and FOE (Montes et al. 1999) have similar spectral resolution to MEGARA-MR and, finally, UVES-POP (Bagnulo et al. 2003), ELODIE high-resolution (Prugniel & Soubiran 2004) and UES (Montes & Martin 1998) surpass the MEGARA-HR spectral resolution. The final library has been produced avoiding any duplicated stars when coming from more than one catalogue.

The GTC at the Observatorio del Roque de los Muchachos (ORM) has geographical coordinates of 28°45′25″ N latitude, 17° 53′ 33″ W longitude and 2396 m altitude. The catalogue coordinate limits have been selected assuming some margin over the GTC operational restrictions (the minimum declination reachable is –35° and the lowest elevation is +25°), to which we added a safety margin, resulting in a declination range for the star library of $-20^\circ \leq \delta \leq +89^\circ$. All coordinates and star data have been checked by parsing the catalogue against the SIMBAD4 release 1.7 database.

Table 4 shows some rows and columns, as an example of the MEGARA-GTC library information. The catalogue will be published with the first release and the observations will be available as soon as the stars are observed and pass our data reduction and quality control processes. The selected columns include the star name, right ascension (RA) and declination (Dec.) equatorial coordinates J2000.0, RA and Dec. proper motions in mas yr$^{-1}$, spectral type and luminosity class, and referenced Johnson magnitudes $V$, $R$, $I$ and $J$ whenever available. Most stars come from other spectral libraries. In these cases, values for $T_{\rm eff}$, log $g$ and [M/H] (usually meaning [Fe/H]) exist and are displayed in Columns 11, 12 and 13, respectively, together with the original catalogue's

**Table 3.** Existing stellar libraries used for MEGARA-GTC library input catalogue.

| Library | Resolving power | Spectral range | Number | MEGARA set-up | Reference |
|---|---|---|---|---|---|
| INDO-US | 5000 | 3460 – 9460 | 1237 | LR | Valdes et al. (2004) |
| MILES | 2100 | 3520 – 7500 | 987 | LR | Sánchez-Blázquez et al. (2006) |
| NGSL | 1000 | 1670 – 10250 | 374 | LR | Gregg et al. (2006) |
| STELIB | 1600 | 3200 – 9300 | 249 | LR | Le Borgne et al. (2003) |
| ELODIE low | 10000 | 3900 – 6800 | 1388 | MR | Prugniel & Soubiran (2001, 2004) |
| FOE | 12000 | 3800 – 10000 | 125 | MR | Montes, Ramsey & Welty (1999) |
| X-SHOOTER | 10000 | 3000 – 25000 | 379 | MR | Chen et al. (2012, 2014) |
| ELODIE high | 42000 | 3900 – 6800 | 1388 | HR | Prugniel & Soubiran (2001, 2004) |
| UES | 55000 | 4800 – 10600 | 83 | HR | Montes & Martin (1998) |
| UVES-POP | 80000 | 3070 – 10300 | 300 | HR | Bagnulo et al. (2003) |

**Table 4.** MEGARA-GTC stellar library catalogue sample. See the text for a description of the columns.

| Name | RA (hh:mm:ss.s) | Dec. (dd:dd:ss.s) | pmRA (masyr$^{-1}$) | pmDec (mas yr$^{-1}$) | Sp.type | $V$ | $R$ | $I$ | $J$ | $T_{\rm eff}$ | log $g$ | [M/H] | Catalogue |
|---|---|---|---|---|---|---|---|---|---|---|---|---|---|
| HD 006229 | 01:03:36.5 | 23:46:06.4 | 14.592 | – 20.505 | G5 IIIw | 8.6 | | | 7.1 | 5218 | 3.00 | – 1.09 | X-SHOOTER |
| HD 006397 | 01:05:05.4 | 14:56:46.1 | 8.265 | 53.750 | F5 III | 5.6 | | | | | | | |
| HD 006461 | 01:05:25.4 | – 12:54:12.1 | 62.973 | 50.091 | G2 V | 7.7 | | | 6.1 | | | | |
| HD 006474 | 01:07:00.0 | 63:46:23.4 | – 2.077 | – 0.304 | G4 Ia | 7.6 | | | 4.8 | | | | |
| HD 006482 | 01:05:36.9 | – 09:58:45.6 | – 31.450 | – 34.294 | K0 III | 6.1 | | | 4.4 | | | | |
| HD 006497 | 01:07:00.2 | 56:56:05.9 | 94.445 | – 108.658 | K2 III | 6.4 | | | 4.7 | | | | |
| HD 006582 | 01:08:16.4 | 54:55:13.2 | 3422.230 | – 1598.930 | G5 Vb | 5.1 | 4.7 | 4.4 | 4.0 | 5320 | 4.49 | – 0.76 | ELODIE low |
| HD 006695 | 01:07:57.2 | 20:44:20.7 | 80.020 | – 94.096 | A3 V | 5.6 | | | | 8266 | 3.91 | – 0.46 | ELODIE low |
| HD 006715 | 01:08:12.5 | 21:58:37.2 | 400.593 | – 46.588 | G5 | 7.7 | 7.2 | 6.9 | 6.3 | 5652 | 4.40 | – 0.20 | ELODIE low |
| HD 006734 | 01:08:00.0 | 01:59:35.0 | 145.370 | – 437.902 | K0 IV | 6.5 | 5.9 | 5.5 | 4.9 | 4934 | 3.18 | – 0.58 | MONTES |

name, shown in the last column. The full catalogue also contains additional information of the stars that have been compiled from the literature. The results for the first library release are in preparation (Carrasco et al., in preparation, hereafter Paper II). However, the assignment of the stellar parameters – initially obtained from the literature – depends on the wavelength range and resolution of each spectrum. For this reason, one of the goals of this work is to propose a method to uniformly determine the stellar parameters of our sample from MEGARA HR spectra (see Section 4.1) and to apply it to all the stars in the library as soon as they are observed.

The dominant spectral types in the basic catalogue are G stars (751), K (705) and F (630), followed by A (335), B (326), M (153) and O (49). We have a minimum number of L, S and R stars and only one WR. We have added an extension to the library with a hot star catalogue composed by 199 Galactic O and B stars from the IACOB data base (Simón-Díaz et al. 2011), plus WR stars and LBV stars (or candidates), with the restriction limits described above to be observed with the GTC. The WR subsample includes 166 galactic,[2] 14 in M81 (Gómez-González, Mayya & González 2016), 205 in M33 (Neugent & Massey 2011) and 53 in M31 (Neugent, Massey & Georgy 2012). We have some of these WR stars scheduled to be observed. LBV stars are rare and only a few are properly confirmed. Our LBV subsample includes eight stars in our Galaxy (plus four candidates), six in M31, four in M33, one in M81 (plus one candidate) and two in NGC 2403.

[2]See the Galactic Wolf–Rayet Catalogue compiled by Crowther, http://pacrowther.staff.shef.ac.uk/WRcat/index.php.

The observational programme is ongoing and has been awarded GTC OT in three consecutive semesters, and we have submitted a proposal for the fourth (see Section 3.3). The MEGARA-GTC library's composition might evolve, so the catalogue will be updated as far as the project progresses to have the most complete data base possible with the available GTC time.

In terms of the spectral region, we have prioritized the library in HR-R and HR-I ($R \simeq 20\,000$) as there are no published empirical catalogues covering these spectral ranges and resolution even though they are in great demand. At present, $R \simeq 20\,000$ is not being offered in any other integral field spectroscopy (IFS) instrument, with a combination of efficiency and telescope collecting area high enough to study the physical properties and kinematics of gas and stellar populations in external galaxies, something particularly powerful in the study of dwarf and face-on disc galaxies. The HR-R set-up is centred at H$\alpha$ at z = 0, so that observations with this grating will provide stellar templates to support subtraction of the underlying stellar population in nearby star-forming galaxies with the same spectral resolution as the gas spectrum. Also, the lines He I 6678 and He II 6683 Å will be crucial for classification of massive and hot stars. The HR-I set-up, centred in the brightest line of Ca II triplet at 8542.09 Å, will trace the presence of both very young (through the Pa series) and intermediate to old (through the Ca II, Mg I, Na I, and Fe I features) populations in nearby galaxies. However, the absence of He I and He II lines will add uncertainty when determining the $T_{\rm eff}$ of hot stars on the basis on their HR-I spectrum alone. The spectra of these set-ups also contain important features used for abundance determination. A more detailed description of the observations in these spectral ranges is given in Sections 4.4 and 4.5 for HR-R and HR-I, respectively.

**Table 5.** Subsample of 21 stars observed with the HR-I spectral configuration during MEGARA commissioning between 2017 June and August. The Johnson magnitudes are shown for the stars if available (note that BD+12 237 is also known as Feige 15 and BD+40 4032 is also known as HD 227900).

| Star name | Sp.type/Lum.class | *U* | *B* | *V* | *R* | *I* | Date | $T_{exp}$ (s) |
|---|---|---|---|---|---|---|---|---|
| Schulte 9 | O4.5 If C | 13.4 | 12.8 | 11.0 | 11.0 | – | 2017/07/30 | 3 × 200 |
| HD 192281 | O4.5 VC | 7.3 | 7.9 | 7.6 | – | – | 2017/08/28 | 3 × 25 |
| BD+25 4655 | sdO6 C | 8.3 | 9.4 | 9.7 | – | – | 2017/07/01 | 3 × 30 |
| HD 218915 | O9.2 Iab | 6.3 | 7.2 | 7.2 | – | – | 2017/08/31 | 1 × 30 |
| BD+40 4032 | B2 III D | 5.0 | 10.8 | 10.6 | – | – | 2017/08/28 | 3 × 100 |
| BD+33 2642 | O7pD (B2 IV) | 9.8 | 10.8 | 10.7 | 10.9 | 11.0 | 2017/06/29 | 3 × 300 |
| HD 220575 | B8 IIIc | 6.4 | 6.7 | 6.7 | – | – | 2017/08/31 | 2 × 15 |
| BD+42 3227 | A0 D | – | 10.1 | 10.1 | – | – | 2017/08/23 | 3 × 60 |
| BD+12 237 | sdA0IVHe1 B | – | 10.4 | 10.2 | – | – | 2017/08/29 | 3 × 90 |
| BD+17 4708 | sdF8 D | 9.7 | 9.9 | 9.5 | 9.0 | 8.7 | 2017/07/30 | 3 × 45 |
| HD 026630 | G0 Ib B | 5.8 | 5.1 | 4.2 | 3.4 | 2.8 | 2017/08/29 | 1 × 20+1 × 10 |
| HD 216219 | G1 II–III-Fe-1 | – | 8.1 | 7.4 | – | – | 2017/06/30 | 3 × 150 |
| HD 011544 | G2 Ib C | – | 8.0 | 6.8 | – | – | 2017/08/23 | 3 × 20 |
| HD 019445 | G2 VFe-3 C | 8.3 | 8.5 | 8.1 | 7.6 | 7.3 | 2017/08/23 | 3 × 30 |
| HD 020123 | G5 Ib–IIa C | 7.0 | 6.2 | 5.0 | – | – | 2017/08/23 | 3 × 15 |
| HD 224458 | G8 III C | – | 9.3 | 8.3 | – | – | 2017/06/30 | 3 × 150 |
| HD 220954 | K0.5 III | 6.4 | 5.4 | 4.3 | 3.5 | – | 2017/08/31 | 1 × 5 |
| HD 025975 | K1 III C | 7.8 | 7.0 | 6.1 | 5.5 | 5.0 | 2017/08/29 | 1 × 60 |
| HD 027971 | K1 III C | – | 6.3 | 5.3 | – | – | 2017/08/29 | 1 × 60 |
| HD 174350 | K1 III C | – | 9.1 | 7.9 | – | – | 2017/06/30 | 3 × 100 |
| HD 185622 | K4 Ib C | – | 8.3 | 6.3 | – | – | 2017/06/24 | 2 × 20 |

Our team is currently developing a new grid of POPSTAR evolutionary synthesis models based on high-resolution theoretical spectra (Mollá et al., in preparation). The POPSTAR code is therefore being prepared to include HR spectra as those resulting from MEGARA stellar library observations and, in particular, HR-R and HR-I set-ups. This will allow us to obtain both SSPs and composed population models, to be used as stellar population templates to interpret MEGARA data.

## 3 MEGARA-GTC LIBRARY OBSERVATIONS

We present in this paper a subsample of 97 stars that will form part of the first release of the MEGARA-GTC library. During MEGARA commissioning at the GTC (2017 June–August), we started a pilot programme whose goal was to obtain the first observations of the MEGARA-GTC library using HR-I. In Section 3.1, we describe these observations. We also observed the centre of the M15 cluster in both HR-R and HR-I configurations, with the MEGARA MOS mode using the robotic positioners. These observations are described in Section 3.2. Finally, we include in this paper 20 stars, also observed in HR-R and HR-I, belonging to the basic library and observed with the filler GTC programme, described in Section 3.3.

### 3.1 Commissioning single-star LCB observations

During the MEGARA commissioning phase, we observed 21 single stars from the MEGARA-GTC catalogue described in Section 2 with the LCB mode in the HR-I set-up. Observations were carried out during twilight or in under-optimum observing conditions, in which the other commissioning tests could not be done. The exposure times ranged between 5 and 900 s. The names and properties of these COM stars are listed in Table 5. The 21 HR-I two-dimensional (2D) spectra have been fully reduced, as described in Section 3.4. Once the final (sky-subtracted) flux-calibrated spectra were obtained, we used the MEGARA Quick Look Analysis (QLA) tool (Gómez-Alvarez et al. 2018) to extract the one-dimensional (1D) spectra by integrating three rings on sky-projection (37 spaxels). Fig. 2 shows the spectra of this COM subsample for the hottest (panel a) and the coolest (panel b) stars, respectively.

### 3.2 Commissioning M15 MOS Observations

We also observed the centre of the M15 globular cluster in both HR-R and HR-I spectral configurations. The observations of 1800 s (3 x 600 s) in each configuration were taken on 2017 August 24, during MEGARA commissioning, with the MOS mode and excellent seeing (0.4 arcsec). The pointing coordinates were chosen to accommodate as many stars as possible in the 88 positioners available. These coordinates were $\alpha$ (J2000.0 FK5) = 21h:29m:58$^{s}$.147 and $\delta$ (J2000.0 FK5) = 12°10′09″.62 with an instrument position angle (IPA) of 196°.146. Calibrations for both set-ups were taken with the same MOS configuration to correct from bias, flat-field and wavelength calibration following the data-reduction steps described in Section 3.4. Corrections for atmospheric extinction and flux calibration were done by observing two standard stars with the IFU (in both set-ups). From these observations, we obtained the master sensitivity curve to correct all the 1D star spectra from spectral response and flux calibration. After performing sky-subtraction with sky spaxels, we used the QLA tool to extract the 1D star spectra. We finally obtained 56 stellar spectra in each set-up to be used in this work. These stars (numbered from 1 to 56) had no previous stellar parameter determination so we have applied the method described in this paper (see section 4.1.2) to obtain them. Fig. 3 shows the spectra of six of these 56 M15 stars in HR-R (a) and HR-I (b). Each star is plotted with a different colour and with a shift for the sake of clarity. From the observations of HR-R and HR-I, we have derived a radial velocity of –106.9 km s$^{-1}$ (after the de-convolution with the instrumental profile), compatible with the value commonly adopted in the literature ($v$ = –106.6 ± 0.6 km s$^{-1}$ from SIMBAD).

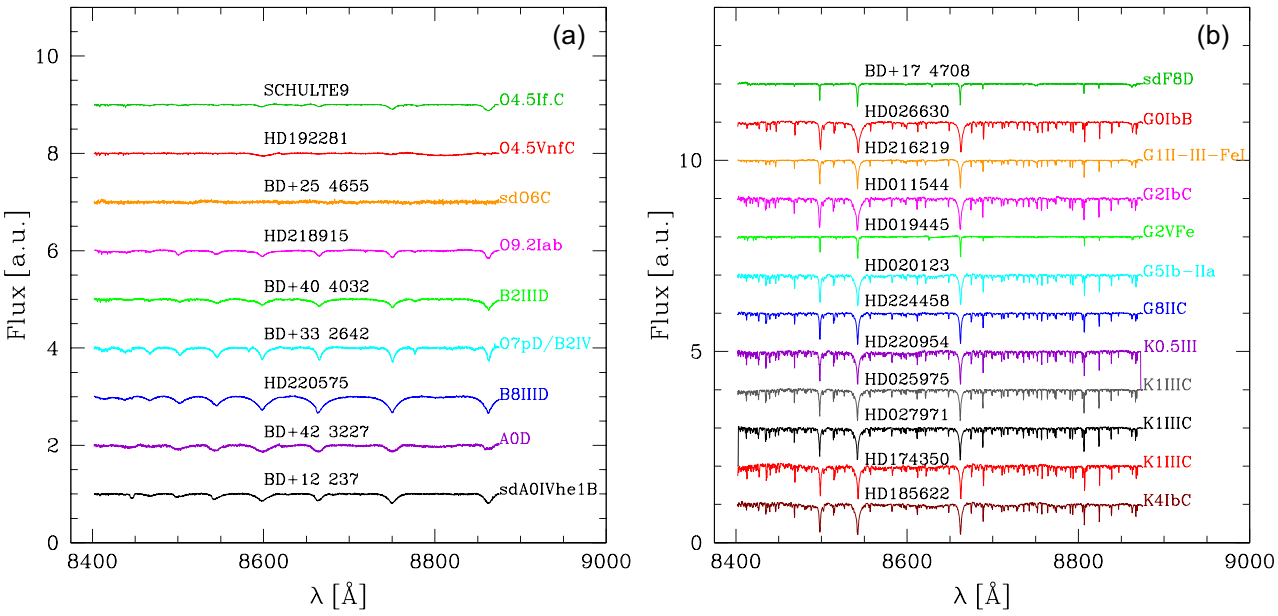


**Figure 2.** Plot showing HR-I spectra in arbitrary units for: (a) the hottest stars of the COM subsample (i.e. nine stars) with spectral types from O (top) to A (bottom); (b) the 12 coolest stars of the COM subsample, with spectral types from F (top) to K (bottom).

### 3.3 Filler programme to observe MEGARA-GTC library

We have proposed a filler-type programme during the last three semesters in the *Call for Proposals for GTC Open Time* to observe stars for the MEGARA-GTC library. We have already been awarded 175 h of observing time (programmes 35-GTC22/18B, 61-GTC37/19A and GTC33-19B; PI, Mollá), and it is our intention to complete this project when we have a high number of stars to do a precise enough evolutionary synthesis code. The motivation of this programme is to finalize, in the shortest time-scale possible, the MEGARA-GTC spectral library. To delimit the goal and, consequently, the telescope time, this filler proposal is focused on the highest spectral resolution configurations: HR-R and HR-I at $R \sim 20\,000$, for the reasons described in Section 2. In the time of submitting this paper, we have more than 260 stars observed and reduced in both set-ups.

GTC filler programmes require relaxed observing conditions to be executed even when no other approved programme in the other regular (higher-priority) bands fits. The MEGARA-GTC library programme fits perfectly as a filler because the star observations can be carried out under almost any conditions, in particular with any seeing, which gives the programme high flexibility. On the one hand, the spectral resolution is preserved as the stop is at the fibre so the slit width remains constant and the resolving power on the detector will not change with seeing. On the other hand, flux can be recovered by adding IFU spaxels on the sky (fibres at the detector) so that flux is always guaranteed regardless of the seeing value. This is explained in Fig. 4, which shows the image of a real star observed with the MEGARA LCB mode at the GTC during the commissioning. This image is taken directly from the QLA tool available at the GTC. The left image shows the full LCB while the right image shows a zoom. The resulting observation is completely valid, regardless tof he seeing conditions. Different circles indicate apertures with different seeing values ,all in the filler range: 2, 3 and 5 arcsec are shown as examples. The spaxel size is 0.62 arcsec on the sky.

Stars can be observed in bright conditions (most of the pilot commissioning observations presented in this paper were carried out during twilight). Therefore, this programme can run up to 1 h after astronomical twilight every night, especially when observing HR-I (very red set-up). Finally, photometric conditions are not required. At least one standard star for flux calibration is taken every night even for a filler-type programme, according to GTC observing policies. However, even in absence of flux calibration the same day, we can use the sensitivity curve taken on another night to correct for the instrument response curve. Therefore, even without a proper (same-night) flux calibration, the goals for determining the stellar parameters and measuring equivalent widths and indices can be completed for the whole stellar library with a high degree of reliability.

The programme is not very demanding in terms of telescope operation. Most of the targets are bright and an accurate pointing in the centre of the LCB is not needed. We have included a large number of short-exposure time observations that can be executed between observing gaps of other programmes, without idle, expensive, telescope time. This filler programme can even be executed in the absence of A&G operation or for high levels of sky brightness. Several strategies have been discussed with GTC staff and are applied to minimize overheads and to increase programme efficiency. On the one hand, the large number of stars in the data base makes the GTC staff's choice very easy and several targets can be selected in the same sky field, reachable with minimum telescope re-pointing. On the other hand, there is a common observing block (OB) with both HR-R and HR-I observations of each star in the GTC Phase-2 tool, guaranteeing a stable data base population of observations in both set-ups. The on-target time per spectral configuration has been estimated with the MEGARA exposure time calculator (ETC) tool to have a signal-to-noise ratio (S/N) between 20 and 300.

The observations are carried out in queue mode with the following strategy: (i) in the GTC Phase-2, search for the most appropriate target according to visibility and priority; (ii) configure MEGARA

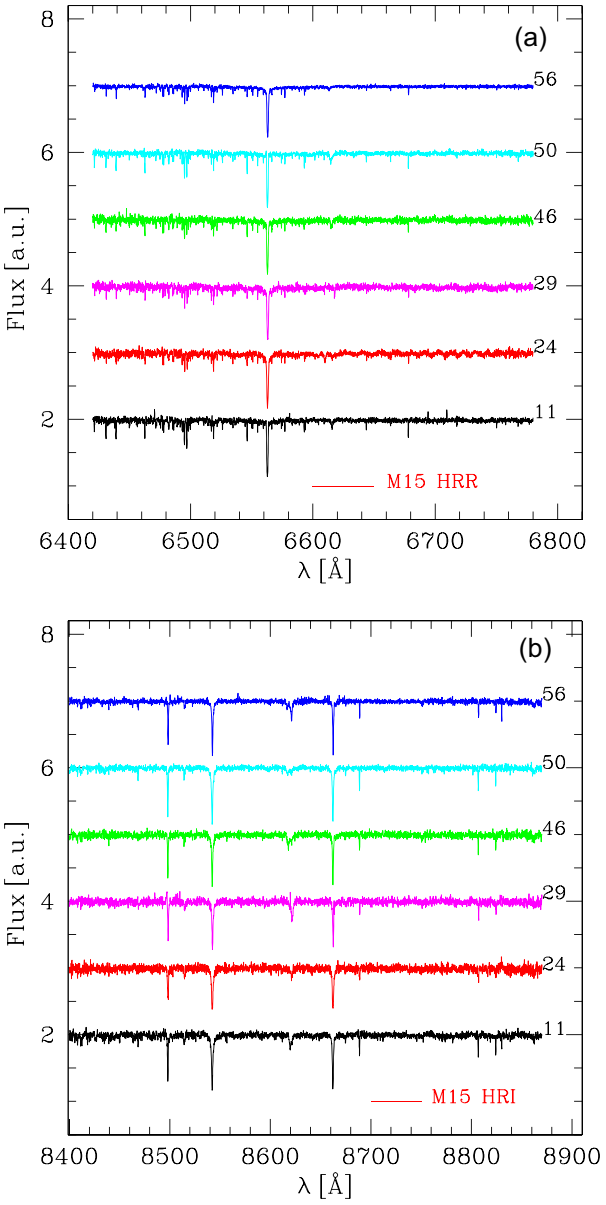


**Figure 3.** Normalized spectra in arbitrary units for six selected stars from M15 in two different set-ups: (a) in HR-R; (b) in HR-I.

while slewing; (iii) acquire the target with LCB image mode; (d) carry out HR-R and then HR-I on the same target. For calibration purposes, we have requested halogen and wavelength calibration lamp images in DayTime and at least one standard star in NightTime, whenever possible. The data are reduced with the MEGARA data-reduction pipeline (MEGARA DRP) by applying the different recipes as described in Section 3.4. Fully reduced and calibrated products are obtained soon after being received, and frequent releases will be delivered to the community, with the first release planned by the first semester of 2020. As the project progresses, we will update the targets in the GTC Phase-2 and manage the priority levels to populate all physical parameter regions of the stellar library. This strategy is possible becase of the high flexibility of the GTC Phase-2 queued observations to accommodate changes within the allocated time. We have included in this paper a subsample of 20 OT stars observed in both HR-R and HR-I, as part of our programme 35-GTC22/18B. A summary of the star data and observations is given in Table 6. Fig. 5 shows the spectra of five of these stars in (a) HR-R and (b) HR-I. The stars are, from bottom to top, HD 220182, HD 147677, HD 206374, HD 221830 and HD 218059, corresponding to spectral types and luminosity classes of K1 V, K0 III, G8 V, F9 V and F8 V, respectively.

### 3.4 Data reduction

All observations were taken with their corresponding calibrations. Whenever the exposure time was longer than 30 s, it was divided into three identical exposures to facilitate the removal of cosmic rays. Halogen and ThNe lamp calibrations were taken in day time for tracing, flat-field and wavelength calibration. Observations of standard stars for flux calibration were taken during night time. Twilight images were taken for the commissioning observations only.

MEGARA DRP is a Python-based software tool operating in the command line (Cardiel & Pascual 2018; Pascual et al. 2018). The DRP uses a file called *control.yaml* that includes all relevant information needed for MEGARA data reduction such as the data directories, the polynomial degree and number of spectral lines used for wavelength calibration and the site's extinction curve. Once MEGARA DRP is installed, the user has to make a local copy of the file tree of the complete calibrations. The MEGARA team has made available a complete set of ready-to-use calibration files for the 36 MEGARA configurations, defined as the combination of the observing mode (LCB or MOS) and the selected VPH set-up (from a total of 18 gratings). These calibration files can be substituted by updated files whenever available. The pipeline operates in a cascade mode so that each step requires processed data with the previous recipes. Each routine has its own input file in which the images to be processed are identified together with the specific parameters needed for that recipe. Once executed, each DRP routine produces a set of output images and quality control files, allowing a full tracking of the reduction process.

The data reduction starts by generating a Master Bias with the *MegaraBiasImage* routine and bias images. In further steps (except the bias itself), all the calibration files have to be taken with the same instrument set-up. The cosmic ray removal routine is automatically applied by default to eliminate the undesired cosmic rays registered on the detector by the combination of several images of the same target whenever available.

The *MegaraTraceMap* recipe uses the halogen lamp images to find the position of the illuminated fibres on the detector, storing the information in a *.json* formatted file and producing a region *.reg* ds9 file (Joye & Mandel 2003) with the trace identification. This ds9 region can be overlapped on any images (wavelength calibration lamp, twilight, standard star and target star) to determine in each case the offset (if needed) between the reference-traced fibres and the actual position. This information allows the matching between the fibres and the traces when extracting the fibre spectra. Although these offsets are predictable as a function of the temperature change, the recommendation is to check the offset position and to apply that as a parameter when calling the subsequent pipeline recipes. The *MegaraModelMap* recipe, starting from the results of the *MegaraTraceMap* and taking the halogen images as input, produces an optimized extraction of the fibre spectra.

The *MegaraArcCalibration* recipe uses the lamp wavelength calibration images, their offset value and the output of the *MegaraModelMap* to produce a wavelength calibration whose parameters are stored in a new *.json* file. After wavelength calibration, the

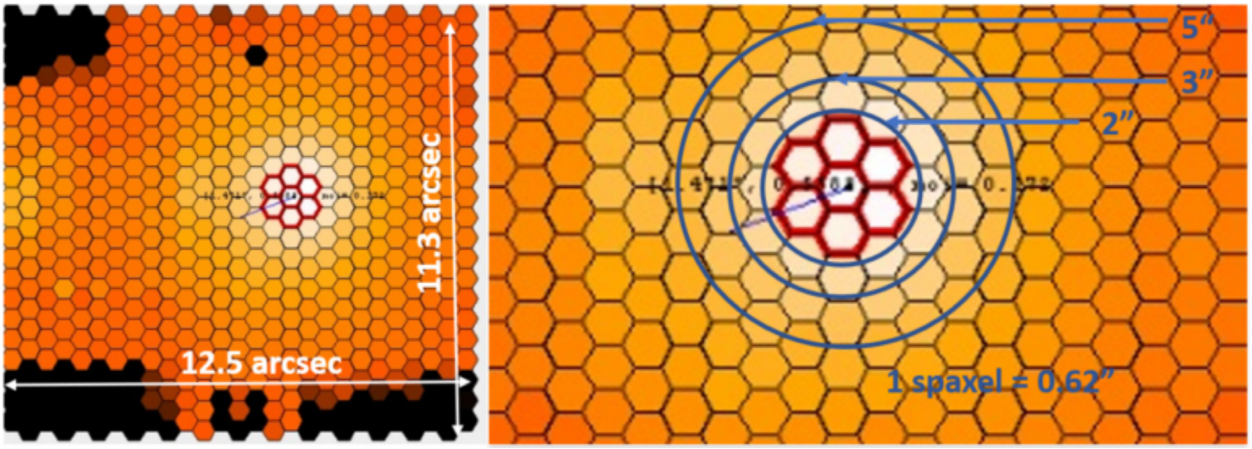


**Figure 4.** Reconstructed image of the star HD 192281 observed with MEGARA LCB mode in HR-I at the GTC during the commissioning, 2017 August 2.

**Table 6.** Subsample of 20 OT stars observed with HR-R and HR-I set-ups from the programme 35-GTC22/18B.

| Star name | Sp.type | *U* | *B* | *V* | *R* | *I* | Date (yy/mm/dd) | $T_{exp}$ (s) HR-R | $T_{exp}$ (s) HR-I | $T_{eff}$ Lit. | log *g* Lit. | [Fe/H] Lit. | Ref. |
|---|---|---|---|---|---|---|---|---|---|---|---|---|---|
| HD 147677 | K0 III | – | 5.8 | 4.9 | – | – | 18/08/23 | 3 × 20 | 1 × 25 | 4910 | 2.98 | −0.08 | INDO-US |
| HD 174912 | F8 V | – | 7.7 | 7.1 | 6.8 | 6.5 | 18/08/21 | 3 × 20 | 3 × 20 | 5746 | 4.32 | −0.48 | MILES |
| HD 200580 | F9 V | – | 7.9 | 7.5 | 7.0 | 6.8 | 18/08/20 | 3 × 20 | 3 × 20 | 5774 | 4.28 | −0.65 | MILES |
| HD 206374 | G8 V | – | 8.2 | 7.5 | 7.0 | 6.7 | 18/08/22 | 3 × 20 | 3 × 20 | 5622 | 4.47 | 0.00 | ELODIE |
| HD 211472 | K1 V | – | 8.3 | 7.5 | 7.6 | 6.6 | 18/08/22 | 3 × 20 | 3 × 20 | 5319 | 4.40 | −0.04 | ELODIE |
| HD 218059 | F8 V | – | 7.5 | 7.1 | 6.8 | 6.6 | 18/08/22 | 3 × 20 | 3 × 20 | 6253 | 4.27 | −0.27 | ELODIE |
| HD 220182 | K1 V | – | 8.2 | 7.4 | 6.8 | 6.5 | 18/08/22 | 3 × 20 | 3 × 20 | 5372 | 4.31 | 0.00 | ELODIE |
| HD 221585 | G8 IV | – | 8.2 | 7.4 | 7.0 | 6.6 | 18/08/22 | 3 × 20 | 3 × 20 | 5352 | 4.24 | 0.27 | ELODIE |
| HD 221830 | F9 V | – | 7.5 | 6.9 | 6.5 | 6.2 | 18/08/22 | 3 × 20 | 3 × 20 | 5688 | 4.16 | −0.44 | MILES |
| BD+08 3095 | G0 V | – | 10.6 | 10.0 | 9.8 | 9.6 | 18/08/22 | 3 × 90 | 3 × 90 | 5728 | 4.12 | −0.36 | INDO-US |
| HD 100696 | K0 III | – | 6.2 | 5.2 | 4.6 | 4.1 | 19/02/10 | 1 × 30 | 1 × 20 | 4890 | 2.27 | −0.25 | INDO-US |
| HD 101107 | F2 II–III | – | 5.9 | 5.6 | 5.4 | 5.2 | 19/02/10 | 1 × 40 | 1 × 40 | 7036 | 4.09 | −0,02 | NGSL |
| HD 104985 | G8 III | – | 6.8 | 5.8 | 5.2 | 4.7 | 19/04/12 | 1 × 40 | 1 × 30 | 4658 | 2.20 | −0.31 | INDO-US |
| HD 113002 | G2 II–III | 9.7 | 9.5 | 8.7 | 8.3 | 8.0 | 19/02/03 | 3 × 40 | 3 × 40 | 5152 | 2.53 | −1.08 | NGSL |
| HD 115136 | K2 III | – | 7.7 | 6.5 | 5.8 | 5.3 | 19/04/12 | 3 × 15 | 1 × 40 | 4541 | 2.40 | 0.05 | INDO-US |
| HD 117243 | G5 III | – | 9.0 | 8.3 | 7.9 | 7.6 | 19/01/29 | 3 × 30 | 3 × 30 | 5902 | 4.36 | 0.24 | INDO-US |
| HD 131111 | K0 III | – | 6.5 | 5.5 | 4.8 | 4.4 | 19/03/03 | 1 × 30 | 1 × 20 | 4710 | 3.11 | −0.29 | INDO-US |
| HD 131507 | K4 III | – | 6.9 | 5.5 | 4.6 | 3.8 | 19/03/03 | 1 × 30 | 1 × 15 | 4140 | 1.99 | −0.20 | INDO-US |
| HD 144206 | B9 III | 4.3 | 4.6 | 4.7 | – | – | 18/09/27 | 3 × 20 | 3 × 20 | 11957 | 3.70 | −0.17 | Stelib |
| HD 175535 | G7 IIIa | – | 5.8 | 4.9 | – | – | 18/09/07 | 3 × 15 | 3 × 10 | 5066 | 2.55 | −0.09 | MILES |

*MegaraFiberFlatImage* recipe is used to correct for the global variations in transmission between fibres while the *MegaraTwilightFlatImage* recipe corrects for the response introduced by the fibre flat (illumination correction).

Flux calibration is applied with the DRP by comparing the reduced standard star spectrum and the corresponding reference template. The *MegaraLcbAcquisition* recipe delivers the position of the standard star on the LCB. This routine uses all the calibrations from the former steps to reduce the standard star images. Once the position of the standard star on the LCB is known, the *MegaraLcbStdStar* routine produces the *Master Sensitivity* curve by comparing the 1D flux spectrum of the standard star (corrected from atmospheric extinction) with its tabulated flux-calibrated template. This sensitivity curve also corrects from the spectral instrument response (mostly dominated by VPH transmission and detector quantum efficiency), so that this step is needed even when non-photometric conditions prevent a reliable flux calibration.

Once all the calibration files are obtained and properly placed on the calibration tree, the scientific observations (MEGARA-GTC library stars) are processed with the recipe *MegaraLcbImage* or *MegaraMosImage*, producing the row-stacked-spectra (RSS) file with the individual flux-calibrated spectra for all fibres (corrected from extinction and flux/spectral response). For the individual stars and the LCB mode, we have used the automatic sky subtraction done by MEGARA DRP resulting from the median of the signal of all the eight sky mini-bundles. In the MOS M15 images, we have used the optimized sky subtraction procedure offered by the QLA, which allows the selection of a customized combination of individual spaxels for sky subtraction. In this case, we took a total of nine sky-spaxels (four in positioner 26 and five in positioner 36).

One of the critical steps before starting the model fitting is the normalization of the observed star spectrum, which needs a reliable continuum fitting that takes into account the proper spectral windows and avoids confusion with the high number of spectral lines due to the high resolution. For that purpose, we have made use of the fitting technique of Cardiel (2009), who described a generalized least-squares method that provides boundary functions

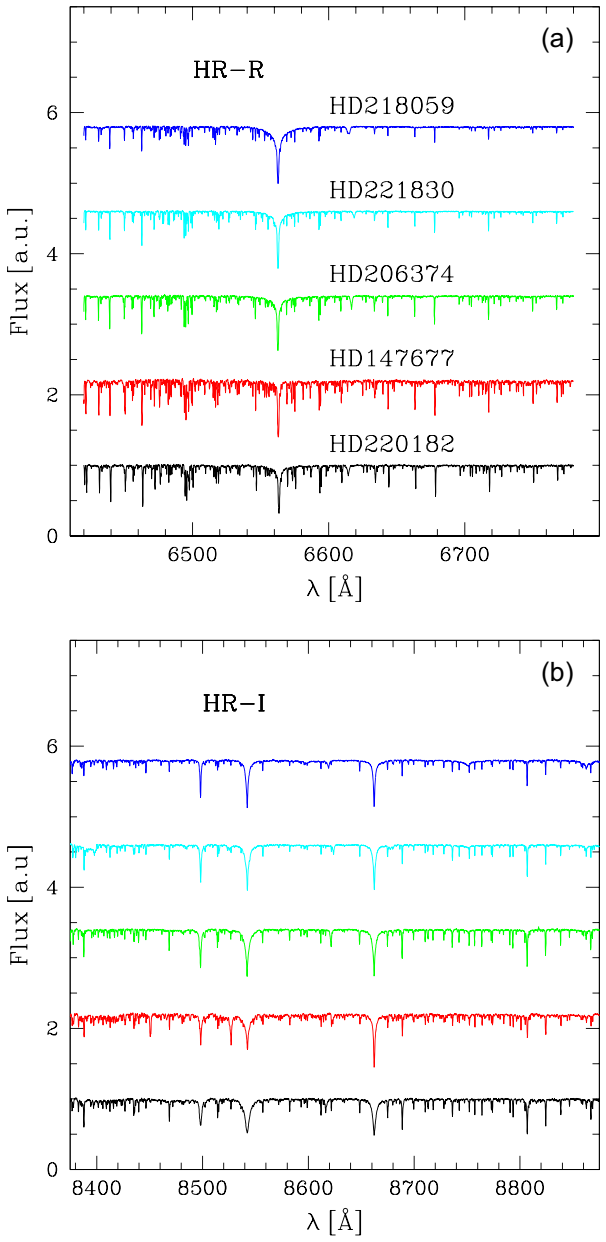


**Figure 5.** Flux of normalized spectra in arbitrary units for five stars, HD 220182, HD 147677, HD 206374, HD 221830 and HD 218059, from bottom to top, in two different set-ups: (a) HR-R and (b) HR-I.

for arbitrary data sets. In particular, this technique can be employed to determine the upper boundary of a particular spectrum. The method is based on the asymmetric treatment of the data on both sides of the boundary. When applied to a particular spectrum, the upper boundary becomes an excellent fit to the expected continuum. This is especially so when using adaptive splines as the mathematical function for the boundary. The flexibility has been improved a step further by splitting the fitted wavelength range of each spectrum into smaller intervals and by smoothly merging the independent adaptive splines to obtain a single continuum fit for the whole spectral range. Before the fitting process, a median filter of a few tens of pixels has been applied to each spectrum to minimize the bias that the data random noise may introduce in this kind of asymmetric fit. Although the fitting process, carried out using the public software `boundfit`,[3] has been completely automatized, all the resulting fits were visually inspected.

## 4 SPECTRA ANALYSIS

### 4.1 Estimates of the stellar physical parameters

Here, we describe the technique we use to estimate the physical stellar parameters, effective temperature $T_{\rm eff}$, surface gravity $\log g$ and metallicity [M/H], of the stars in our sample. We apply a $\chi^2$ technique to compare the observed spectra with each of the modelled spectra from a theoretical grid. This method has been proven to be successful in the determination of physical stellar parameters, such as the ULyss code by Koleva et al. (2009), MA$\chi$ by Jofré et al. (2010) and SP_ACE by Boeche & Grebel (2016).

We use the models of MUN05 for the spectra comparison. MUN05 present a complete library of synthetic spectra based on Kurucz's covering the 250–10500 Å range at different values of the spectral resolution, from which we have selected the ones at $R = 20\,000$. This theoretical stellar library has 71 754 wavelength values, selected to fit the ranges corresponding to the MEGARA gratings HR-R (6420–6800 Å) and HR-I (8400–8850 Å). The effective temperature $T_{\rm eff}$ ranges between 3500 and 47 500 K, with a 250 K step for models between 3500 and 10 000 K, and having less resolution for temperatures hotter than 10 000 K, which leads to a total of 58 models with different values of $T_{\rm eff}$. The gravity ranges from 0.0 to 5.0 dex, with 0.5 dex steps, giving 11 models with different values of $\log g$ for any value of $T_{\rm eff}$, except for the hottest models that have a smaller number of models with different $\log g$. Finally, the abundance varies from [M/H] = −2.5 to +0.5 dex, with +0.5 dex steps, giving a total of seven abundance values. The total number of models is 2665, with an average number of ∼380 different models for each metallicity.

The $\chi^2$ technique uses the flux-normalized spectra of both observations and models, and computes the differences at any given wavelength on a certain range with the well-known equation:

$$\chi^2 = \sum_{i=1}^{nl} \frac{[F_{\rm mod}(\lambda) - F_{\rm obs}(\lambda)]^2}{\sigma^2}. \quad (1)$$

Here, $F_{\rm mod}$ and $F_{\rm obs}$ are the model and the observed normalized fluxes, respectively, $nl$ is the number of available wavelengths and $\sigma$ is the flux error, which we have calculated with the continuum S/N averaged over the whole spectral range. We have obtained the modelled spectra with the same spectral sampling as observed by polynomial interpolation, and then we have computed $\chi^2$ (equation 1) by comparing the observed spectrum with each single modelled spectra in the theoretical grid. Then, we have assigned to each observed star the physical stellar parameters corresponding to the model that gives the minimum $\chi^2$, and we have labelled these values $T_{\rm eff}$, $\log g$ and [M/H]. As an example of these fitting results, Fig. 6 shows the detailed spectra of the $\chi^2_{\rm min}$ model in three consecutive spectral ranges within the HR-I set-up for a cool star (left panel) and a hot star (right panel) of the COM subsample.

When the $\chi^2$ technique is used, a likelihood or confidence level, $P$, for a $\chi^2$ distribution is obtained, given by

$$P = 1 - \alpha(\chi^2 < x) = 1 - \int_0^x \chi^2_k \, {\rm d}u = 1 - \int_0^x \frac{u^{k/2} e^{-u/2}}{2^{k/2}\Gamma(k/2)} {\rm d}u. \quad (2)$$

[3] https://boundfit.readthedocs.io/en/latest/

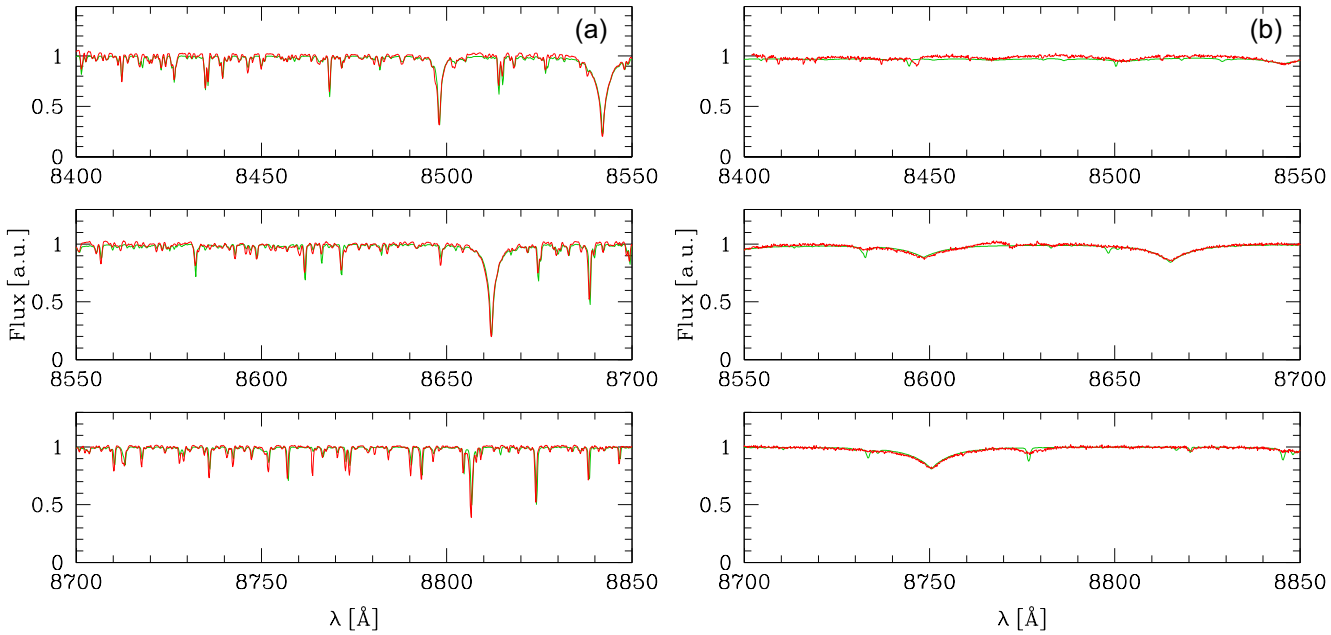


**Figure 6.** MEGARA HR-I normalized spectra of (a) the cool giant K1 III star HD 025975 and (b) the hot B2 IIID star BD+40 4032. Observed spectra are plotted in red while the MUN05 model, which gives the best fit, is overplotted in green. The $\chi^2_{\rm min}$ model for HD 025975 has $T_{\rm eff}$ = 4750 K, $\log g$ = 3.0 and [M/H] = −0.5, while the one for BD+40 4032 has $T_{\rm eff}$ = 28 000 K, $\log g$ = 3.5 and [M/H] = 0.0. Each star spectrum is divided into three panels to show the fitting details.

The minimum $\chi^2$ technique described above gives the most likely model, obtaining the most probable stellar parameters. However, when analysing the table with the $\chi^2$ values obtained from the fitting of each single model of the theoretical grid to a given observed star, we usually find several models with similar likelihood, which, therefore, still provide a good fit to the observational data. We have performed an analysis of the $\chi^2$ results of all models of each observed spectrum, to find those with likelihood similar to the corresponding one for $\chi^2_{\rm min}$. Thus, we derive the likelihood contours around the best-fitting model that define the parameter region offering results within a given confidence level, $L_{\rm sel}$. To select models within a region $R_{\nu,\alpha}$ (Avni 1976),

$$\chi^2 - \chi^2_{\rm min} \leq \Delta(\nu, \alpha), \quad (3)$$

it is necessary to define $\nu$, which is the number of free parameters (three in our case), and $\alpha$, the significance level. We have considered all the models with $\alpha$ = 0.01, implying differences as

$$\chi^2 - \chi^2_{\rm min} \leq \Delta(3, 0.01) = 0.115. \quad (4)$$

Every model within this contoured region has a likelihood $L_{\rm sel}$ similar to the maximum $L_{\rm max} = 1$ (corresponding to the best model with $\chi^2 = \chi^2_{\rm min}$), within a 1 per cent error, $L_{\rm sel} \geq L_{\rm max} - 0.01$. This means that the probability of choosing the best model will be better than 99 per cent when selecting the results within this region $R_{\nu,\alpha}$. The number of models, $N$, fulfilling equation (4) is different, obviously, from star to star, as can be seen in the tables that present the fitting results (Tables 7, 8, 9 and 10for the COM, M15 and OT stars, respectively), as this depends on the characteristics of each spectrum.

We can apply this method to each observed spectrum, either in the HR-R set-up or in the HR-I set-up. In fact, we have performed the calculations in each separately, and then combining both spectra for each star in only one fit. Fig. 7 shows, as an example, the results for the OT star BD+08 3095 observed in both HR-R and HR-I set-ups. This figure plots the resulting models in the $T_{\rm eff}$–$\log g$ plane for all metallicities (although we have also tabulated our results separately for each value of [M/H]). The colours represent the probability scale, as labelled on the right in the plot. The top and middle panels show the results when fitting the models to the HR-R and HR-I observed spectra, respectively. The effective temperature obtained when using $\chi^2_{\rm min}$ are similar $T_{\rm eff}$ = 6000 K (from the fit to the HR-R spectrum) and 6500 K (HR-I), and a similar abundance ([M/H] = −1.0 and −0.5) is set for each set-up. However, the value of $\log g$ obtained from the fit to the observed spectra is very different in HR-R ($\log g = 1.5$) and HR-I ($\log g = 5.0$). We have then run our fit taking both spectra and doing a single fit to the combined HR-R and HR-I spectrum. The $\chi^2_{\rm min}$ fitting gives values of $T_{\rm eff} = 6250$ K, $\log g = 4.5$ and [M/H] = −0.5, closer to the values in the literature ($T_{\rm eff} = 5728$ K, $\log g = 4.1$ and [M/H] = −0.36) plotted as a green dot. These results are shown in the bottom panel of Fig. 7.

We have also carried out a second analysis by choosing those models with $P > 0.99$, within a small region of the parameter space. In the case of BD+08 3095 we have obtained 36, 78 and 42 compliant models when using the HR-R spectrum only, the HR-I spectrum only, or the combination of both set-ups in a single spectrum, respectively. These models are over-plotted with small grey dots over the blue region where the best models are located, and a large black cross indicates the averaged stellar parameters, with their dispersion given by an ellipse, obtained with those models in the top, middle and bottom panels, respectively.

For the top panel (fitting to HR-R spectrum), these averaged values are $T_{\rm eff} = 5972 \pm 285$ K and $\log g = 1.8 \pm 1.1$ dex. For the middle panel (fitting to HR-I spectrum), the averaged results are $T_{\rm eff} = 5356 \pm 663$ K and $\log g = 4.0 \pm 0.9$ dex. The relative errors for $\log g$ are very high (61 and 23 per cent) compared with the errors found for $T_{\rm eff}$ (5 and 12 per cent). This can be attributed to the larger step size in $\log g$ in the MUN05 models, given the much smaller number of models with different $\log g$ than those

**Table 7.** Stellar parameters for the 21 commissioning stars derived from the fitting with the theoretical models for the HR-I set-up, and from the literature. References are: (1) Cenarro et al. (2001b); (2) Chen et al. (2014); (3) Prugniel & Soubiran (2004); (4) Prugniel, Vauglin & Koleva (2011); (5) Cameron (2003); (6) Valdes et al. (2004); (7) Holgado et al. (in preparation); (8) Blomme et al. (2013); (9) Martins, Schaerer & Hillier (2005). See the text for a description of the table.

| Star name | $\chi^2_{\rm min}$ | $P_{\rm max}$ | Results with minimum $\chi^2$ | | | $N$ | Average results and dispersion with $N$ models | | | Data from the literature | | | Ref. |
|---|---|---|---|---|---|---|---|---|---|---|---|---|---|
| | | | $T_{\rm eff}$ | $\log g$ | [M/H] | | $\langle T_{\rm eff}\rangle$ | $\langle \log g\rangle$ | $\langle$[M/H]$\rangle$ | $T_{\rm eff,\,lit}$ | $\log g_{\rm lit}$ | [M/H]$_{\rm lit}$ | |
| Schulte 9 | 0.06 | 0.996 | 37 500 | 4.5 | − 2.5 | 200 | 32 808 ± 5320 | 4.41 ± 0.59 | − 0.92 ± 0.98 | 38 520 | 3.57 | | (8, 9) |
| HD 192281 | 0.13 | 0.988 | 40 000 | 4.5 | − 2.5 | 118 | 35 725 ± 4839 | 4.60 ± 0.45 | − 1.01 ± 0.99 | 40 800 | 3.73 | | (7) |
| BD 254655 | 0.08 | 0.994 | 40 000 | 5.0 | − 2.5 | 134 | 35 295 ± 4583 | 4.67 ± 0.37 | − 1.01 ± 0.98 | | | | |
| HD 218915 | 0.06 | 0.996 | 24 000 | 3.0 | 0.5 | 249 | 31 347 ± 5717 | 4.28 ± 0.65 | − 0.96 ± 0.99 | 31 100 | 3.21 | | (7) |
| BD+40 4032 | 0.05 | 0.997 | 28 000 | 3.5 | 0.0 | 305 | 29 543 ± 5199 | 4.21 ± 0.65 | − 0.97 ± 0.99 | 33 813 | 3.13 | 0.0 | (5) |
| BD+33 2642 | 0.17 | 0.983 | 17 000 | 2.5 | 0.0 | 145 | 21 131 ± 3797 | 3.13 ± 0.37 | − 0.96 ± 0.99 | | | | |
| HD 220575 | 0.23 | 0.974 | 18 000 | 3.5 | − 2.5 | 219 | 18 183 ± 2936 | 3.36 ± 0.51 | − 1.03 ± 1.01 | 12 293 | 3.70 | 0.50 | (1) |
| | | | | | | | | | | 12 241 ± 402 | 4.09 ± 0.13 | 0.27 ± 0.15 | (4) |
| BD+42 3227 | 0.07 | 0.995 | 28 000 | 3.5 | − 0.5 | 349 | 28 117 ± 5177 | 4.12 ± 0.69 | − 0.98 ± 0.99 | | | | |
| BD+12 2237 | 0.29 | 0.962 | 28 000 | 3.5 | − 2.5 | 286 | 25 615 ± 4735 | 3.77 ± 0.59 | − 0.96 ± 0.99 | | | | |
| BD+17 4708 | 0.02 | 0.999 | 5750 | 4.0 | − 1.5 | 285 | 5244 ± 776 | 3.17 ± 1.41 | − 1.91 ± 0.55 | 5993 | 3.94 | − 1.65 | (3) |
| HD 026630 | 1.03 | 0.794 | 5500 | 0.5 | − 0.5 | 14 | 5357 ± 306 | 0.50 ± 0.55 | − 0.54 ± 0.31 | 5643 | 1.54 | 0.10 | (6) |
| HD 216219 | 0.05 | 0.997 | 5500 | 3.0 | − 0.5 | 179 | 5159 ± 654 | 3.00 ± 1.48 | − 0.93 ± 0.56 | | | | |
| HD 011544 | 0.42 | 0.935 | 5000 | 1.0 | − 0.5 | 22 | 4943 ± 336 | 1.02 ± 0.75 | − 0.48 ± 0.39 | | | | |
| HD 019445 | 0.07 | 0.996 | 5000 | 5.0 | − 2.5 | 238 | 5283 ± 730 | 3.20 ± 1.40 | − 2.00 ± 0.50 | 5929 | 4.36 | − 2.02 | (2) |
| HD 020123 | 0.48 | 0.924 | 5000 | 1.5 | − 0.5 | 42 | 5101 ± 445 | 1.43 ± 0.94 | − 0.54 ± 0.45 | 4901 | | | (6) |
| HD 224458 | 0.19 | 0.979 | 5000 | 2.0 | − 0.5 | 104 | 4892 ± 558 | 2.40 ± 1.43 | − 0.63 ± 0.54 | 4722 | 2.20 | − 0.50 | (1) |
| | | | | | | | | | | 4819 ± 67 | 2.29 ± 0.17 | −0.44 ± 0.08 | (4) |
| HD 220954 | 0.22 | 0.974 | 4750 | 1.5 | − 0.5 | 49 | 4500 ± 430 | 1.83 ± 1.15 | − 0.51 ± 0.47 | 4664 | 2.37 | − 0.10 | (4) |
| | | | | | | | | | | 4731 ± 46 | 2.61 ± 0.11 | 0.07 ± 0.05 | (4) |
| HD 025975 | 0.18 | 0.981 | 4750 | 3.0 | − 0.5 | 114 | 4752 ± 563 | 3.11 ± 1.35 | − 0.52 ± 0.49 | 4941 | 3.40 | − 0.20 | (6) |
| HD 027971 | 0.29 | 0.962 | 4750 | 2.0 | − 0.5 | 62 | 4746 ± 491 | 2.40 ± 1.33 | − 0.45 ± 0.52 | 4860 | 2.82 | − 0.08 | (6) |
| HD 174350 | 1.60 | 0.659 | 4750 | 0.0 | − 1.0 | 21 | 5190 ± 353 | 0.81 ± 0.72 | − 0.48 ± 0.37 | 4537 | 2.56 | − 0.02 | (2) |
| HD 185622 | 0.24 | 0.972 | 5000 | 1.5 | − 0.5 | 42 | 4958 ± 431 | 1.60 ± 1.08 | − 0.55 ± 0.47 | | | | |

**Table 8.** Stellar parameters for the M15 stars derived from the fit of the theoretical models to the observed spectra in HR-R and HR-I, and the simultaneous fitting to the combined spectrum with HR-R and HR-I. See the text for a description of the table. The full table with the results for the 56 stars is available online (Table A1 in Appendix A, given as supporting information online).

| Star | $\chi^2_{\rm min}$ | $P_{\rm max}$ | Results with minimum $\chi^2$ | | | Average results with $N$ models | | | |
|---|---|---|---|---|---|---|---|---|---|
| | | | $T_{\rm eff}$ | $\log g$ | [M/H] | $N_{\rm p}$ | $\langle T_{\rm eff}\rangle$ | $\langle \log g\rangle$ | $\langle$[M/H]$\rangle$ |
| | | | | | HR-R | | | | |
| 1 | 5.251 | 0.15 | 7000 | 0.5 | − 1.5 | 10 | 7125 ± 132 | 0.50 ± 0.00 | − 1.50 ± 0.00 |
| 2 | 0.731 | 0.87 | 7250 | 1.5 | − 1.5 | 246 | 7494 ± 489 | 1.59 ± 0.74 | − 1.88 ± 0.39 |
| 3 | 0.910 | 0.82 | 5250 | 0.0 | − 2.0 | 102 | 5551 ± 271 | 0.81 ± 0.63 | − 1.93 ± 0.39 |
| 4 | 1.935 | 0.59 | 5750 | 0.0 | − 1.5 | 10 | 5800 ± 197 | 0.20 ± 0.26 | − 1.50 ± 0.00 |
| 5 | 1.960 | 0.58 | 6000 | 0.0 | − 2.0 | 60 | 6117 ± 289 | 0.68 ± 0.54 | − 1.90 ± 0.38 |
| | | | | | HR-I | | | | |
| 1 | 0.884 | 0.83 | 6250 | 0.5 | 1.50 | 52 | 6457 ± 504 | 1.3 ± 1.0 | − 1.73 ± 0.30 |
| 2 | 0.558 | 0.91 | 6750 | 3.0 | 1.50 | 65 | 6673 ± 470 | 2.5 ± 1.0 | − 1.98 ± 0.41 |
| 3 | 0.710 | 0.87 | 4500 | 0.0 | 2.50 | 131 | 4616 ± 545 | 2.1 ± 1.3 | − 2.00 ± 0.39 |
| 4 | 0.614 | 0.89 | 4250 | 0.0 | 2.50 | 73 | 4497 ± 481 | 1.3 ± 0.9 | − 1.95 ± 0.39 |
| 5 | 1.144 | 0.77 | 5000 | 0.0 | 1.50 | 17 | 4750 ± 375 | 0.3 ± 0.4 | − 1.59 ± 0.20 |
| | | | | | HR-R and HR-I in a combined single spectrum | | | | |
| 1 | 375.217 | 0.00 | 7250 | 0.5 | − 1.5 | 2 | 7125 ± 177 | 0.50 ± 0.00 | − 1.50 ± 0.00 |
| 2 | 11.126 | 0.09 | 7500 | 1.0 | − 1.5 | 14 | 7304 ± 223 | 1.43 ± 0.65 | − 1.57 ± 0.18 |
| 3 | 6.303 | 0.36 | 5750 | 0.0 | − 1.5 | 11 | 5477 ± 284 | 0.27 ± 0.41 | − 1.64 ± 0.23 |
| 4 | 10.614 | 0.16 | 6750 | 0.5 | − 1.5 | 7 | 6357 ± 690 | 0.36 ± 0.24 | − 1.50 ± 0.00 |
| 5 | 5.322 | 0.31 | 6000 | 0.0 | − 1.5 | 3 | 5750 ± 250 | 0.00 ± 0.00 | − 1.50 ± 0.00 |

with eligible values of $T_{\rm eff}$. However, the result shown in the bottom panel for the fitting to the combined spectrum of both HR-R and HR-I spectral ranges gives $T_{\rm eff} = 5917 \pm 356$ K, $\log g = 3.6 \pm 1.2$ and [M/H] $= -0.88 \pm 0.33$, closer, as before, to those found by other authors and reported in the literature (green point in the bottom panel). Differences can still be attributed mostly to the model-error dominated by the large step size in all physical parameters in the MUN05 grid.

The results are presented as histograms for $T_{\rm eff}$, $\log g$ and [M/H] in Fig. 8, which shows the values resulting from the fit of the models to the observed spectrum of BD+08 3095 in HR-R (left column), HR-I (middle column) and the combined spectrum with the two spectral windows HR-R and HR-I (right column) for an easy comparison. We have plotted a Gaussian function (blue dashed line), showing the averaged and the dispersion values obtained for each stellar parameter. The results obtained with the $\chi^2_{\rm min}$ model are shown with a green arrow. To complete the figure, we have over-plotted with a cyan short-dashed arrow the stellar parameters obtained from the SP_ACE model (see Section 4.3) that best fits each observed spectrum. The values from the literature, usually obtained from a spectrum with a wider wavelength range and much lower spectral resolution, are represented as a magenta dot-dashed arrow.

**Table 9.** Stellar parameters for the 20 OT stars derived from the fitting with the theoretical models and from the literature for the HR-R and HR-I separately. See the text for a description of the table.

| Star name | HR-R | | | | | | | | | | | HR-I | | | | |
|---|---|---|---|---|---|---|---|---|---|---|---|---|---|---|---|---|
| | $\chi^2_{min}$ | $P_{max}$ | Results with $\chi^2_{min}$ | | | $N$ | Average results with $N$ models | | | $\chi^2_{min}$ | $P_{max}$ | Results with $\chi^2_{min}$ | | | $N$ | Average results with $N$ models | | |
| | | | $T_{eff}$ | log $g$ | [M/H] | | $\langle T_{eff}\rangle$ | $\langle \log g\rangle$ | $\langle$[M/H]$\rangle$ | | | $T_{eff}$ | log $g$ | [M/H] | | $\langle T_{eff}\rangle$ | $\langle \log g\rangle$ | $\langle$[M/H]$\rangle$ |
| HD 147677 | 1.240 | 0.74 | 5250 | 1.0 | 0.0 | 25 | 5360 ± 307 | 1.6 ± 1.0 | 0.18 ± 0.32 | 1.005 | 0.80 | 7250 | 5.0 | 0.0 | 8 | 7156 ± 352 | 4.8 ± 0.3 | 0.00 ± 0.00 |
| HD 174912 | 0.963 | 0.81 | 6250 | 2.0 | −0.5 | 40 | 6088 ± 292 | 1.3 ± 1.0 | −0.86 ± 0.36 | 0.428 | 0.93 | 6250 | 5.0 | −0.5 | 42 | 5548 ± 539 | 4.3 ± 0.8 | −0.87 ± 0.38 |
| HD 200580 | 1.784 | 0.62 | 6000 | 0.0 | −2.5 | 39 | 6910 ± 1436 | 1.1 ± 0.7 | −1.51 ± 0.97 | 1.150 | 0.77 | 6000 | 5.0 | −0.5 | 26 | 5760 ± 541 | 4.6 ± 0.5 | −0.71 ± 0.40 |
| HD 206374 | 0.466 | 0.93 | 6000 | 3.0 | 0.0 | 27 | 5806 ± 313 | 2.3 ± 1.2 | −0.20 ± 0.25 | 0.112 | 0.99 | 5500 | 5.0 | −0.5 | 79 | 5472 ± 602 | 4.0 ± 0.9 | −0.55 ± 0.37 |
| HD 211472 | 0.503 | 0.92 | 5500 | 4.5 | 0.0 | 18 | 5444 ± 251 | 3.6 ± 1.1 | −0.03 ± 0.21 | 0.227 | 0.97 | 5000 | 5.0 | −0.5 | 58 | 5379 ± 644 | 4.4 ± 0.6 | −0.44 ± 0.36 |
| HD 218059 | 0.366 | 0.95 | 6250 | 2.0 | −0.5 | 39 | 6192 ± 295 | 1.6 ± 1.1 | −0.58 ± 0.34 | 0.187 | 0.98 | 6250 | 4.0 | −0.5 | 59 | 5661 ± 551 | 3.8 ± 1.1 | −0.84 ± 0.40 |
| HD 220182 | 3.347 | 0.34 | 6500 | 3.5 | −1.5 | 218 | 7409 ± 2355 | 3.0 ± 1.4 | −1.40 ± 0.86 | 0.418 | 0.94 | 6000 | 5.0 | 0.0 | 62 | 5657 ± 659 | 4.2 ± 0.7 | −0.35 ± 0.33 |
| HD 221585 | 0.842 | 0.84 | 5500 | 1.0 | 0.0 | 31 | 5718 ± 340 | 1.8 ± 1.2 | 0.10 ± 0.30 | 0.606 | 0.90 | 6500 | 4.0 | 0.0 | 52 | 6062 ± 634 | 4.2 ± 0.9 | −0.03 ± 0.30 |
| HD 221830 | 0.511 | 0.92 | 5750 | 1.5 | −0.5 | 27 | 5815 ± 299 | 1.7 ± 1.1 | −0.41 ± 0.31 | 0.336 | 0.95 | 6000 | 5.0 | −0.5 | 107 | 5493 ± 697 | 3.9 ± 1.1 | −0.81 ± 0.48 |
| BD+08 3095 | 0.397 | 0.94 | 6000 | 1.5 | −1.0 | 36 | 5972 ± 285 | 1.8 ± 1.1 | −1.06 ± 0.39 | 0.117 | 0.99 | 6500 | 5.0 | −0.5 | 78 | 5356 ± 663 | 4.0 ± 0.9 | −1.21 ± 0.48 |
| HD 100696 | 0.731 | 0.87 | 5500 | 2.0 | −0.5 | 37 | 5615 ± 304 | 2.3 ± 1.2 | −0.49 ± 0.34 | 1.296 | 0.73 | 5250 | 0.5 | −1.0 | 17 | 5382 ± 332 | 1.2 ± 0.9 | −0.71 ± 0.36 |
| HD 101107 | 0.233 | 0.97 | 9750 | 2.5 | −2.5 | 106 | 9316 ± 1843 | 3.2 ± 0.9 | −1.73 ± 0.73 | 0.704 | 0.87 | 6750 | 5.0 | −0.5 | 24 | 6469 ± 332 | 4.3 ± 0.6 | −0.77 ± 0.25 |
| HD 104985 | 1.042 | 0.79 | 5250 | 1.0 | 0.0 | 21 | 5405 ± 349 | 1.5 ± 1.2 | 0.07 ± 0.33 | 0.873 | 0.83 | 4500 | 0.5 | −1.0 | 29 | 4931 ± 433 | 1.1 ± 0.9 | −0.67 ± 0.47 |
| HD 113002 | 1.692 | 0.64 | 5750 | 0.5 | −1.5 | 30 | 5867 ± 243 | 0.8 ± 0.7 | −1.52 ± 0.50 | 0.369 | 0.95 | 5000 | 0.5 | −1.5 | 34 | 5066 ± 400 | 1.5 ± 1.1 | −1.15 ± 0.47 |
| HD 115136 | 0.390 | 0.94 | 5000 | 0.5 | 0.0 | 13 | 5212 ± 247 | 1.5 ± 0.9 | 0.27 ± 0.33 | 0.159 | 0.98 | 4250 | 0.5 | −1.0 | 33 | 4462 ± 415 | 1.7 ± 1.1 | −0.44 ± 0.51 |
| HD 117243 | 0.227 | 0.97 | 6000 | 2.0 | 0.0 | 26 | 5942 ± 319 | 1.9 ± 1.1 | −0.15 ± 0.24 | 0.336 | 0.95 | 5500 | 2.5 | −0.5 | 73 | 5479 ± 520 | 3.2 ± 1.5 | −0.47 ± 0.46 |
| HD 131111 | 0.106 | 0.99 | 6250 | 4.0 | 0.0 | 30 | 6158 ± 191 | 3.7 ± 0.9 | −0.23 ± 0.25 | 0.063 | 1.00 | 4750 | 3.0 | −0.5 | 62 | 4819 ± 460 | 3.4 ± 1.2 | −0.52 ± 0.44 |
| HD 131507 | 1.384 | 0.71 | 5250 | 1.5 | 0.5 | 19 | 5184 ± 261 | 1.6 ± 1.1 | 0.32 ± 0.25 | 2.053 | 0.56 | 5500 | 0.0 | −0.5 | 14 | 5357 ± 389 | 0.5 ± 0.5 | −0.32 ± 0.25 |
| HD 144206 | 0.301 | 0.96 | 7250 | 2.5 | −1.5 | 201 | 8141 ± 1221 | 2.2 ± 0.9 | −1.15 ± 0.88 | 0.393 | 0.94 | 21 000 | 3.0 | 0.5 | 50 | 17825 ± 6607 | 3.2 ± 0.4 | −0.97 ± 1.15 |
| HD 175535 | 0.552 | 0.91 | 5500 | 1.5 | 0.0 | 29 | 5638 ± 331 | 2.2 ± 1.2 | 0.10 ± 0.31 | 0.207 | 0.98 | 4750 | 2.0 | −0.5 | 49 | 5138 ± 487 | 3.0 ± 1.3 | −0.18 ± 0.49 |

Fig. 8 illustrates the discrepancies found in the derived stellar parameter when using different methods, and the sensitivity to spectral resolution, mathematical algorithms (i. e.fitting and parameter selection) and model set (among other effects). It is more difficult to determine the stellar parameter (mainly gravity) in the HR-I set-up, for which we cannot find SP_ACE's solutions for many of the stars in our sample. We return to this discussion in Sections 4.2 and 4.3, after estimating the stellar parameters of the 97 stars from three different samples presented in this work.

We emphasize the importance of the spectral range involved in the fitting. In the case of individual fits to the HR-R and HR-I spectra, the resulting average parameters are not very different in both set-ups, for $T_{\rm eff}$ and [M/H], within the error bars. However, this is not the case for log $g$, for which an important discrepancy is obtained. This can be explained by the very different information in the spectral lines existing in the two (and short) spectral ranges. The effect is magnified because of the high spectral resolution. To try to take advantage of all the information in our observed spectra, we repeated the model fitting to allow the code to use the spectral information in the two spectral ranges HR-R and HR-I simultaneously. The average parameters are then found to be in better agreement with the ones from the literature. This conclusion reinforces the decision to make the spectral library by always observing all stars in both high-resolution MEGARA set-ups.

### *4.1.1 Stellar parameters for the commissioning stars*

We have applied the technique described in the previous section to our 21 COM stars, in order to assign the stellar parameters $T_{\rm eff}$, log $g$ and [M/H] with the $\chi^2_{\rm min}$ model fitted to the observed spectrum. We have also obtained the mean values $\langle T_{\rm eff}\rangle$, $\langle \log g\rangle$ and $\langle$[M/H]$\rangle$, as the average of the parameters of $N$ models with $\chi^2$ similar to $\chi^2_{\rm min}$, within the allowed probability value.

Table 7 summarizes the results for the 21 commissioning stars, sorted by spectral type, from the hottest (top) to the coolest (bottom). Column 1 displays the star name; column 2 shows the $\chi^2_{\rm min}$ obtained from the fitting process of the observed normalized spectrum to the MUN05 theoretical catalogue; column 3 displays the associated maximum probability $P_{\rm max}$, associated with the $\chi^2_{\rm min}$. Columns 4, 5 and 6 show the derived stellar parameters, $T_{\rm eff}$, log $g$ and [M/H], from the MUN05 model corresponding to the $\chi^2_{\rm min}$ model. Column 7 gives the number of models, $N$, in the likelihood region $R_{v,\alpha}$. Columns 8, 9 and 10 have the average stellar parameters, $\langle T_{\rm eff}\rangle$, $\langle \log g\rangle$ and $\langle$[M/H]$\rangle$, respectively, obtained as the averaged values of the set of $N$ models, with their corresponding errors. Finally, columns 11, 12 and 13 give the stellar parameters, $T_{\rm eff,lit}$, $\log g_{\rm lit}$ and $[{\rm M/H}]_{\rm lit}$, from the literature whenever available, given the reference code in column 14. The stellar parameters come from: Holgado et al. (private communication) for HD 218915 and HD 192281; the GOSSS catalogue (Sota et al. 2014) for the spectral type of Schulte 9, whose $T_{\rm eff}$ has been obtained from Blomme et al. (2013) and log $g$ from the calibration for O stars (Martins et al. 2005); MILES stellar parameters (Cenarro et al. 2001b) for HD 220575, HD 224458 and HD 220954; XSL, XSHOOTER spectral library (Chen et al. 2014) for HD 019445, HD 174350 and HD 216219; ELODIE (Prugniel & Soubiran 2004) for BD+17 4708 and HD 026630; INDO-US (Valdes et al. 2004) for HD 020123, HD 025975 and HD 027971. Values for BD+40 4032 come from Cameron (2003). Stars from MILES were re-calibrated by Prugniel et al. (2011) and the new values appear in an additional row. Table 7 shows that the $\langle T_{\rm eff}\rangle$ values obtained are in agreement with those from the literature – we will revisit this point in Section 4.2 – except

**Table 10** Stellar parameters for the 20 OT stars derived from the fitting with the combined spectrum of both HR-R and HR-I set-ups. See the text for a description of the table.

| Star name | $\chi^2_{min}$ | $P_{max}$ | Simultaneous fitting of HR-R and HR-I: Results with $\chi^2_{min}$ | | | $N$ | Average results with $N$ models | | | Data from Literature | | | |
|---|---|---|---|---|---|---|---|---|---|---|---|---|---|
| | | | $T_{eff}$ | log $g$ | [M/H] | | $\langle T_{eff}\rangle$ | $\langle \log g\rangle$ | $\langle$[M/H]$\rangle$ | $\langle T_{eff}\rangle$ | $\langle \log g\rangle$ | $\langle$[M/H]$\rangle$ | $R$ |
| HD 147677 | 0.627 | 0.89 | 5500 | 4.0 | 0.0 | 29 | 5422 ± 402 | 3.6 ± 0.9 | −0.14 ± 0.30 | 4910 | 3.0 | −0.08 | 5000 |
| HD 174912 | 0.288 | 0.96 | 6250 | 4.0 | −0.5 | 34 | 6088 ± 369 | 3.6 ± 1.1 | −0.63 ± 0.31 | 5746 | 4.3 | −0.48 | 2000 |
| HD 200580 | 0.292 | 0.96 | 6250 | 4.5 | −0.5 | 43 | 5849 ± 354 | 3.3 ± 1.3 | −0.87 ± 0.35 | 5774 | 4.3 | −0.65 | 2000 |
| HD 206374 | 0.202 | 0.98 | 6000 | 4.5 | 0.0 | 38 | 5770 ± 336 | 3.8 ± 0.9 | −0.25 ± 0.25 | 5622 | 4.5 | 0.00 | 42 000 |
| HD 211472 | 0.209 | 0.98 | 5500 | 5.0 | 0.0 | 27 | 5380 ± 305 | 4.1 ± 0.8 | −0.22 ± 0.25 | 5319 | 4.4 | −0.04 | 42 000 |
| HD 218059 | 0.237 | 0.97 | 6250 | 4.0 | −0.5 | 31 | 6210 ± 360 | 3.6 ± 1.2 | −0.55 ± 0.35 | 6253 | 4.3 | −0.27 | 42 000 |
| HD 220182 | 0.479 | 0.92 | 5750 | 5.0 | 0.0 | 28 | 5455 ± 347 | 4.3 ± 0.6 | −0.23 ± 0.25 | 5272 | 4.3 | 0.00 | 42 000 |
| HD 221585 | 0.684 | 0.88 | 6250 | 5.0 | 0.5 | 35 | 5921 ± 352 | 4.1 ± 0.8 | 0.19 ± 0.25 | 5352 | 4.2 | 0.27 | 42 000 |
| HD 221830 | 0.299 | 0.96 | 6000 | 3.5 | −0.5 | 56 | 5911 ± 373 | 3.3 ± 1.3 | −0.55 ± 0.38 | 5688 | 4.2 | −0.44 | 2000 |
| BD 08+3095 | 0.191 | 0.98 | 6250 | 4.5 | −0.5 | 42 | 5917 ± 356 | 3.6 ± 1.2 | −0.88 ± 0.33 | 5728 | 4.1 | −0.36 | 80 000 |
| HD 100696 | 0.337 | 0.95 | 5500 | 2.5 | −0.5 | 55 | 5505 ± 410 | 2.7 ± 1.3 | −0.45 ± 0.41 | 4890 | 2.3 | −0.25 | 5000 |
| HD 101107 | 0.384 | 0.94 | 7000 | 5.0 | −0.5 | 24 | 6823 ± 250 | 4.5 ± 0.5 | −0.94 ± 0.40 | 7036 | 4.0 | −0.02 | 1000 |
| HD 104985 | 0.262 | 0.97 | 5250 | 2.5 | 0.0 | 26 | 5212 ± 398 | 2.5 ± 1.1 | −0.10 ± 0.45 | 4658 | 2.2 | −0.31 | 5000 |
| HD 113002 | 0.180 | 0.98 | 5500 | 1.5 | −1.0 | 38 | 5454 ± 343 | 1.8 ± 1.2 | −0.95 ± 0.38 | 5152 | 2.5 | −1.08 | 1000 |
| HD 115136 | 0.243 | 0.97 | 5000 | 2.0 | 0.0 | 27 | 5102 ± 375 | 2.5 ± 1.1 | 0.09 ± 0.39 | 4541 | 2.4 | 0.05 | 5000 |
| HD 117243 | 0.171 | 0.98 | 6000 | 4.0 | 0.0 | 33 | 5955 ± 327 | 3.6 ± 1.0 | −0.08 ± 0.28 | 5902 | 4.4 | 0.24 | 5000 |
| HD 131111 | 0.163 | 0.98 | 6000 | 4.5 | 0.0 | 39 | 5846 ± 323 | 3.7 ± 0.9 | −0.26 ± 0.25 | 4710 | 3.1 | 0.29 | 5000 |
| HD 131507 | 0.632 | 0.89 | 4750 | 2.0 | 0.0 | 29 | 4871 ± 370 | 2.0 ± 1.2 | 0.02 ± 0.45 | 4140 | 2.0 | −0.20 | 5000 |
| HD 144206 | 0.344 | 0.95 | 7500 | 4.0 | −2.0 | 27 | 7417 ± 240 | 3.9 ± 0.4 | −1.72 ± 0.59 | 11957 | 3.7 | −0.17 | 2000 |
| HD 175535 | 0.163 | 0.98 | 5500 | 3.0 | 0.0 | 38 | 5586 ± 395 | 3.3 ± 1.1 | 0.04 ± 0.36 | 5066 | 2.6 | −0.09 | 2000 |

in three cases (HD 218915, HD 220575 and HD 174350). The metallicity, when available, is in general in agreement but there are important discrepancies in the ⟨[M/H]⟩ obtained from both set-ups.

The $T_{eff}$ difference found in the hottest stars between our estimates and the values from the literature might come, on the one hand, from the lack of He I and He II lines in the HR-I spectral range and, on the other hand, from the less dense grid in the MUN05 models for the larger values of $T_{eff}$. In the particular case of Schulte 9, we also know that this star is an SB2-type binary (Nazé et al. 2012; Maíz-Apellániz et al. 2019).

Figs 9 and 10 show the observed spectra (in red) from the commissioning pilot programme for hot and cool stars, respectively. The name of each star and its spectral type are given in each panel. The $\chi^2_{min}$ fitted model is displayed as a green continuum line. The averaged spectrum is obtained from the MUN05 set, by selecting those models with the closest values to the averaged stellar parameters according to the likelihood criterion of $L \geq L_{max} - 0.01$. For example, if we obtain $\langle T_{eff}\rangle = 4300$ K, log $g = 2.6$ dex and ⟨[M/H]⟩ = –0.3 dex, we take the spectra corresponding to $T_{eff} = 4000$ and 4500 K, log $g = 2.5$ and 3.0 dex and ⟨[M/H]⟩ = –0.5 and 0.0 dex. With these eight models, and interpolating between each two among them, we obtain the spectrum corresponding to the averaged stellar parameters plotted as the blue dashed line. This method is the same as that used in next sections for the M15 and OT stars. Both models are almost indistinguishable. The bottom panel shows the residuals (the difference between the observed and theoretical spectra). Each panel also displays the stellar parameters derived from the literature (black, whenever available), the $\langle\chi^2\rangle$ model (blue) and the model with $\chi^2_{min}$ (green).

### *4.1.2 Stellar parameters for the M15 stars*

We have repeated the process described in the previous section for deriving the stellar parameters of the 56 stars obtained with MEGARA MOS within the central 12-arcsec region of the M15 cluster. We have not found any identification of these stars in the literature, or their stellar parameters, except for the global metallicity of the cluster, which is estimated between [Fe/H] ∼ −2.15 (McNamara, Harrison & Baumgardt 2004) and −2.30 (Sneden et al. 2000; Caretta et al. 2009). A detailed discussion on M15 abundance is presented in Sobeck et al. (2011).

Taking into account this M15 metallicity commonly agreed in the literature, we have restricted the possible MUN05 models to the three sets with the lowest value of [M/H] (–2.5, –2.0 and –1.0). We have done the fit of the models to the observed spectra in each of the two different set-ups, HR-R and HR-I, obtaining two sets of physical stellar parameters. Also, as described in Section 4.1 and also done for OT stars (Section 4.1.3), we have repeated the fit to a combined spectrum containing the two spectral ranges (HR-R and HR-I).

Table 8 summarizes the results (this table is given in electronic format but we show here some rows as an example). Column 1 displays the star number; column 2 shows the $\chi^2_{min}$ obtained from the fitting process of the observed normalized spectrum to the MUN05 theoretical catalogue; column 3 displays the associated maximum probability, $P_{max}$. Columns 4, 5 and 6 show the derived stellar parameters, $T_{eff}$, log $g$ and [M/H], from the MUN05 model corresponding to $\chi^2_{min}$. Column 7 gives the number of models, $N$, in the likelihood region $R_{\nu,\alpha}$. Columns 8, 9 and 10 give the mean stellar parameters: $\langle T_{eff}\rangle$, $\langle \log g\rangle$ and ⟨[M/H]⟩, with their corresponding errors, obtained as the averaged values from the set of $N$ models. The first five rows correspond to our results for HR-R; the next five rows give the results of the fitting to the HR-I spectra. Finally, the last five rows show the parameters when fitting the models to the combination of HR-R and HR-I observations into a single spectrum. In this case, as said before, there are no stellar parameters from the literature to compare with, except the average cluster abundance, which is found to be around [M/H] ∼ –2 dex. We analyse these results in Section 4.2.

Fig. 11 shows the observed spectra of six selected M15 stars (labelled Star-11, Star-24, Star-29, Star-46, Star-50 and Star-56).

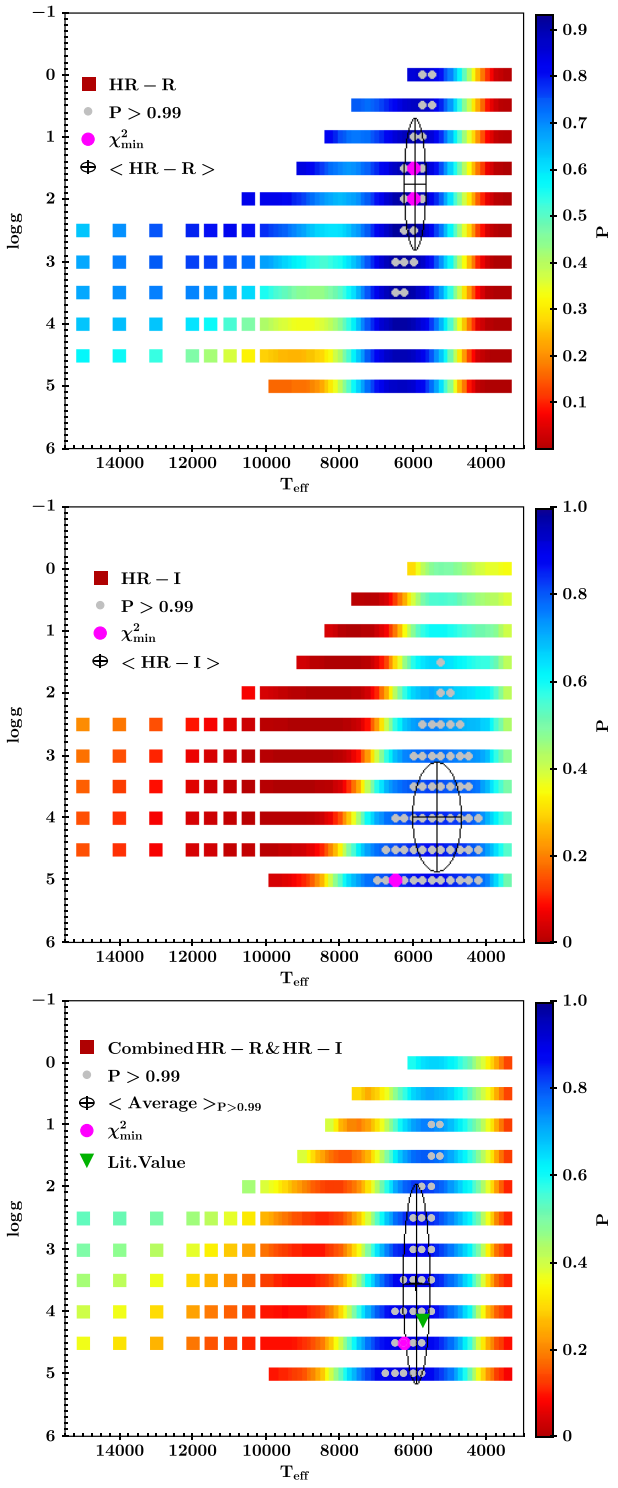


**Figure 7.** Probability maps of models (representing log $g$ on the $y$-axis and $T_{\rm eff}$ on the $x$-axis as in a Hertzsprung–Russell diagram) fitted to the observed spectrum in HR-R (top panel), HR-I (medium panel), and the combined HR-R and HR-I spectrum of the OT star BD+08 3095 (bottom panel). The colour scale indicates the probability $P$ obtained from the reduced $\chi^2_{\rm red} = \chi^2 - \chi^2_{\rm min}$, whose value gives the closeness to the $\chi^2_{\rm min}$ model. The selected models with $P \geq 0.99$ are represented with grey dots over-plotted on the blue region, and the large magenta dot is the model of $\chi^2_{\rm min}$ ($P = 1$). Over each diagram we have also plotted the averaged value, with its dispersion, using a large black cross and an ellipse. The green triangle in the bottom panel indicates the values given by the literature.

The first row of this figure shows the panels with HR-R spectra and their fitted models of the stars 11, 24 and 29, while the second row displays the corresponding HR-I spectra of stars whose HR-R spectrum are shown just above. The sequence is repeated with rows 3 (HR-R) and 4 (HR-I) for stars 46, 50 and 56. We have over-plotted the $\chi^2_{\rm min}$ model (displaying in green both the line fitting and the derived stellar parameters) and the average model (in blue). The fits represented in these figures are those to the combined spectra of HR-R and HR-I, with the two spectral windows in a single spectrum. The observed and fitted models for the 56 stars are given in Fig. A1 of Appendix A, which is in the supporting information online.

Fig. 12 displays the histograms of the stellar metallicity distribution for all 56 stars in our sample of M15 resulting from the fit of the models to HR-R (blue line) and HR-I (red line). We have over-plotted a Gaussian fit to the data of each set-up, obtaining mean abundance values of [M/H] $= -1.72 \pm 0.19$ dex and [M/H] $= -1.84 \pm 0.17$ dex, for HR-R and HR-I, respectively. We have also fitted the model to the combined spectrum of HR-R and HR-I for each star, obtaining [M/H] $= -1.66 \pm 0.16$ dex. The resulting abundance we derive for the 56 stars in the centre of the cluster is slightly higher than the average value for the whole cluster ([M/H] $= -2.15$ dex), claimed in previous published papers (Sobeck et al. 2011).

The purpose of including the M15 commissioning stars has been primarily to increase the number of stars in the sample analysed in this work. However, a complete analysis of M15 with these observations, and all the set-ups throughout the complete optical spectra range, is being carried out by the MEGARA commissioning team.

### *4.1.3 Stellar parameters for the 20 OT stars*

We have also applied our fitting method to the HR-R and HR-I spectra of the 20 OT stars in our MEGARA-GTC library sample. In this case, each star may have different stellar parameters (not for M15 stars, whose members are expected to share a common metallicity and age, implying close values of their physical parameters). As in the case of the COM stars, and as will be the case in all the stars of the MEGARA-GTC library, the stars from the OT subsample have reported estimates of the stellar parameters usually obtained from spectra with a wider spectral range and lower spectral resolution than MEGARA spectra. The observations in HR-R and HR-I, with much higher spectral resolution, can substantially change the results of the previous estimates.

Tables 9 and 10 summarize our results for these stars. In Table 9, the star name is given in column 1. Columns 2–10 contain the results for the fitting to HR-R spectra while columns 11–19 have the corresponding values when using the HR-I observed spectra. The value of $\chi^2_{\rm min}$ in columns 2 and 11, the corresponding maximum probability $P$ in columns 3 and 12, and the stellar parameters that correspond to the $\chi^2_{\rm min}$ model in columns 4, 5 and 6 (13, 14 and 15 for HR-I). Then, we have in column 7 the number of models $N$ with similar $\chi^2$ as $\chi^2_{\rm min}$, and the averaged values of stellar parameters obtained with these $N$ models in columns 8, 9 and 10, with their corresponding errors; and the equivalent parameters for HR-I fittings in columns 16, 17, 18 and 19. The stellar parameters from the literature are given in Table 6. Table 10 shows the values when fitting the models to the combined spectrum with the information of both HR-R and HR-I set-ups, as these spectra are two windows of a single spectrum. Again, the star name is given in column 1; columns 2–10 contain the results for the fitting to the

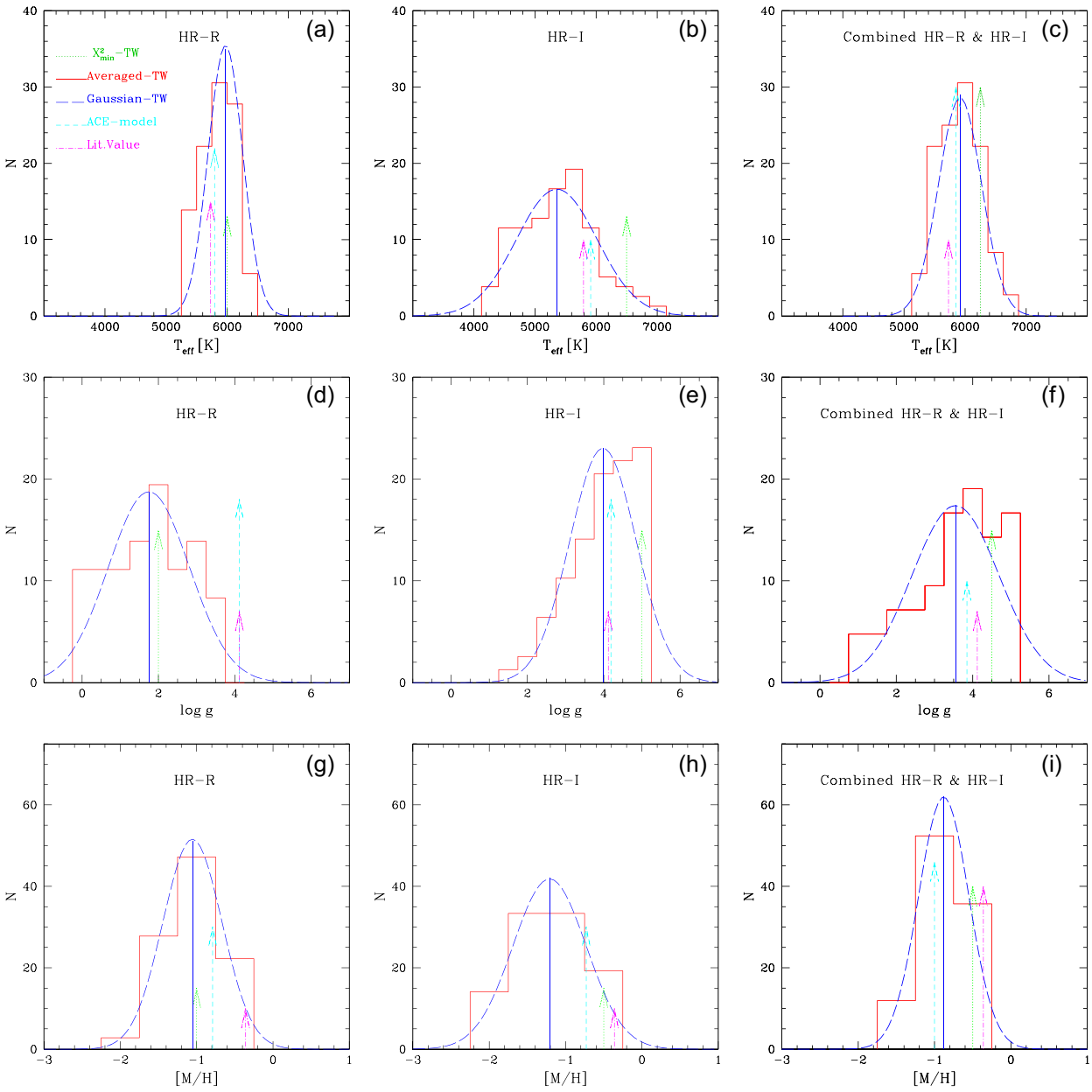


**Figure 8.** Histograms of $T_{\rm eff}$, $\log g$ and [M/H], in the top, middle and bottom panels, for the selected models ($P > 0.99$) fitted to HR-R (left panels), HR-I (centre panels) and both combined into a single spectrum (right panels) for star BD+08 3095. Over each histogram in red, we add a Gaussian as a blue dashed line, which gives the averaged value marked as a blue solid line. The value given by the $\chi^2_{\rm min}$ model is plotted with a green dotted arrow, the value from the literature is the magenta arrow and the cyan dashed arrow indicates the result obtained when applying the SP_ACE model to the observed spectrum.

combined spectra, corresponding to the parameters as labelled in the table; columns 11–13 repeat the physical parameters from the literature obtained with spectra of resolving power, $R$, shown in column 14.

Fig. 13 shows the fitting to the HR-R (upper panel) and to the HR-I (lower panel) observed spectra of three stars from the OT subsample. The fits represented in these figures are those to the combined spectra of HR-R and HR-I, with the two spectral windows in a single spectrum. We have repeated the analysis for the whole OT star subsample and the fittings are shown in Fig. B1 of Appendix B, in the supporting information online.

### 4.2 Analysis of the stellar parameter estimates

We have found physical parameters in the literature for some of the stars in our COM and OT subsamples. These parameters have been derived from spectra with lower resolution and wider wavelength range than our observations taken with MEGARA and HR-R/HR-I set-ups. We have, however, used these data to check the correlation between the stellar parameters derived from the literature and our estimates from the model fittings. The comparison presented in this section is between the previous published values and the values we obtain when fitting the models to the HR-I spectrum only (in the case of the COM subsample) and to the combined spectrum with

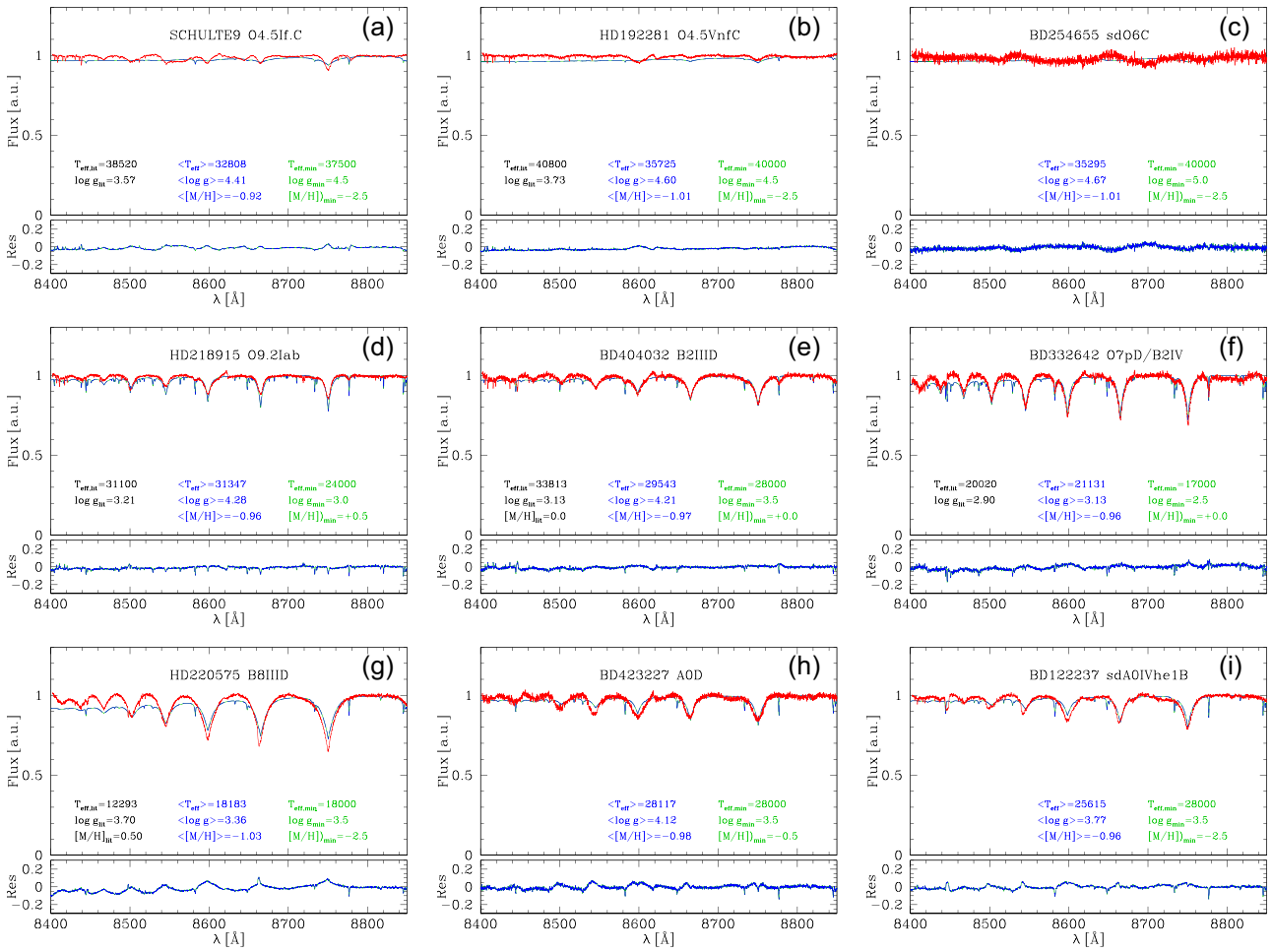


**Figure 9.** The observed spectrum of the commissioning hot stars with the best-fitting MUN05 models over-plotted. The top panel shows the observed spectrum (red solid line), the averaged fitted model (blue long-dashed line) and the $\chi^2_{\rm min}$ model (green short-dashed line). The bottom panel shows the residuals as $\rm Flux_{obs}$ – $\rm Flux_{mod}$ (blue and green lines as the corresponding fitted models).The stellar parameters derived from the literature (black, whenever available), from the averaged model (blue) and from the $\chi^2_{\rm min}$ model (green) are shown in each panel.

HR-R and HR-I, in the OT subsample. The wider the spectral range available for the fitting, the more reliable the values of the physical parameters, as discussed in Section 4.1star-par.

Fig. 14 shows the comparison between the stellar parameters found in this work after fitting the observed spectra (*y*-axis) with those obtained by previous works (*x*-axis). Open symbols represent the parameters of the $\chi^2_{\rm min}$ model and the solid synbols denote the averaged parameters from the models whose $\chi^2$ fulfils equation (4). We plot the results for the COM stars as blue triangles, and the OT stars as green dots. For COM stars, we have parameters from the fitting to HR-I spectra only, while for the OT stars, we have plotted the fit to the combined HR-R and HR-I spectra (i.e. using the complete spectral information; see values in Tables 7, 9and 10).

Fig. 14(a) shows our estimates of $T_{\rm eff}$ versus the values from the literature. When all points are used together, we obtained the minimum square straight line shown by the black solid line. This fit follows closely the 1 : 1 line within the error bars. The inset figure shows the same plot including the hottest stars, which reach 40 000 K, where there are only a certain number of COM stars. The blue line is the fit obtained only for these COM stars. The correlation between the averaged values of $\log g$ and the values from the literature (Fig. 14b) is in general quite good for the stellar parameters derived from the fitting to the observed spectra, with which we compute the black line fit. Finally, Fig. 14(c) shows that the metallicity derived from the models also follows a clear trend, showing values similar to the ones from the literature ($\rm [M/H]_{Lit}$), within the errors. Note that the theoretical catalogue (MUN05 in our case) provides a discrete sampling of $T_{\rm eff}$, $\log g$ and [M/H], which introduces an important source of uncertainty.

For example, $T_{\rm eff}$ reaches a maximum value of 47 500 K. In summary, the stellar parameters obtained from our fitting are in good agreement with the ones from the literature, and near the 1 : 1 line slope, better for the OT stars, in which the models have been fitted to a spectral range (combination of HR-R and HR-I) wider than the COM stars. We will extend this analysis with a statistically significant sample of the MEGARA-GTC library stars in Paper II.

### 4.3 Comparison with the SP_ACE model

In the literature, there are a certain number of methods (Heiter et al. 2015; Texeira et al. 2017; Jofré et al. 2019) to derive stellar physical parameters for different combinations of spectral range and resolution. Also, there are public codes, such as FERRE by Allende-Prieto et al. (2015) and SP_ACE (Stellar Parameters And Chemical Abundances Estimator) by Boeche & Grebel (2016), with which it is possible to compute the best fit among a set of models (complete

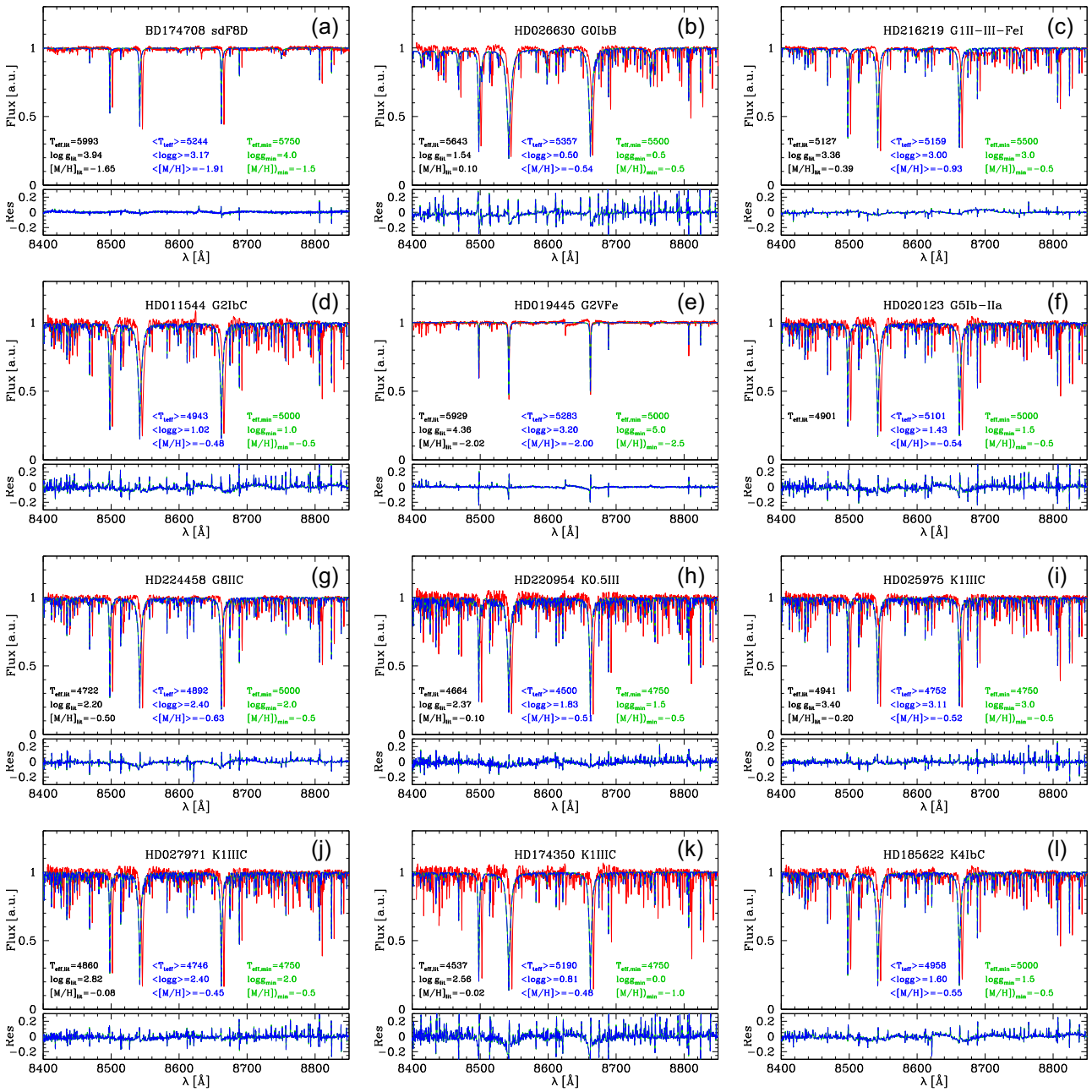


**Figure 10.** The observed spectra of the commissioning cool stars with the best-fitting MUN05 models over-plotted. The top panel shows the observed spectrum (red solid line), the averaged fitted model (blue long-dashed line) and the $\chi^2_{\rm min}$ model (green short-dashed line). The bottom panel shows the residuals as $\rm Flux_{obs}$ – $\rm Flux_{mod}$ (blue and green lines as the corresponding fitted models). The stellar parameters derived from the literature (black, whenever available), from the averaged model (blue) and from the $\chi^2_{\rm min}$ model (green) are shown in each panel.

spectra or equivalent-width line catalogues) that reproduces the observed data and, simultaneously, yields stellar parameters with good precision. In this subsection, we compare our derived stellar parameters with those obtained with the SP_ACE model whenever this code gives a solution.

We have compared our stellar parameter results with the estimates obtained with the SP_ACE code (Boeche & Grebel 2016). This model is available online (http://dc.g-vo.org/SP_ACE), offering a friendly graphical user interface, in which the input spectrum is introduced as a two-column table text file. The model is based on the generation of a library of the equivalent widths of 4363 absorption lines created as a function of the stellar parameters and abundances, and it can find the best fit of the spectra by applying a $\chi^2_{\rm min}$ technique. This code computes the estimated spectral parameters for spectra in the ranges 5212–6860 and 8400–8924 Å, with resolving power 2000–20 000, and is highly optimized for the fitting of FGK-type stars, which implies stars cooler than $T_{\rm eff} \leq 7000$ K.

We have used this code to compute the stellar spectra for all stars from the OT subsample. The code SP_ACE fails when trying to fit some spectra. We have obtained the parameters found from SP_ACE using the combined spectrum of HR-R and HR-I for the OT stars subsample, finding a solution for 13 of them.

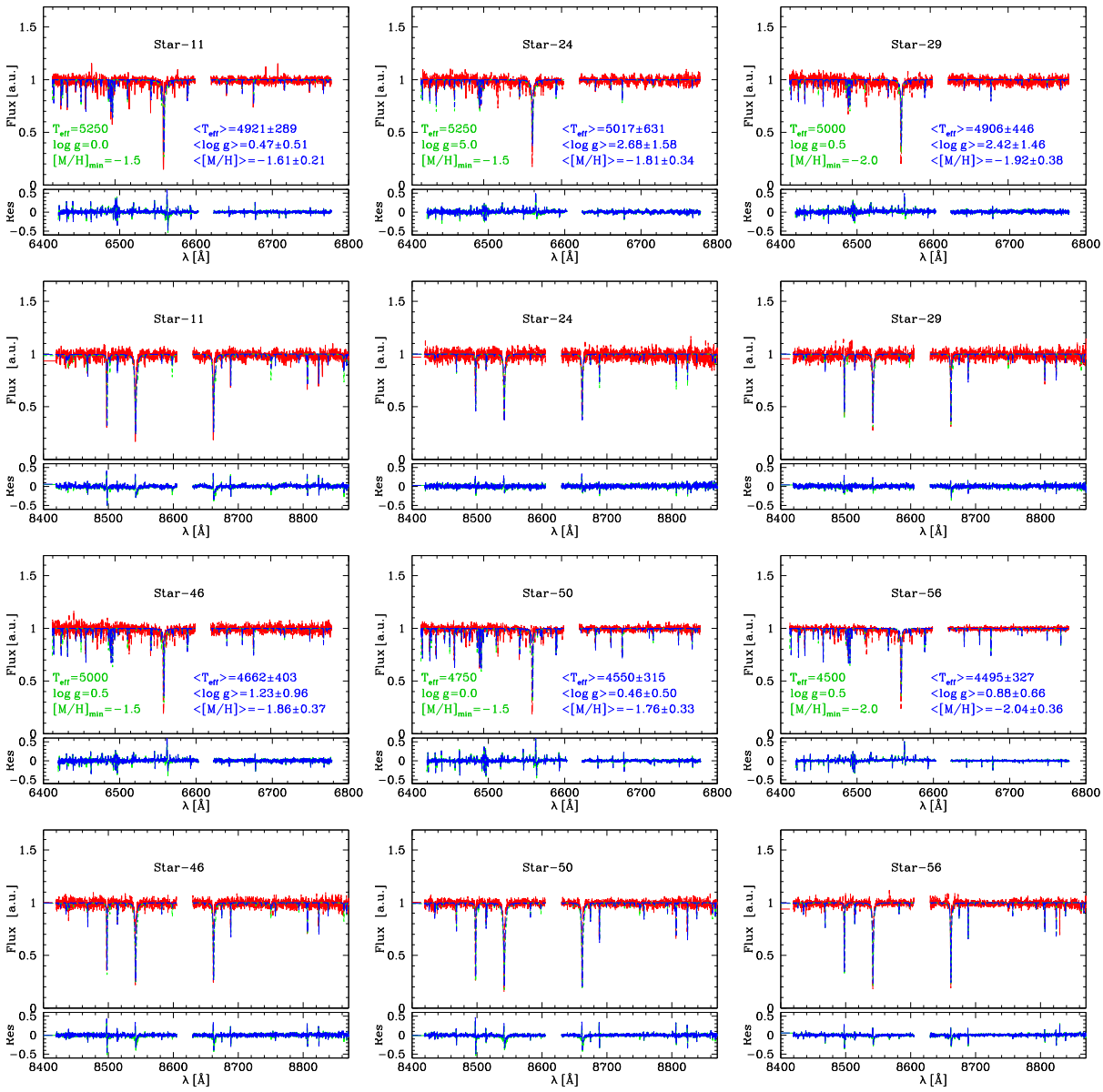


**Figure 11.** Six selected M15 stars, from the sample of 56, have been chosen to show the fitting results. The best-fitting MUN05 model is over-plotted to the observed spectrum for each star. The top panel of each star shows the observed spectrum (red solid line), the averaged fitted model (blue long-dashed line) and the $\chi^2_{\rm min}$ model (green short-dashed line). The bottom subpanel shows the residuals as $\rm Flux_{obs} - Flux_{mod}$ (blue and green lines as the corresponding fitted models). For each set of two rows, we present the spectra of three stars: in the top panel the HR-R spectrum of the star is shown and just below the corresponding HR-I spectrum. The stellar parameters from the average model (blue) and the $\chi^2_{\rm min}$ model (green) are shown in each panel. The spectra and their fitting results for the rest of the M15 stars are available online (Fig. A1 in Appendix A, which is in the supporting information online).

Fig. 15 shows the comparison of the averaged values obtained in this work ($y$-axis, and plotted as red circles) against the SP_ACE model results ($x$-axis) of (a) $\langle T_{\rm eff}\rangle$, (b) $\langle \log g\rangle$ and (c) $\langle$[M/H]$\rangle$. The stellar parameters existing in the literature are plotted as black squares. We find, in general, a good correlation. However, as explained throughout this paper, this sample is not statistically significant to derive conclusions, and does not cover the complete stellar parameter space.

As an example, to study the fitting, the determination of stellar parameters and the comparison of results, we have carefully studied the star BD+08 3095 (OT subsample), classified as GO V in the literature, and thus within the range of optimization of the SP_ACE code. We have not considered the correction from the star velocity profile.

Fig. 16 shows the detail of the observed spectrum in HR-R (Fig. 16a) and HR-I (Fig. 16b), around two strong absorption lines: H$\alpha$ in HR-R and the strongest line of the Ca II triplet in HR-I. These top panels represent the best fits separately for each set-up. In both panels, the MEGARA observed spectra are plotted as a red line. The best MUN05 models obtained when fitting to the spectrum of each individual set-up, HR-R in (a) and HR-I in (b), are shown as green long-dashed lines when applying our $\chi^2_{\rm min}$ method, and as blue short-dashed lines for our average model. The SP_ACE fits obtained for our spectra are shown as dashed orange lines. The MUN05

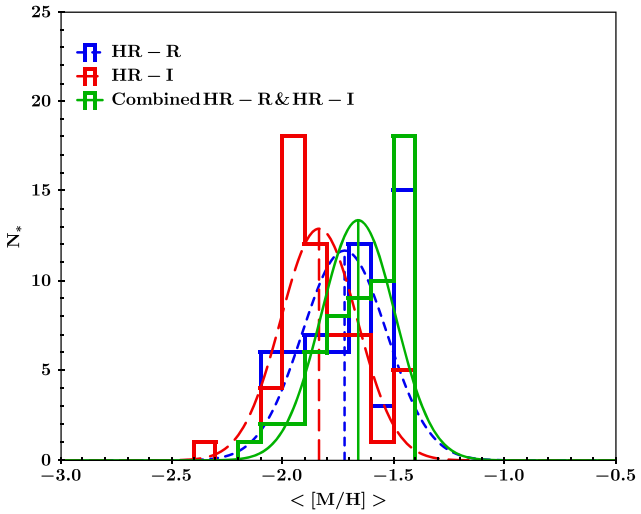


**Figure 12.** Distribution of averaged [M/H] obtained for the M15 stars after using the $\chi^2$ technique for all of them. The blue lines correspond to the HR-R results while the red lines are the fit to HR-I spectra. The green line represents the results for the fit to the combined spectrum with HR-R and HR-I. We have added a Gaussian fit for each set of data.

model corresponding to the stellar parameters resulting from the SP_ACE model is displayed as a dotted black line.

We see in Fig. 16(a) that both MUN05 models fitted with our method are quite deep and the fitting to the peak of the observed spectrum is good enough. Both models have a lower level of continuum out of the H$\alpha$ spectral window fitting this level well. The SP_ACE model model is, however, deeper and wider than the observations. The MUN05 model corresponding to the estimates of the SP_ACE is, in turn, less deep than the observed data. This outlines the fact that the MUN05 models corresponding to the stellar parameters derived from the SP_ACE code and ours are different, which is a result of the different fitting methods (SP_ACE is based on the equivalent width fitting while our method fits the entire continuum spectrum).

The problem for interpreting this plot comes from the difficulty of fitting simultaneously the depth and the width of the H$\alpha$ line. That is, if we use the SP_ACE stellar parameters and compare the corresponding spectra of MUN model, the H$\alpha$ profile is not well reproduced (at least in this example). Taking into account that the increase of the gravity reduces the depth of the line, it is difficult to understand how to create such a deep profile with a large value such as $\log g \sim 4$. In this example, our resulting spectrum, either because of our method or the models we have used, produces a better fit to the spectral lines, although the SP_ACE estimated stellar parameters have good agreement with those previously obtained in the literature.

Something similar occurs in Fig. 16(b) with the Ca II line. In this case, the SP_ACE model is deeper than the observed profile, as in Fig. 16(a), but it is also narrower. For this set-up, however, all the stellar parameters are in good agreement among them.

In the bottom panels, we represent the same fits best obtained using both HR-R and HR-I spectra in one only fit. In that case, the stellar parameters are the same in both windows (Figs 16c and d). In Fig. 16(c), we see that our fits (green or blue lines) are not deep enough compared with the observed spectrum, while the SP_ACE model is deeper than necessary. Moreover, the wings of the H$\alpha$ absorption feature are better fitted with our method, while the SP_ACE one has too wide a line. For Fig. 16(d), the whole spectrum is well fitted for all cases, except the depth of the three CaT absorption lines, which are very strong in the SP_ACE model.

Probable causes for the discrepancies found could be the different theoretical model set used in each case and the limitations of the models themselves. The SP_ACE library of equivalent widths can model many weak lines while MUN05 models are not as good for this purpose. Also, SP_ACE models are mostly limited by the adoption of LTE 1D atmosphere models, and by the microturbulence treatment and other minor effects discussed in detail elsewhere (Boeche & Grebel 2016). The high spectral resolution of MEGARA set-ups HR-R and HR-I allows us to obtain the information from the detailed absorption-line structure, which might be very important to study non-LTE effects and the impact on the kinematics of stellar populations composed of low-velocity dispersion; in order to understand these effects, it is crucial to have reliable models at this high resolution.

We will derive parameters for all the stars of the first release of the MEGARA-GTC library, expected in 2020, which will contain between 200 and 300 stars (see Paper II).

The purpose of determining the stellar parameters in this work was not a precise and absolute determination of these values, but the development of a fitting code that allows the classification of the MEGARA-GTC library stars and cluster members with a uniform criterion and based on the same MEGARA high-resolution data (HR-R and HR-I). The final goal is to find a reliable technique that can be used to assign stellar parameters in a homogeneous way to all the observed stars of the MEGARA-GTC library. Then, we can use these values to assign the right star to each point of the synthetic Hertzsprung–Russell diagrams when computing the isochrones in the next generation of high-resolution POPSTAR models.

### 4.4 HR-R spectra

We have identified the main absorption lines detected in the HR-R spectra of the observed stars. We have labelled the strongest lines in Fig. 17, left and right panels, for the stars HD 144206 (B0 III) and HD 147677 (K0 III), respectively, both belonging to the OT subsample. The HR-R hottest stars spectra are dominated by helium (He I 6678.15 and 6867.48 Å; He II 6560.10 Å) and hydrogen H$\alpha$ 6562.76 Å (6562.71, 6562.72, 6562.85 Å). For spectral types later than A, the range starts to be populated with metal lines from: Fe I (6430.85, 6469.19, 6475.62, 6481.87, 6495.74, 6496.47, 6498.94, 6518.37, 6533.93, 6546.24, 6574.23, 6581.21, 6591.31, 6592.91, 6593.87, 6597.54, 6608.02, 6609.11, 6627.54, 6633.41, 6633.75, 6703.57, 6710.32, 6713.74, 6716.24, 6725.36, 6750.15 and 6752.71 Å); Ca I (6439.08, 6449.81, 6455.60, 6471.66, 6493.78, 6499.65, 6508.85, 6572.78, 6717.68 and 6798.48 Å); Al I (6696.02 and 6698.67 Å); Si I (6721.85 and 6741.63 Å); Ti I (6497.68, 6554.22, 6599.10 and 6743.12 Å); Co I (6454.99 and 6771.03 Å); Ni I (6482.80, 6586.31, 6598.60, 6635.12, 6643.63, 6767.77 and 6772.31 Å); V I (6504.16 Å); Cr I (6537.92, 6630.01, 6537.92 and 6630.01 Å); Th I (6457.28, 6462.61, 6531.34 and 6989.65 Å); and single ionized lines such as Fe II (6516.08, 6432.68 and 6456.38 Å), Ti II (6491.57 Å), Sc II (6604.60 Å) and Mg II (6545.97 Å).

### 4.5 HR-I spectra

We have also identified the main spectral lines in the HR-I set-up that appear in the observed stars. Fig. 18 shows the spectra of a hot and a cool star (left and right panel, respectively) from the COM subsample.

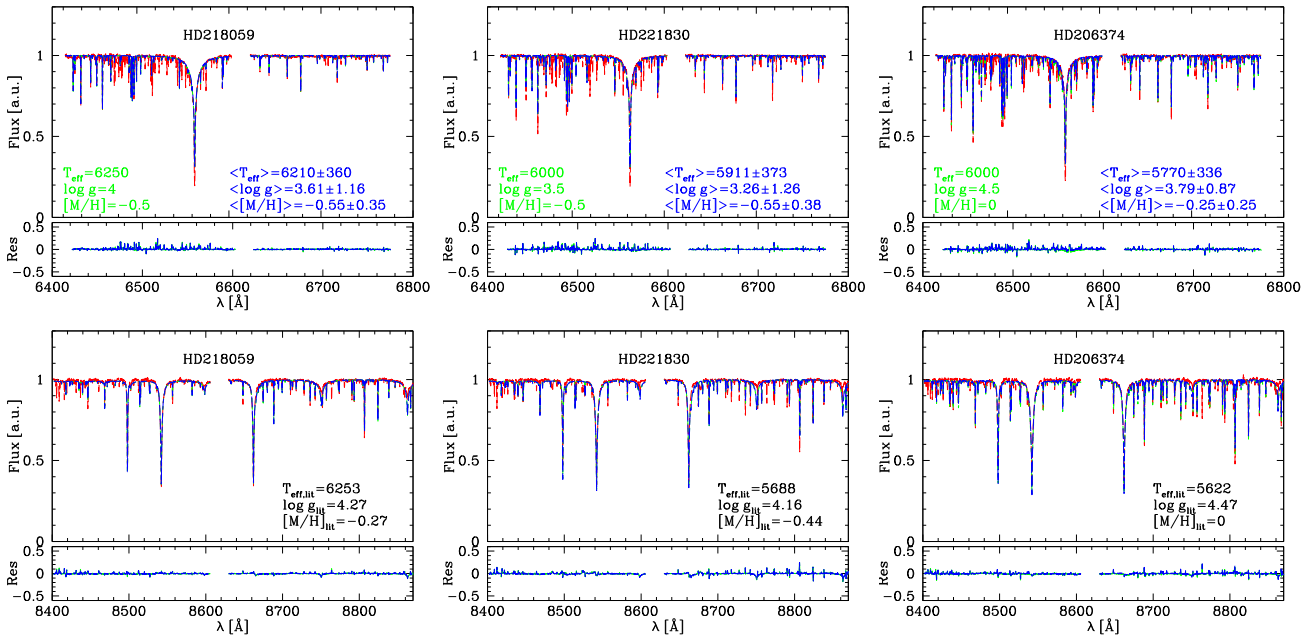


**Figure 13.** The best-fitting MUN05 model is over-plotted to each observed spectrum for three selected OT stars. The top panel of each star shows the observed spectrum (red solid line), the averaged fitted model (blue long-dashed line) and the minimum $\chi^2$ model (green short-dashed line). The corresponding bottom panel shows the residuals as $\mathrm{Flux_{obs}} - \mathrm{Flux_{mod}}$ (blue and green lines as the corresponding fitted models). Three spectra in HR-R are shown in the top row while the ones in HR-I are just below. The spectra and their fitting results for the rest of the OT stars are available online (Fig. B1 in Appendix B, in the supporting information online).

The observed COM hot stars shown in Fig. 2(a) show hydrogen (Paschen) and helium lines in the spectral-type sequence from O4 to A0. The Paschen series H I lines (Pa19 8413.33, Pa18 8437.96, Pa17 8467.27, Pa16 8502.50, Pa15 8545.39, Pa14 8598.40, Pa13 8665.03 and Pa 12 8750.47 Å) are clear and strong along the whole sequence, with maximum strength and width for giant B stars. The He I lines are identified at 8444 Å (3po–3d at 8444.44, 8444.46, 8444.65 Å), 8481 Å (3p0–3s at 8480.67, 8480.68, 8480.88 Å), 8518 Å (1S–1p0 at 8518.04 Å), 8531 Å (1d–1p0 at 8530.93 Å), 8532 Å (3d–3p0 at 8532.10, 8532.11, 8532.13 Å), 8583 Å (3p0–3d at 8582.51, 8582.52 Å), 8633 Å (3p0–3s at 8632.71, 8632.73, 8632.93 Å), 8777 Å (3p0–3d at 8776.65, 8776.67, 8776.88 Å) and 8849 Å (3p0–3s at 8849.16, 8849.37 Å).

The observed cool stars from the commissioning single-star subsample shown in Fig. 2(b) shows the Ca II and Mg I strong lines and a large number of Fe I, Th I, Ti I and Na I lines. The spectral-type sequence ranges from F8 to K4. The calcium triplet lines (Ca II 2d–2p0 at 8498.03, 8542.09, 8662.14 Å) are the most prominent ones of the spectra in all cool stars; followed in intensity by Mg I 1p0–1d 8806.76. Fe I lines are easily identified in the spectra at 8468.41, 8514.07, 8611.80, 8661.90, 8674.75, 8688.62, 8757.19, 8763.97, 8793.34, 8824.22 and 8838.43 Å. The strongest Th I lines can be detected at 8416.73, 8421.22, 8446.51, 8478.36, 8748.03 and 8758.24 Å. Ti I detected lines are at 8412.36, 8426.50, 8434.96, 8435.65 and 8675.37 Å. Finally, Na I lines are at 8649.93, 8650.90 and 8793.08 Å.

We have measured the indices of Ca II (Ca1, Ca2, Ca3), centred on the lines 8498.03, 8542.09 and 8662.14 Å respectively, and Pa (Pa1, Pa2, Pa3), centred on the series lines P17, P14 and P12, as defined by Cenarro et al. (2001a), using the same line and continuum windows in the MEGARA spectra. From these measurements, we have derived the composed index CaT = Ca1 + Ca2 + Ca3. We have measured this index on the 97 stars using their spectra normalized to the continuum.

For the CaT lines, we have redefined the windows of both continuum and lines to decontaminate the indices from the contribution of other metallic lines that become only apparent at the high spectral resolution of MEGARA HR-I. The new proposed continuum windows for Ca II lines are (wavelength in Å), for Ca1 and Ca2 lines, 8450.0–8460.0 (blue) and 8565.5–8575.0 (red), while for Ca3 we use 8619.5–8642.5 (blue) and 8700.5–8710.0 (red). The feature windows are 8482.0–8512.0 (Ca1), 8531.0–8554.0 (Ca2) and 8650.0–8673.0 (Ca3).

Table 11 summarizes the measurement of Ca II line equivalent widths (in Å) using Cenarro et al. (2001a) windows and the new windows defined in this paper, for the 21 COM stars and the 20 OT stars. This table also includes the Mg I and sTiO indices as defined in Cenarro et al. (2009), for which we have kept the same spectral windows. Table 12 has the same information as Table 11 but for the subsample of M15 stars.

The columns in Tables 11 and 12 are as follows: the first column identifies the star; column 2 gives the continuum S/N averaged over the whole spectrum as defined by Stoehr et al. (2008); columns 3–5 are the equivalent widths (in Å) of the three Ca II lines as defined by Cenarro et al. (2001a); column 6 is the Mg I equivalent width (Å); columns 7–9 are the equivalent widths of the Pa lines; columns 10–12 are the equivalent widths (in Å) of the three Ca II lines with the windows redefined in this work. The last column is the sTiO colour, as defined by Cenarro et al. (2009). All the values include the random errors due to continuum and are related to the spectra S/N. These errors are below 3 per cent in all cases (S/N $\geq$ 100).

The results of all measurements and the conclusions will be included in Paper II with a statistically significant sample and stars within a wide range of physical stellar parameters.

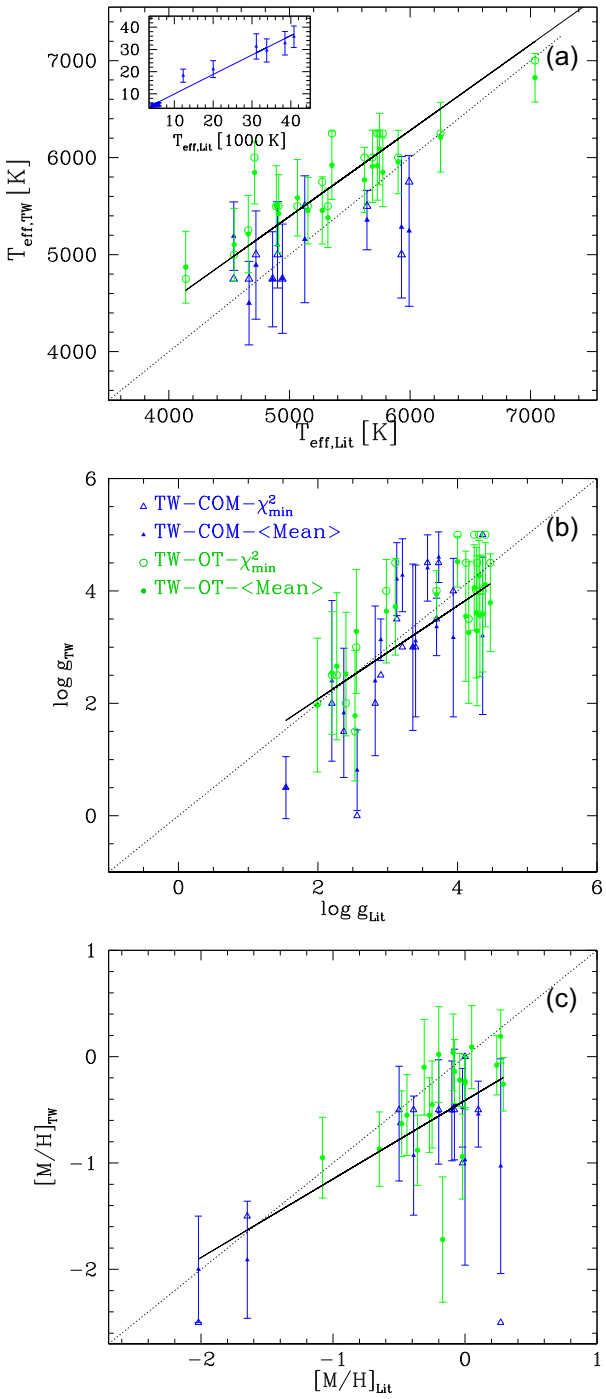


**Figure 14.** Values of $T_{\rm eff}$, $\log g$ and [M/H] resulting from our fitting compared with those from the literature for COM and OT stars. Open symbols correspond to the $\chi^2_{\rm min}$ parameters, while the solid dots with error bars refer to the averaged values; blue triangles and green dots correspond to COM and OT stars, respectively. The minimum square straight line in black is set for the whole set of points. The dotted identity line is in all panels.

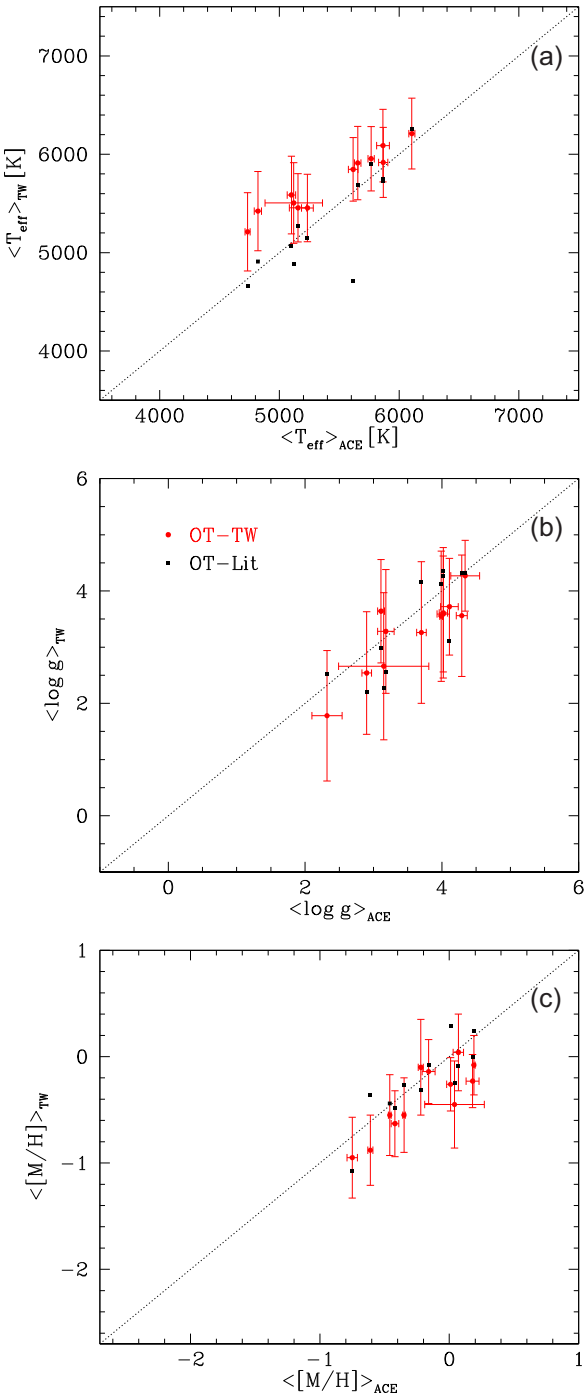


**Figure 15.** Comparison of the stellar parameters estimated in this work for the OT stars subsample (red circles) with the results from the SP_ACE code: (a) $\langle T_{\rm eff}\rangle$; (b) $\langle \log g\rangle$; (c) $\langle$[M/H]$\rangle$. Black filled squares are the estimates given in the literature.

Fig. 19 plots on the *y*-axis the values of the redefined CaT index in this work, CaT(TW), against the results (*x*-axis) when measuring the index with Cenarro et al. (2001a) windows, CaT(CEN), for all 97 stars. The dashed line represents the 1 : 1 relation, while the solid line is the actual fitting to the observations, showing values of the new CaT index slightly lower than the ones measured with CaT(CEN). This is particularly noticeable for the largest index values obtained in giant and supergiant stars. The reason is the contamination of the CaT(CEN) index with other metallic lines that do not fall in the line window defined in the new (high-resolution) index.

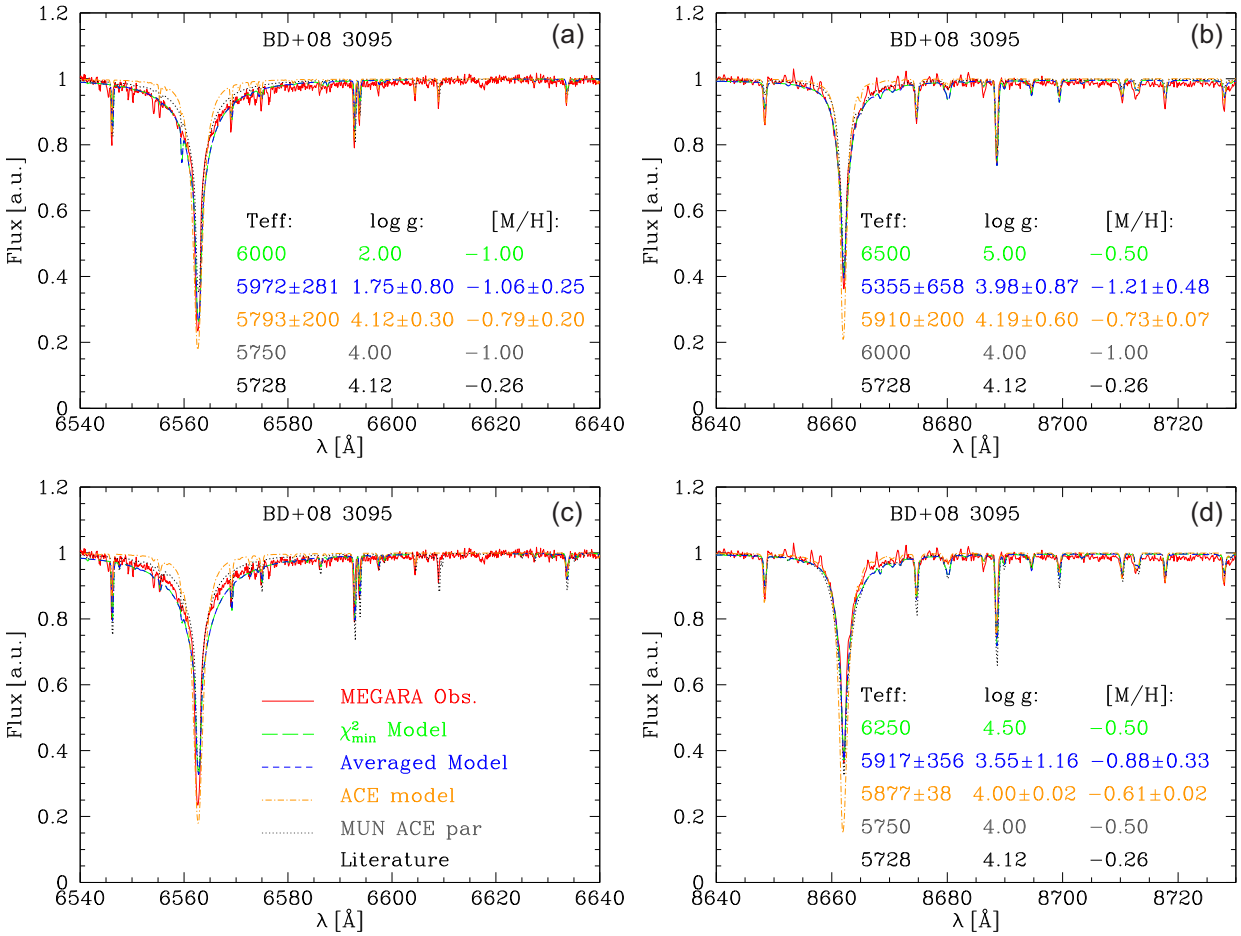


**Figure 16.** The spectra for the OT star BD+08 3095 (red line) in HR-R (panels a and c) and in HR-I (panels b and d), compared with our best models obtained with the $\chi^2_{\rm min}$ (green long-dashed line) and the averaged (blue short-dashed line) models, and with the spectrum fitting using the SP_ACE model (orange dot-dashed line). The dotted black line is the MUNARI model for the closest stellar parameters to the SP_ACE model estimates. Top panels represent the best fits obtained separately for each set-up, while the bottom panels represent the best fit obtained simultaneously with both HR-R and HR-I spectra.

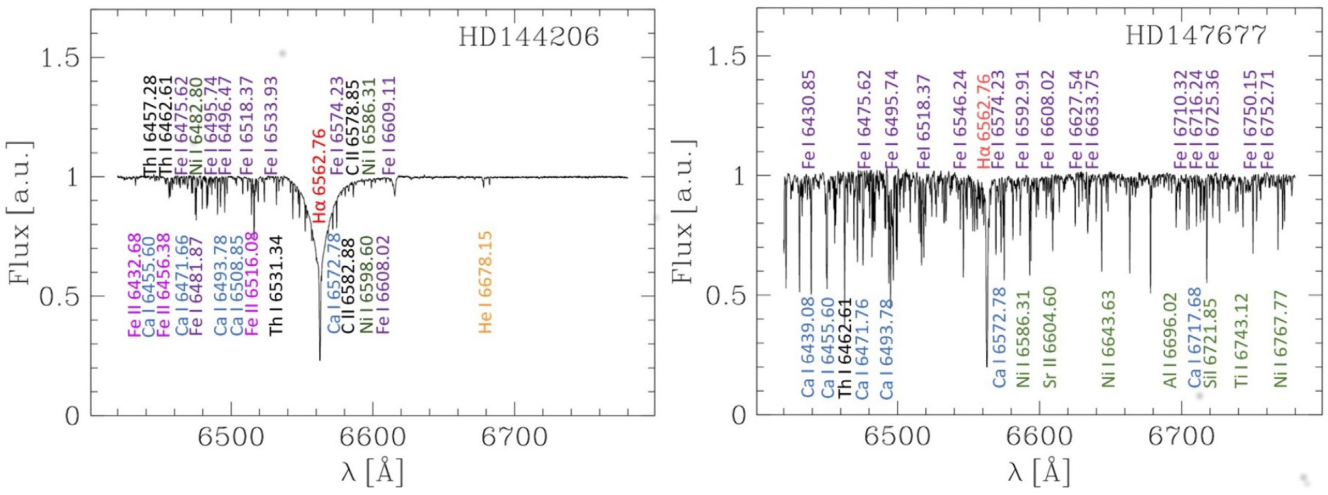


**Figure 17.** Left panel: spectrum of HD 144206 (B0 III) with the identification of the strongest spectral lines. Right panel: spectrum of HD 147677 (K0 III) with the identification of a representative number of lines.

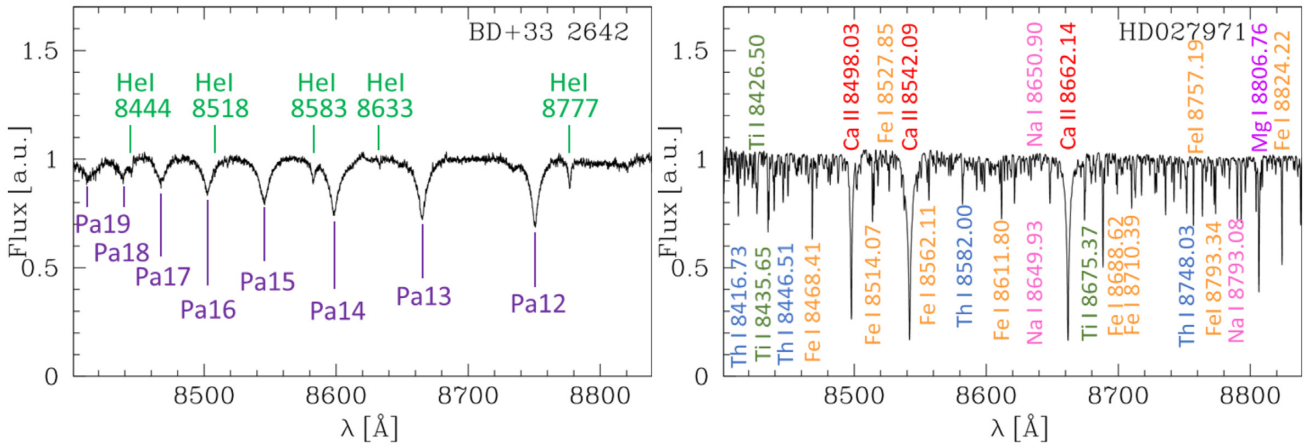


**Figure 18.** Left panel: spectrum of the hot star BD+33 2642 (O7pD) and spectral lines identified. Pa series and He I lines are clearly identified. Right panel: spectrum of the cool star HD 027971 (K1 III). The strongest lines of Ca II, Fe I, Th I and Ti I are identified.

## 5 MEGARA-GTC LIBRARY DATA BASE

The goals of the MEGARA-GTC stellar library are to compile input spectra for POPSTAR models and to produce a useful, public and accessible data base of fully reduced and calibrated star spectra for other MEGARA users. Handling the data for several thousands of stars and their GTC observations in different set-ups, which have to be prepared for execution, and be reduced and analysed, requires a specific software tool. We have developed a data base in MySQL with all library data and a web-based tool that allows the management of stellar parameters and observed spectra. There are several permission levels, allowing different actions on the data base, from manipulating and updating both the library and the observations, to just making queries and retrieving reduced spectra.

The data base also supports the MEGARA-GTC library team for preparing and uploading the OBs to the GTC-Phase 2 tool. To prepare a new OB set, we search for unobserved stars in the MEGARA-GTC library filtered by a certain magnitude range in both *R* and *I* bands and/or by spectral type, considering that all stars within that group and for a given set-up will have a similar S/N when choosing the appropriate exposure time in each set-up. The tool has the capability of exporting a file suited to the GTC-Phase 2 format. Because of the GTC Phase-2 flexibility for changing, adding or removing OBs, we use the data base functionality to make decisions on the queued observations, tuning the priorities to guarantee a good coverage of the stellar parameters.

Fig. 20 shows some views of the graphical user interface. The *Source* form functionality allows authorized users to upload, change and delete library stars and/or their properties, while the *Observation* menu includes the functions of listing, searching, modifying, deleting, uploading and retrieving fully reduced library spectra obtained with MEGARA at the GTC. The tool also includes a *Statistics* menu with information on the observations distribution as a function of the physical stellar parameters and MEGARA set-ups, and a *Download* Menu for getting the released observations. A complete description of the tool will be given in Paper II. The MEGARA-GTC stellar library data base and the web-based tools can be found at https://www.fractal-es.com/megaragtc-stellarlibrary/.

## 6 CONCLUSIONS

MEGARA, an instrument at the GTC 10-m telescope facility, is a fibre-fed spectrograph with medium-high spectral resolution ($R$ = 6000, 12 000, 20 000), covering the range 3650–9750 Å. The instrument was successfully commissioned at the Observatorio del Roque de los Muchachos (La Palma, Spain) in the summer of 2017 and has been in operation since 2018 July. In this paper, we have introduced the MEGARA-GTC spectral library, an empirical star catalogue whose spectra shall be used as the seed of the new generation of POPSTAR models for interpretation of the contribution of the stellar populations in a wide range of MEGARA observations with the same instrument configuration. The maximum priority has been given to the HR-R and HR-I set-ups, centred, in rest frame, at H$\alpha$ and the brightest line of the Ca II triplet, respectively.

We have presented a first sample of 97 stars. We observed 21 of these in the HR-I set-up during the MEGARA commissioning as a pilot programme to demonstrate the feasibility of the MEGARA-GTC library project, 56 stars at both HR-R and HR-I at the centre of the M15 cluster and 20 stars, also in HR-R and HR-I, obtained from our ongoing GTC filler OT programme.

For all these 97 stars, we have derived the stellar parameters: effective temperature $T_{\rm eff}$, surface gravity $\log g$ and metallicity [M/H]. To obtain them, we have developed a code that uses a $\chi^2$ technique to fit the theoretical modelled spectra of MUN05 to the high-resolution MEGARA observations, both normalized to their respective continuum. The best results are found when using the complete information in both HR-R and HR-I spectral windows, combining them in a single spectrum to which the model is compared. This allows us to use all the spectral information. We have used this combined spectrum to derive the stellar parameters. We have compared our results with the parameters published in the literature, when available, and with the ones obtained when using the SP_ACE code (when offering a solution). In general, we find very good agreement in the values derived for $T_{\rm eff}$, $\log g$ and [M/H] from all these different methods and sources, within the error bars and the intrinsic model limitations, whose grid's density puts a limit on the errors of the derived stellar parameters. The quality of our method is probed in this sample of observations, and we will apply it to the MEGARA-GTC library, sampling a wider range of stellar parameters.

**Table 11.** Equivalent widths of the Ca II, Mg I and Pa lines, in Å, as defined by Cenarro et al. (2001a) and sTiO colour defined by Cenarro et al. (2009) for the subsample of 21 COM stars observed in HR-I and the 20 stars of the OT subsample. See the text for a description of the table.

| Star name | S/N | Ca1CEN | Ca2CEN | Ca3CEN | Mg I | Pa1 | Pa2 | Pa3 | Ca1MEG | Ca2MEG | Ca3MEG | sTiO |
|---|---|---|---|---|---|---|---|---|---|---|---|---|
| Schulte 9 | 548 | −0.181 ± 0.006 | −0.030 ± 0.002 | −0.109 ± 0.003 | +0.089 ± 0.002 | −0.177 ± 0.003 | −0.214 ± 0.003 | −0.720 ± 0.005 | −0.024 ± 0.002 | −0.038 ± 0.005 | −0.123 ± 0.002 | +0.635 |
| HD 192281 | 280 | −0.104 ± 0.011 | −0.037 ± 0.008 | +0.161 ± 0.045 | −0.245 ± 0.000 | −0.070 ± 0.009 | −0.848 ± 0.010 | +0.289 ± 0.038 | −0.015 ± 0.005 | −0.020 ± 0.007 | −0.060 ± 0.006 | +0.636 |
| BD+25 4655 | 71 | −0.159 ± 0.047 | +0.444 ± 0.045 | +0.201 ± 0.116 | +0.052 ± 0.017 | +0.014 ± 0.023 | +0.244 ± 0.042 | +0.025 ± 0.001 | −0.034 ± 0.000 | +0.465 ± 0.040 | +0.285 ± 0.035 | +0.626 |
| BD+33 2642 | 105 | −1.360 ± 0.026 | −1.911 ± 0.032 | −1.580 ± 0.023 | +0.112 ± 0.745 | −0.871 ± 0.015 | −2.150 ± 0.030 | −1.893 ± 0.029 | −1.284 ± 0.028 | −1.843 ± 0.024 | −1.810 ± 0.020 | +0.634 |
| HD 218915 | 256 | −0.735 ± 0.012 | −0.897 ± 0.014 | −0.908 ± 0.010 | −0.011 ± 0.006 | −0.235 ± 0.007 | −1.884 ± 0.012 | −1.150 ± 0.013 | −0.645 ± 0.012 | −0.729 ± 0.011 | −0.930 ± 0.009 | +0.633 |
| BD+40 4032 | 146 | −0.507 ± 0.020 | −1.039 ± 0.023 | −1.942 ± 0.019 | +0.046 ± 0.009 | −0.192 ± 0.012 | −1.841 ± 0.021 | −1.959 ± 0.024 | −0.578 ± 0.021 | −1.015 ± 0.019 | −1.686 ± 0.015 | +0.630 |
| HD 220575 | 232 | −1.725 ± 0.012 | −2.544 ± 0.013 | −5.451 ± 0.011 | −0.123 ± 0.001 | −0.659 ± 0.007 | −4.529 ± 0.012 | −5.208 ± 0.013 | −1.711 ± 0.013 | −2.377 ± 0.011 | −4.377 ± 0.008 | +0.624 |
| BD+42 3227 | 111 | −1.170 ± 0.025 | −1.264 ± 0.028 | −1.230 ± 0.020 | −0.106 ± 0.011 | −0.238 ± 0.020 | −2.001 ± 0.025 | −1.209 ± 0.023 | −1.221 ± 0.026 | −1.419 ± 0.023 | −1.378 ± 0.018 | +0.630 |
| BD+12 237 | 171 | −0.693 ± 0.016 | −1.144 ± 0.019 | −1.370 ± 0.017 | +0.007 ± 0.005 | −0.360 ± 0.011 | −2.039 ± 0.017 | −2.362 ± 0.018 | −0.737 ± 0.018 | −1.210 ± 0.015 | −1.281 ± 0.012 | +0.623 |
| BD+17 4708 | 172 | −0.492 ± 0.022 | −0.909 ± 0.019 | −0.852 ± 0.019 | −0.131 ± 0.007 | −0.061 ± 0.011 | −0.092 ± 0.018 | −0.190 ± 0.018 | −0.548 ± 0.026 | −0.991 ± 0.017 | −0.789 ± 0.014 | +0.625 |
| HD 026630 | 235 | −2.371 ± 0.016 | −6.029 ± 0.016 | −4.285 ± 0.014 | −0.512 ± 0.006 | −0.357 ± 0.010 | −1.198 ± 0.013 | −0.545 ± 0.017 | −2.526 ± 0.019 | −5.417 ± 0.010 | −3.795 ± 0.010 | +0.638 |
| HD 216219 | 346 | −1.154 ± 0.011 | −2.625 ± 0.011 | −1.945 ± 0.009 | −0.282 ± 0.004 | −0.150 ± 0.006 | −0.342 ± 0.008 | −0.254 ± 0.011 | −1.125 ± 0.011 | −2.457 ± 0.008 | −1.749 ± 0.007 | +0.632 |
| HD 011544 | 147 | −2.070 ± 0.021 | −4.754 ± 0.022 | −3.697 ± 0.022 | −0.698 ± 0.012 | −0.385 ± 0.015 | +0.051 ± 0.015 | −0.683 ± 0.026 | −2.409 ± 0.027 | −4.747 ± 0.016 | −3.218 ± 0.015 | +0.616 |
| HD 019445 | 227 | −0.246 ± 0.010 | −0.819 ± 0.017 | −0.292 ± 0.007 | −0.131 ± 0.006 | −0.007 ± 0.001 | +0.150 ± 0.160 | +0.025 ± 0.006 | −0.339 ± 0.016 | −0.861 ± 0.014 | −0.353 ± 0.007 | +0.624 |
| HD 020123 | 134 | −1.345 ± 0.020 | −3.418 ± 0.023 | −2.002 ± 0.017 | −0.457 ± 0.010 | −0.122 ± 0.008 | +0.071 ± 0.010 | −0.017 ± 0.002 | −1.751 ± 0.028 | −3.506 ± 0.018 | −1.765 ± 0.013 | +0.615 |
| HD 224458 | 225 | −1.286 ± 0.015 | −2.760 ± 0.016 | −2.335 ± 0.015 | −0.613 ± 0.007 | −0.286 ± 0.010 | −0.407 ± 0.015 | −0.177 ± 0.022 | −1.215 ± 0.015 | −2.669 ± 0.012 | −2.126 ± 0.011 | +0.627 |
| HD 220954 | 66 | −1.276 ± 0.044 | −4.290 ± 0.062 | −2.600 ± 0.049 | −0.734 ± 0.026 | −0.116 ± 0.014 | −1.539 ± 0.046 | −0.259 ± 0.049 | −1.123 ± 0.042 | −3.494 ± 0.040 | −2.559 ± 0.038 | +0.619 |
| HD 025975 | 110 | −1.205 ± 0.029 | −3.980 ± 0.038 | −2.590 ± 0.033 | −0.664 ± 0.014 | −0.149 ± 0.013 | −0.448 ± 0.029 | +0.042 ± 0.019 | −1.168 ± 0.031 | −3.384 ± 0.027 | −2.284 ± 0.023 | +0.634 |
| HD 027971 | 88 | −1.519 ± 0.041 | −4.050 ± 0.044 | −3.074 ± 0.042 | −0.657 ± 0.019 | −0.277 ± 0.025 | −0.457 ± 0.038 | −0.722 ± 0.040 | −1.533 ± 0.044 | −3.674 ± 0.031 | −2.768 ± 0.031 | +0.618 |
| HD 174350 | 75 | −1.543 ± 0.042 | −2.959 ± 0.046 | −1.497 ± 0.027 | −0.549 ± 0.019 | +0.244 ± 0.029 | −0.298 ± 0.151 | +1.065 ± 0.335 | −2.533 ± 0.071 | −2.991 ± 0.036 | −1.895 ± 0.027 | +0.632 |
| HD 185622 | 136 | −1.656 ± 0.022 | −2.497 ± 0.018 | −1.394 ± 0.013 | −0.204 ± 0.005 | +0.161 ± 0.011 | +0.400 ± 0.054 | +1.480 ± 0.027 | −2.857 ± 0.037 | −3.536 ± 0.019 | −1.631 ± 0.012 | +0.623 |
| HD 100696 | 212 | −0.878 ± 0.012 | −2.598 ± 0.016 | −2.321 ± 0.016 | −0.477 ± 0.007 | −0.444 ± 0.009 | −0.625 ± 0.017 | −0.670 ± 0.016 | −0.477 ± 0.008 | −2.691 ± 0.013 | −2.351 ± 0.012 | +0.645 |
| HD 101107 | 690 | −1.090 ± 0.005 | −2.332 ± 0.005 | −2.633 ± 0.005 | −0.395 ± 0.002 | −0.378 ± 0.003 | −1.048 ± 0.005 | −1.780 ± 0.005 | −0.760 ± 0.004 | −2.260 ± 0.004 | −2.439 ± 0.003 | +0.636 |
| HD 104985 | 104 | −0.899 ± 0.024 | −2.692 ± 0.032 | −2.402 ± 0.030 | −0.618 ± 0.015 | −0.431 ± 0.035 | −0.602 ± 0.036 | −0.706 ± 0.035 | −0.467 ± 0.014 | −2.798 ± 0.027 | −2.399 ± 0.025 | +0.645 |
| HD 113002 | 174 | −0.853 ± 0.018 | −2.147 ± 0.020 | −1.854 ± 0.018 | −0.280 ± 0.008 | −0.374 ± 0.027 | −0.489 ± 0.112 | −0.641 ± 0.020 | −0.537 ± 0.013 | −2.285 ± 0.017 | −1.916 ± 0.015 | +0.642 |
| HD 115136 | 59 | −0.910 ± 0.038 | −3.004 ± 0.058 | −2.670 ± 0.055 | −0.725 ± 0.026 | −0.488 ± 0.026 | −0.760 ± 0.082 | −0.810 ± 0.067 | −0.364 ± 0.018 | −2.979 ± 0.045 | −2.621 ± 0.045 | +0.647 |
| HD 117243 | 138 | −1.052 ± 0.023 | −2.732 ± 0.025 | −2.502 ± 0.026 | −0.587 ± 0.012 | −0.382 ± 0.014 | −0.610 ± 0.029 | −0.828 ± 0.023 | −0.770 ± 0.019 | −2.824 ± 0.020 | −2.467 ± 0.018 | +0.642 |
| HD 131111 | 130 | −0.837 ± 0.020 | −2.573 ± 0.028 | −2.307 ± 0.028 | −0.528 ± 0.012 | −0.417 ± 0.031 | −0.634 ± 0.028 | −0.649 ± 0.029 | −0.390 ± 0.011 | −2.561 ± 0.022 | −2.291 ± 0.021 | +0.644 |
| HD 131507 | 65 | −0.928 ± 0.033 | −3.133 ± 0.051 | −2.677 ± 0.049 | −0.705 ± 0.024 | −0.565 ± 0.025 | −0.726 ± 0.034 | −0.829 ± 0.185 | −0.249 ± 0.010 | −3.218 ± 0.041 | −2.702 ± 0.040 | +0.651 |
| HD 144206 | 378 | −1.929 ± 0.007 | −2.877 ± 0.009 | −4.991 ± 0.006 | −0.597 ± 0.002 | −0.686 ± 0.005 | −3.042 ± 0.008 | −4.855 ± 0.008 | −1.643 ± 0.008 | −2.509 ± 0.006 | −4.241 ± 0.005 | +0.619 |
| HD 147677 | 109 | −0.241 ± 0.010 | −2.376 ± 0.044 | −1.932 ± 0.032 | −0.297 ± 0.014 | −0.143 ± 0.014 | −0.294 ± 0.085 | −0.462 ± 0.034 | +0.926 ± 0.054 | −1.376 ± 0.022 | −1.900 ± 0.024 | +0.643 |
| HD 174912 | 210 | −0.856 ± 0.016 | −2.159 ± 0.017 | −2.092 ± 0.016 | −0.253 ± 0.007 | −0.260 ± 0.021 | −0.583 ± 0.027 | −1.161 ± 0.016 | −0.551 ± 0.012 | −2.226 ± 0.014 | −2.013 ± 0.011 | +0.639 |
| HD 175535 | 110 | −1.046 ± 0.024 | −2.964 ± 0.031 | −2.638 ± 0.031 | −0.520 ± 0.015 | −0.476 ± 0.015 | −0.719 ± 0.045 | −0.811 ± 0.030 | −0.625 ± 0.017 | −3.034 ± 0.025 | −2.617 ± 0.024 | +0.647 |
| HD 200580 | 232 | −0.611 ± 0.012 | −1.960 ± 0.016 | −1.804 ± 0.014 | −0.328 ± 0.007 | −0.265 ± 0.019 | −0.384 ± 0.013 | −0.693 ± 0.014 | −0.141 ± 0.003 | −1.881 ± 0.013 | −1.786 ± 0.012 | +0.637 |
| HD 206374 | 164 | −0.838 ± 0.016 | −2.503 ± 0.021 | −2.272 ± 0.020 | −0.589 ± 0.010 | −0.315 ± 0.022 | −0.182 ± 0.035 | −0.493 ± 0.019 | −0.760 ± 0.015 | −2.667 ± 0.016 | −2.214 ± 0.016 | +0.643 |
| HD 220182 | 145 | −0.782 ± 0.017 | −2.704 ± 0.022 | −2.241 ± 0.022 | −0.617 ± 0.010 | −0.438 ± 0.025 | −0.716 ± 0.031 | −0.777 ± 0.026 | −0.340 ± 0.009 | −2.662 ± 0.018 | −2.212 ± 0.016 | +0.641 |
| HD 211472 | 144 | −0.612 ± 0.014 | −2.508 ± 0.024 | −2.123 ± 0.020 | −0.706 ± 0.010 | −0.381 ± 0.021 | −0.324 ± 0.052 | −0.692 ± 0.027 | −0.278 ± 0.007 | −2.521 ± 0.017 | −2.146 ± 0.016 | +0.640 |
| HD 218059 | 201 | −0.851 ± 0.018 | −2.143 ± 0.020 | −2.055 ± 0.018 | −0.342 ± 0.008 | −0.286 ± 0.009 | −0.565 ± 0.000 | −0.848 ± 0.017 | −0.560 ± 0.013 | −2.190 ± 0.015 | −2.057 ± 0.015 | +0.639 |
| HD 221585 | 100 | −1.237 ± 0.036 | −3.152 ± 0.033 | −1.940 ± 0.033 | −0.388 ± 0.013 | −0.417 ± 0.018 | −0.307 ± 0.034 | +1.130 ± 0.052 | −0.749 ± 0.025 | −3.132 ± 0.026 | −2.023 ± 0.025 | +0.675 |
| HD 221830 | 220 | −1.367 ± 0.021 | −2.415 ± 0.017 | −2.341 ± 0.018 | −0.377 ± 0.006 | −0.243 ± 0.018 | −0.179 ± 0.012 | −0.545 ± 0.013 | −1.542 ± 0.026 | −2.553 ± 0.013 | −2.035 ± 0.012 | +0.648 |
| BD+08 3095 | 124 | −0.697 ± 0.026 | −1.740 ± 0.028 | −1.679 ± 0.028 | −0.327 ± 0.013 | −0.243 ± 0.015 | −0.429 ± 0.025 | −0.582 ± 0.027 | −0.459 ± 0.021 | −1.865 ± 0.025 | −1.725 ± 0.023 | +0.637 |

**Table 12.** Equivalent widths of the Ca II, Mg I and Pa lines, in Å, as defined by Cenarro et al. (2001a) and sTiO colour defined by Cenarro et al. (2009) for the 56 stars in the M15 subsample observed in HR-I during MEGARA commissioning. See the text for a description of the table.

| Star name | S/N | Ca1CEN | Ca2CEN | Ca3CEN | Mg I | Pa1 | Pa2 | Pa3 | Ca1MEG | Ca2MEG | Ca3MEG | sTiO |
|---|---|---|---|---|---|---|---|---|---|---|---|---|
| M15_01 | 7 | −0.152 ± 0.160 | −0.534 ± 0.356 | +0.007 ± 0.005 | −0.580 ± 0.419 | −0.058 ± 0.130 | +0.877 ± 0.000 | −1.495 ± 1.207 | −0.972 ± 0.447 | −2.231 ± 0.383 | +0.138 ± 0.076 | +0.606 |
| M15_02 | 12 | −2.318 ± 0.230 | −2.397 ± 0.272 | −4.151 ± 0.246 | −0.539 ± 0.096 | −0.897 ± 0.140 | −2.240 ± 0.267 | −4.315 ± 0.280 | −2.624 ± 0.251 | −3.110 ± 0.210 | −3.509 ± 0.169 | +0.625 |
| M15_03 | 15 | −0.657 ± 0.268 | −1.381 ± 0.349 | −0.532 ± 0.137 | −0.035 ± 0.023 | −0.226 ± 0.227 | +0.063 ± 0.050 | +0.108 ± 0.173 | −0.644 ± 0.282 | −1.550 ± 0.295 | −0.613 ± 0.130 | +0.646 |
| M15_04 | 14 | −0.580 ± 0.249 | −0.499 ± 0.115 | −0.184 ± 0.049 | +0.112 ± 0.066 | −0.256 ± 0.176 | +0.284 ± 0.893 | +0.124 ± 0.254 | −1.258 ± 0.534 | −1.379 ± 0.239 | −0.433 ± 0.091 | +0.633 |
| M15_05 | 11 | +0.028 ± 0.014 | +0.025 ± 0.007 | +0.543 ± 0.209 | −0.187 ± 0.099 | +0.086 ± 0.156 | +0.419 ± 0.538 | −0.281 ± 0.205 | −0.575 ± 0.273 | −1.299 ± 0.279 | +0.206 ± 0.071 | +0.619 |
| M15_06 | 11 | −0.068 ± 0.049 | −1.713 ± 0.599 | −3.565 ± 0.251 | −0.775 ± 0.100 | +0.278 ± 0.114 | −3.000 ± 0.287 | −1.444 ± 0.267 | +0.282 ± 0.183 | −0.568 ± 0.173 | −3.422 ± 0.178 | +0.605 |
| M15_07 | 12 | +0.087 ± 0.045 | −0.926 ± 0.214 | −0.714 ± 0.156 | +0.048 ± 0.042 | +0.109 ± 0.196 | +2.326 ± 0.208 | +0.549 ± 0.096 | +0.277 ± 0.149 | −1.254 ± 0.229 | −0.405 ± 0.078 | +0.643 |
| M15_08 | 9 | −0.320 ± 0.270 | −1.995 ± 0.427 | −1.969 ± 0.661 | −0.290 ± 0.161 | −0.483 ± 0.191 | −1.245 ± 0.270 | −0.330 ± 0.169 | +0.813 ± 0.001 | −0.620 ± 0.316 | −1.533 ± 0.443 | +0.643 |
| M15_09 | 16 | −0.551 ± 0.211 | −1.225 ± 0.228 | −0.500 ± 0.099 | −0.116 ± 0.057 | −0.194 ± 0.098 | −0.160 ± 0.094 | −0.405 ± 0.191 | −0.335 ± 0.143 | −1.492 ± 0.220 | −0.606 ± 0.095 | +0.632 |
| M15_10 | 7 | +0.213 ± 0.227 | +0.323 ± 0.129 | +1.198 ± 0.506 | −0.199 ± 0.116 | +0.064 ± 0.041 | +2.241 ± 0.522 | +0.063 ± 0.087 | −0.912 ± 0.931 | −1.186 ± 0.346 | +0.953 ± 0.353 | +0.622 |
| M15_11 | 35 | −0.531 ± 0.074 | −1.495 ± 0.096 | −0.923 ± 0.065 | +0.042 ± 0.010 | −0.231 ± 0.042 | +0.367 ± 1.908 | +0.133 ± 0.065 | −0.567 ± 0.081 | −1.616 ± 0.083 | −0.891 ± 0.053 | +0.646 |
| M15_12 | 8 | −0.051 ± 0.045 | −0.116 ± 0.052 | +1.086 ± 0.138 | +0.005 ± 0.004 | −0.430 ± 0.315 | +1.883 ± 3.746 | +1.766 ± 0.321 | −0.902 ± 0.798 | −1.351 ± 0.413 | +1.347 ± 1.631 | +0.645 |
| M15_13 | 17 | −0.445 ± 0.176 | −0.843 ± 0.170 | −0.700 ± 0.143 | −0.169 ± 0.095 | −0.182 ± 0.088 | +0.283 ± 0.407 | +0.088 ± 0.246 | −0.568 ± 0.239 | −0.975 ± 0.154 | −0.400 ± 0.069 | +0.640 |
| M15_14 | 17 | −0.637 ± 0.234 | −1.156 ± 0.208 | −0.896 ± 0.172 | −0.463 ± 0.122 | −0.109 ± 0.124 | +0.288 ± 0.166 | −0.586 ± 0.163 | −0.318 ± 0.139 | −1.244 ± 0.177 | −0.379 ± 0.062 | +0.632 |
| M15_15 | 30 | −0.445 ± 0.082 | −1.371 ± 0.121 | −0.927 ± 0.088 | −0.006 ± 0.002 | −0.235 ± 0.050 | −0.252 ± 0.095 | −0.347 ± 0.123 | −0.370 ± 0.075 | −1.560 ± 0.105 | −1.182 ± 0.090 | +0.636 |
| M15_16 | 22 | −0.305 ± 0.074 | −1.054 ± 0.131 | −0.758 ± 0.093 | +0.099 ± 0.042 | −0.247 ± 0.077 | +0.297 ± 0.117 | −0.141 ± 1.023 | −0.494 ± 0.133 | −1.495 ± 0.140 | −1.163 ± 0.121 | +0.640 |
| M15_17 | 22 | −0.308 ± 0.075 | −1.048 ± 0.132 | −0.763 ± 0.093 | +0.096 ± 0.039 | −0.248 ± 0.075 | +0.306 ± 0.124 | −0.125 ± 66.06 | −0.499 ± 0.13 | −1.496 ± 0.135 | −1.157 ± 0.111 | +0.640 |
| M15_18 | 20 | −0.126 ± 0.036 | −0.637 ± 0.089 | −0.652 ± 0.101 | −0.143 ± 0.065 | +0.186 ± 0.000 | +1.359 ± 0.625 | +0.094 ± 0.189 | −0.056 ± 0.017 | −1.099 ± 0.125 | −0.613 ± 0.078 | +0.633 |
| M15_19 | 20 | −0.231 ± 0.070 | −0.949 ± 0.153 | −0.590 ± 0.111 | −0.141 ± 0.058 | −0.064 ± 0.144 | +0.234 ± 0.000 | −0.149 ± 0.086 | −0.246 ± 0.082 | −1.264 ± 0.163 | −0.578 ± 0.089 | +0.629 |
| M15_20 | 15 | +0.433 ± 0.190 | −0.763 ± 0.140 | −0.710 ± 0.138 | −0.205 ± 0.132 | +0.073 ± 0.130 | +1.682 ± 0.177 | +0.345 ± 0.559 | +0.666 ± 0.330 | −1.006 ± 0.161 | −0.778 ± 0.129 | +0.632 |
| M15_21 | 33 | −1.069 ± 0.122 | −2.065 ± 0.117 | −0.991 ± 0.062 | +0.030 ± 0.005 | −0.588 ± 0.053 | −0.782 ± 0.179 | +0.358 ± 0.077 | −0.380 ± 0.049 | −2.013 ± 0.087 | −1.560 ± 0.075 | +0.669 |
| M15_22 | 42 | −0.471 ± 0.049 | −1.658 ± 0.084 | −1.104 ± 0.063 | −0.131 ± 0.028 | −0.234 ± 0.040 | −0.252 ± 0.053 | −0.244 ± 0.074 | −0.310 ± 0.038 | −1.721 ± 0.069 | −1.221 ± 0.054 | +0.638 |
| M15_23 | 51 | −0.459 ± 0.038 | −1.802 ± 0.073 | −1.305 ± 0.059 | −0.172 ± 0.019 | −0.101 ± 0.024 | −0.003 ± 0.002 | −0.578 ± 0.127 | −0.316 ± 0.028 | −1.884 ± 0.060 | −1.264 ± 0.045 | +0.633 |
| M15_24 | 27 | −0.318 ± 0.060 | −1.617 ± 0.149 | −0.809 ± 0.074 | −0.047 ± 0.016 | −0.125 ± 0.003 | −0.116 ± 1.147 | −0.537 ± 0.118 | −0.040 ± 0.009 | −1.493 ± 0.106 | −0.948 ± 0.072 | +0.637 |
| M15_25 | 41 | −0.458 ± 0.056 | −1.257 ± 0.073 | −0.978 ± 0.064 | −0.099 ± 0.018 | −0.189 ± 0.041 | +0.185 ± 0.256 | −0.190 ± 0.082 | −0.159 ± 0.022 | −1.339 ± 0.067 | −1.071 ± 0.061 | +0.639 |
| M15_26 | 39 | −0.747 ± 0.096 | −1.656 ± 0.116 | −1.381 ± 0.098 | −0.144 ± 0.026 | −0.256 ± 0.044 | −0.798 ± 11.78 | −0.294 ± 0.08 | −0.018 ± 0.00 | −1.276 ± 0.068 | −1.525 ± 0.083 | +0.645 |
| M15_27 | 57 | −0.524 ± 0.036 | −2.153 ± 0.075 | −1.452 ± 0.050 | −0.178 ± 0.020 | −0.122 ± 0.033 | −0.038 ± 0.026 | −0.619 ± 0.062 | −0.426 ± 0.034 | −2.146 ± 0.062 | −1.408 ± 0.041 | +0.633 |
| M15_28 | 63 | −0.639 ± 0.040 | −1.968 ± 0.062 | −1.190 ± 0.041 | −0.225 ± 0.020 | −0.266 ± 0.062 | +0.046 ± 0.033 | −0.333 ± 0.059 | −0.530 ± 0.037 | −2.025 ± 0.050 | −1.235 ± 0.033 | +0.644 |
| M15_29 | 30 | −0.410 ± 0.077 | −1.346 ± 0.126 | −0.614 ± 0.074 | −0.071 ± 0.022 | −0.130 ± 0.131 | +0.360 ± 8.544 | +0.335 ± 0.583 | −0.351 ± 0.073 | −1.382 ± 0.102 | −0.508 ± 0.053 | +0.641 |
| M15_30 | 34 | −0.186 ± 0.029 | −1.229 ± 0.089 | −0.803 ± 0.063 | −0.151 ± 0.029 | −0.115 ± 0.063 | +0.251 ± 88.55 | −0.314 ± 0.11 | −0.381 ± 0.06 | −1.675 ± 0.090 | −0.922 ± 0.059 | +0.631 |
| M15_31 | 21 | −0.029 ± 0.008 | −0.748 ± 0.122 | −0.275 ± 0.045 | −0.133 ± 0.052 | +0.164 ± 0.082 | +0.503 ± 0.000 | −0.450 ± 0.143 | −0.020 ± 0.006 | −1.129 ± 0.144 | −0.283 ± 0.039 | +0.622 |
| M15_32 | 51 | −0.667 ± 0.057 | −1.874 ± 0.079 | −1.189 ± 0.050 | −0.278 ± 0.032 | −0.272 ± 0.031 | −0.057 ± 0.056 | −0.242 ± 0.051 | −0.625 ± 0.060 | −1.865 ± 0.059 | −1.354 ± 0.050 | +0.642 |
| M15_33 | 28 | +1.305 ± 0.111 | +0.810 ± 0.070 | +2.430 ± 0.108 | +0.253 ± 0.046 | +1.175 ± 0.072 | +2.384 ± 0.141 | +2.101 ± 1.147 | +0.994 ± 0.094 | +0.688 ± 0.049 | +2.499 ± 0.096 | +0.619 |
| M15_34 | 31 | −0.665 ± 0.101 | −1.712 ± 0.129 | −0.800 ± 0.065 | −0.064 ± 0.014 | −0.040 ± 0.029 | +0.065 ± 0.286 | +0.009 ± 0.000 | −0.648 ± 0.104 | −1.749 ± 0.107 | −1.083 ± 0.075 | +0.640 |
| M15_35 | 56 | −0.770 ± 0.054 | −2.119 ± 0.073 | −1.159 ± 0.044 | −0.163 ± 0.023 | −0.411 ± 0.030 | +0.009 ± 0.007 | +0.022 ± 0.019 | −0.558 ± 0.045 | −2.113 ± 0.055 | −1.301 ± 0.041 | +0.652 |
| M15_36 | 62 | −0.368 ± 0.026 | −1.481 ± 0.049 | −1.047 ± 0.039 | −0.216 ± 0.020 | −0.216 ± 0.042 | +0.079 ± 0.185 | −0.279 ± 0.119 | −0.270 ± 0.020 | −1.794 ± 0.049 | −1.186 ± 0.035 | +0.637 |
| M15_37 | 125 | −0.524 ± 0.018 | −1.725 ± 0.029 | −1.227 ± 0.022 | −0.196 ± 0.010 | −0.318 ± 0.014 | −0.205 ± 0.054 | −0.405 ± 0.027 | −0.232 ± 0.009 | −1.758 ± 0.023 | −1.345 ± 0.020 | +0.641 |
| M15_38 | 27 | −0.371 ± 0.091 | −1.291 ± 0.136 | −0.941 ± 0.109 | −0.163 ± 0.048 | −0.175 ± 0.049 | +0.149 ± 0.516 | −0.239 ± 0.117 | −0.384 ± 0.102 | −1.460 ± 0.123 | −1.083 ± 0.101 | +0.635 |
| M15_39 | 74 | −0.565 ± 0.038 | −1.765 ± 0.056 | −1.175 ± 0.040 | −0.192 ± 0.017 | −0.176 ± 0.022 | −0.050 ± 0.092 | −0.164 ± 0.040 | −0.481 ± 0.036 | −1.717 ± 0.042 | −1.173 ± 0.034 | +0.640 |
| M15_40 | 44 | −0.717 ± 0.068 | −1.874 ± 0.087 | −1.134 ± 0.055 | −0.216 ± 0.029 | −0.303 ± 0.085 | −0.109 ± 0.069 | −0.093 ± 0.023 | −0.644 ± 0.069 | −1.907 ± 0.071 | −1.286 ± 0.051 | +0.646 |
| M15_41 | 19 | −0.171 ± 0.063 | −0.554 ± 0.113 | +0.060 ± 0.014 | +0.055 ± 0.085 | −0.079 ± 0.044 | +1.024 ± 0.034 | −0.136 ± 0.111 | −0.485 ± 0.185 | −1.178 ± 0.186 | +0.002 ± 0.000 | +0.632 |
| M15_42 | 45 | −0.219 ± 0.024 | −1.633 ± 0.087 | −1.037 ± 0.058 | −0.079 ± 0.013 | −0.229 ± 0.072 | −0.271 ± 0.109 | −0.389 ± 0.076 | +0.166 ± 0.021 | −1.496 ± 0.061 | −1.150 ± 0.050 | +0.635 |
| M15_43 | 13 | −0.227 ± 0.117 | −0.586 ± 0.158 | −0.062 ± 0.020 | −0.209 ± 0.083 | +0.067 ± 0.054 | +0.036 ± 0.052 | −0.406 ± 0.224 | −0.710 ± 0.402 | −1.556 ± 0.309 | −0.266 ± 0.070 | +0.622 |
| M15_44 | 41 | −0.656 ± 0.056 | −2.144 ± 0.076 | −1.823 ± 0.073 | −0.372 ± 0.028 | −0.194 ± 0.071 | −0.154 ± 0.054 | −0.452 ± 0.084 | −0.375 ± 0.036 | −2.341 ± 0.065 | −2.111 ± 0.065 | +0.641 |
| M15_45 | 18 | −0.361 ± 0.127 | −0.959 ± 0.184 | −0.511 ± 0.093 | −0.118 ± 0.066 | −0.108 ± 0.086 | +0.129 ± 0.099 | −0.521 ± 0.201 | −0.304 ± 0.117 | −1.182 ± 0.173 | −0.666 ± 0.101 | +0.630 |
| M15_46 | 33 | −0.407 ± 0.068 | −1.232 ± 0.105 | −0.842 ± 0.074 | −0.081 ± 0.030 | −0.238 ± 0.060 | −0.325 ± 0.093 | −0.425 ± 0.136 | −0.250 ± 0.046 | −1.383 ± 0.099 | −0.937 ± 0.071 | +0.633 |
| M15_47 | 10 | +0.249 ± 0.216 | +0.840 ± 0.341 | −0.045 ± 0.018 | −0.141 ± 0.128 | +0.217 ± 0.317 | +1.046 ± 25.21 | −0.815 ± 0.38 | −0.839 ± 0.72 | −1.293 ± 0.370 | −0.228 ± 0.073 | +0.599 |
| M15_48 | 18 | −0.620 ± 0.214 | −1.134 ± 0.182 | −0.662 ± 0.128 | −0.156 ± 0.041 | −0.242 ± 0.205 | −0.211 ± 0.212 | −0.333 ± 0.160 | −0.567 ± 0.205 | −1.286 ± 0.169 | −0.533 ± 0.080 | +0.635 |
| M15_49 | 15 | −0.834 ± 0.339 | −1.041 ± 0.205 | −0.243 ± 0.049 | −0.098 ± 0.111 | −0.198 ± 0.121 | +0.202 ± 0.153 | −0.197 ± 0.152 | −1.010 ± 0.414 | −1.577 ± 0.243 | −0.322 ± 0.053 | +0.642 |
| M15_50 | 43 | −0.498 ± 0.056 | −1.570 ± 0.084 | −1.102 ± 0.067 | −0.139 ± 0.023 | −0.266 ± 0.039 | −0.239 ± 0.075 | −0.296 ± 0.172 | −0.383 ± 0.047 | −1.648 ± 0.069 | −1.265 ± 0.059 | +0.639 |
| M15_51 | 5 | −1.905 ± 0.496 | −1.433 ± 0.441 | −3.244 ± 0.483 | −0.294 ± 0.188 | −1.279 ± 0.286 | −0.881 ± 0.295 | −5.944 ± 0.567 | −3.978 ± 0.541 | −4.143 ± 0.465 | −2.416 ± 0.344 | +0.599 |
| M15_52 | 20 | −0.001 ± 0.000 | −0.961 ± 0.149 | +0.167 ± 0.027 | +0.078 ± 0.064 | +0.011 ± 0.012 | +1.915 ± 0.201 | +0.184 ± 0.422 | −0.285 ± 0.096 | −1.476 ± 0.174 | +0.371 ± 0.054 | +0.635 |
| M15_53 | 31 | −0.299 ± 0.056 | −1.027 ± 0.105 | −0.200 ± 0.024 | −0.056 ± 0.013 | −0.043 ± 0.028 | +0.249 ± 0.161 | −0.220 ± 1.329 | −0.356 ± 0.072 | −1.349 ± 0.110 | −0.450 ± 0.044 | +0.632 |
| M15_54 | 24 | +0.213 ± 0.059 | −0.498 ± 0.070 | −0.093 ± 0.014 | −0.019 ± 0.009 | 0.079 ± 0.063 | 1.801 ± 2.050 | +0.096 ± 0.181 | −0.186 ± 0.056 | −1.263 ± 0.134 | +0.022 ± 0.003 | +0.631 |
| M15_55 | 15 | +0.475 ± 0.209 | −0.496 ± 0.103 | +0.898 ± 0.227 | −0.037 ± 0.037 | +0.246 ± 0.000 | +1.808 ± 0.272 | +0.129 ± 0.261 | −0.307 ± 0.133 | −1.676 ± 0.249 | +0.748 ± 0.169 | +0.619 |
| M15_56 | 45 | −0.356 ± 0.048 | −1.114 ± 0.076 | −0.544 ± 0.040 | −0.100 ± 0.021 | −0.139 ± 0.034 | +0.022 ± 0.007 | −0.142 ± 0.123 | −0.544 ± 0.080 | −1.429 ± 0.079 | −0.663 ± 0.040 | 0.630 |

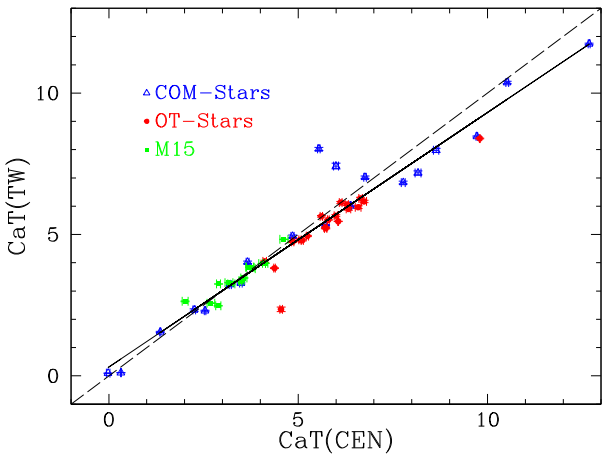


**Figure 19.** CaT index measured in all the HR-I spectra presented in this work (TW) versus the same index CaT measured following the Cenarro et al. (2001a) definition. Different sample stars are drawn with different symbols, as labelled in the plot. The dashed line represents the 1 : 1 relation while the solid line is the actual fit to the observed data.

We have measured known stellar indices (based on measurements of equivalent widths) and we have proposed updated indices based on new spectral windows more suitable to the MEGARA spectral resolution. We have also tested the reliability of measuring these indices with non-flux-calibrated observations. The complete study of the indices and their relationship with stellar parameters are left for future papers.

We are running a filler-type programme with MEGARA at the GTC that has been granted so far with 175 h of observing time in the semesters 2018B, 2019A and 2019B, which should provide around 300 stars observed in both HR-R and HR-I set-ups. All spectra are being reduced with the MEGARA DRP and pass through proper quality control, analysis and classification processes. The MEGARA IFU mode has an enormous advantage for these filler observations with respect to a long-slit instrument, especially in bad observing conditions: MEGARA data always have identical spectral resolution because the pupil stop is at the fibre at the spectrograph pseudo-slit, keeping it independent from sky conditions, and flux is always recovered by adding spaxels according to the actual seeing.

To manage the MEGARA-GTC library, we have put together a MySQL data base residing on https://www.fractal-es.com/megaragtc-stellarlibrary/, to handle both data and observations. We

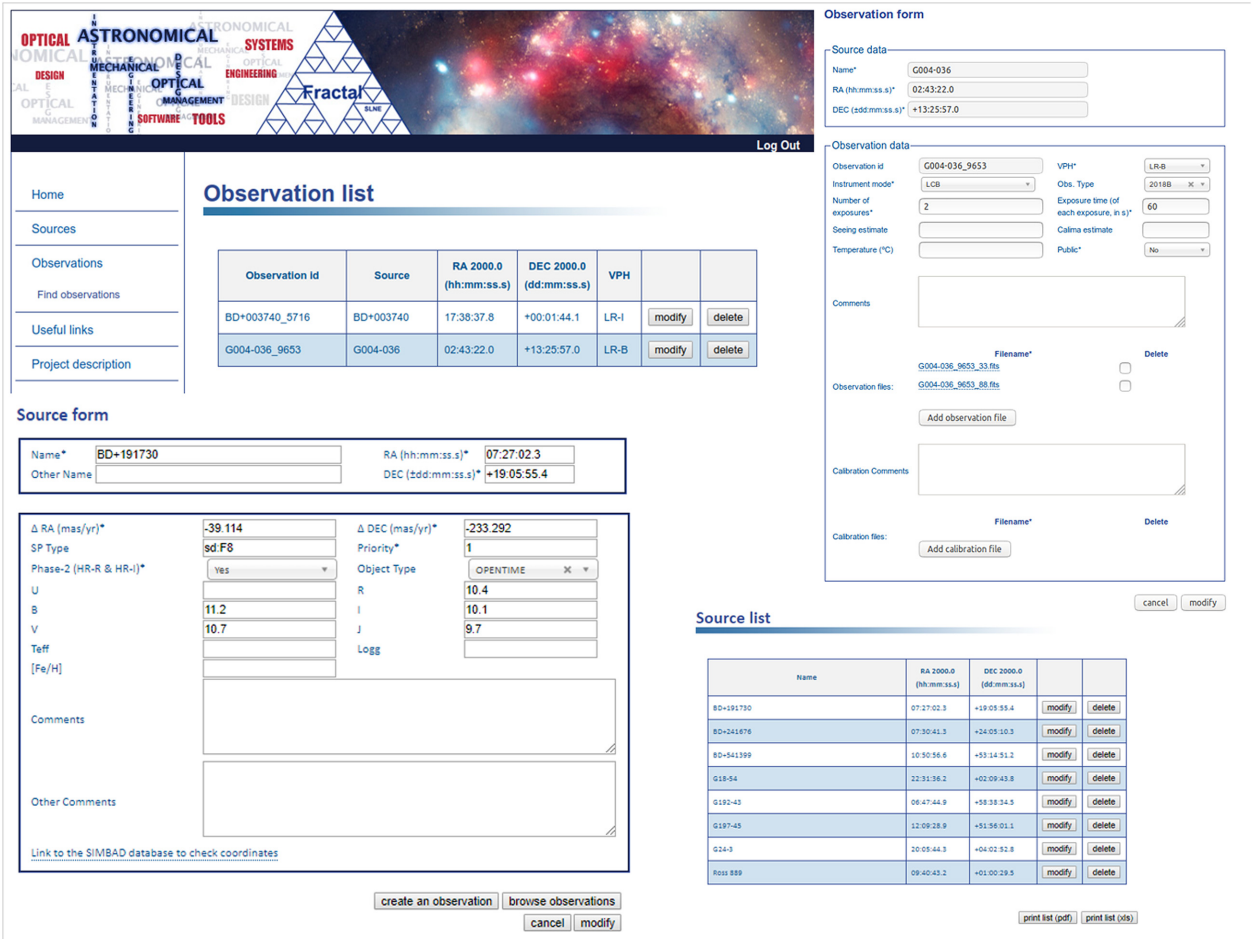


**Figure 20.** MEGARA-GTC library data base. The figure shows some views of the web-based tool. Top left: home page and main menus. Top right: observation form where the proper observed data can be handled. Bottom left: source form to handle library stars. Bottom right: source list after a searching process with the options of examining the content of each record in more detail and printing the filtered list in different formats for further analysis.

will upload all quality-checked spectra to deliver a first release of the MEGARA spectral library in 2020, which will allow users to retrieve the spectra along with the evolutionary synthesis models to support the interpretation of the observations.

We will use these observations to produce the first synthetic spectra with POPSTAR for the MEGARA highest-resolution modes, which will be refined as the library observations progress.

## ACKNOWLEDGEMENTS

This work has been supported by MINECO-FEDER grants AYA2016-75808-R and AYA2016-79724-C4-3-P, and has been partially funded by FRACTAL, INAOE and CIEMAT. This work is based on observations made with the Gran Telescopio Canarias (GTC), installed at the Spanish Observatorio del Roque de los Muchachos, on the island of La Palma. This work is based on data obtained with MEGARA instrument, funded by the European Regional Development Funds (ERDF), through *Programa Operativo Canarias FEDER 2014–2020*. The authors are grateful for the support given by Dr Antonio Cabrera and Dr Daniel Reverte, GTC Operations Group staff, during the preparation and execution of the observations at the GTC. The authors acknowledge an anonymous referee for comments that have substantially improved the manuscript.

## REFERENCES

Allende-Prieto C. et al., 2015, AAS Meeting 225, 422.07
Avni Y., 1976, ApJ, 210, 642
Bagnulo S., Jehin E., Ledoux C., Cabanac R., Melo C., Gilmozzi R., ESO Paranal Science Operations Team, 2003, Msngr, 114, 10
Blomme R., Nazé Y., Volpi D., De Becker M., Prinja R. K., Pittard J. M., Parkin E. R., Absil O., 2013, A&A, 550, A90
Boeche C., Grebel E. K., 2016, A&A, 587, A2
Bohlin R. C., Mèszáros S., Fleming S. W., Gordon K. D., Koekemoer A. M., Kovács J., 2017, AJ, 153, 234
Bruzual G., Charlot S., 2003, MNRAS, 344, 1000
Cameron R. B., 2003, AJ, 125, 2531
Cardiel N., 2009, MNRAS, 396, 680
Cardiel N., Pascual S., 2018
Carrasco E. et al., 2018, Proc. SPIE, 10702, 1070216,
Carretta E., Bragaglia A., Gratton R., D'Orazi V., Lucatello S., 2009, A&A, 508, 695
Cenarro A. J., Cardiel N., Gorgas J., Peletier R. F., Vazdekis A., Prada F., 2001a, MNRAS, 326, 959
Cenarro A. J., Gorgas J., Cardiel N., Pedraz S., Peletier R. F., Vazdekis A., 2001b, MNRAS, 326, 981
Cenarro A. J., Cardiel N., Vazdekis A., Gorgas J., 2009, MNRAS, 396, 1895
Chen Y. P., Trager S. C., Peletier R. F., Lançon A., Prugniel P., Koleva M., 2012, ASInC, 6, 13
Chen Y. P., Trager S. C., Peletier R. F., Lançon A., 2014, ASInC, 11, 17
Cid Fernandes R., Mateus A., Sodré L., Stasińska G., Gomes J. M., 2005, MNRAS, 358, 363
Coelho P. R. T., 2014, MNRAS, 440, 1027
Coelho P., Barbuy B., Meléndez J., Schiavon R. P., Castilho B. V., 2005, A&A, 443, 735
Coelho P., Bruzual G., Charlot S., Weiss A., Barbuy B., Ferguson J. W., 2007, MNRAS, 382, 498
de Laverny P., Recio-Blanco A., Worley C. C., Plez B., 2012, A&A, 544, A126
Dullo B. T. et al., 2019, ApJ, 871, 1
Eldridge J. J., Stanway E. R., 2009, MNRAS, 400, 1019
Frémaux J., Kupka F., Boisson C., Joly M., Tsymbal V., 2006, A&A, 449, 109
Fritze-v. Alvensleben U., Bicker J., 2006, A&A, 454, 67
García-Vargas M. L., Díaz A. I., 1994, ApJS, 91, 553
García-Vargas M. L., Bressan A., Díaz A. I., 1995, A&AS, 112, 13
García-Vargas M. L., Mollá M., Martín-Manjón M. L., 2013, MNRAS, 432, 2746
Gil de Paz A. et al., 2018, Proc. SPIE, 10702, 1070217
Gomes J. M., Papaderos P., 2018, A&A, 618, C3
Gómez-Alvarez P. et al., 2018, Proc. SPIE, 10707, 107071L
Gómez-González V. M. A., Mayya Y. D., González R., 2016, MNRAS, 460, 1555
González-Delgado R. M., Cerviño M., Martins L. P., Leitherer C., Hauschildt P. H., 2005, MNRAS, 357, 945
Gregg M. D. et al., 2006, in Koekemoer A. M., Goudfrooij P., Dressel L. L., eds, Proc. 2005 HST Calibration Workshop: Hubble after the transition to two-gyro mode. NASA, Greenbelt, MD, p. 209
Gustafsson B., Edvardsson B., Eriksson K., Jørgensen U. G., Nordlund Å., Plez B., 2008, A&A, 486, 951
Heiter U., Jofré P., Gustafsson B., Korn A. J., Soubiran C., Thévenin F., 2015, A&A, 582, A49
Jofré P., Panter B., Hansen Cote J., Weiss A., 2010, A&A, 517, A57
Jofré P., Heiter U., Soubiran C., 2019, ARA&A, 57, 571
Joye W. A., Mandel E., 2003, in Payne E., Jedrzejewski R. I., Hook R. N., eds, ASP Conf. Ser. Vol. 295, Astronomical Data Analysis Software and Systems XII. Astron. Soc. Pac., San Francisco, CA, p. 489
Kirby E. N., 2011, PASP, 123, 531
Koleva M., Prugniel P., Bouchard A., Wu Y., 2009, A&A, 501, 1269
Kurucz R. L., 1993, yCat, 6039
Le Borgne J.-F. et al., 2003, A&A, 402, 433
Leitherer C. et al., 1999, ApJS, 123, 3
Leitherer C. et al., 2010, ApJS, 189, 309
Maíz-Apellániz J., et al., 2019, A&A, 626, A20
McNamara B. J., Harrison T. E., Baumgardt H., 2004, ApJ, 602, 264
Maraston C., Strömbäck G., 2011, MNRAS, 418, 2785
Maraston C. et al., 2019, preprint (arXiv:1911.05748v2)
Martín-Manjón M. L., García-Vargas M. L., Mollá M., Díaz A. I., 2010, MNRAS, 403, 2012
Martins L. P., González-Delgado R. M., Leitherer C., Cerviño M., Hauschildt P., 2005, MNRAS, 358, 49
Martins F., Schaerer D., Hillier D. J., 2005, A&A, 436, 1049
Mas-Hesse J. M., Kuntz D., 1991, A&AS, 88, 3
Mollá M., García-Vargas M. L., Bressan A., 2009, MNRAS, 398, 451
Montes D., Martin E. L., 1998, A&AS, 128, 485
Montes D., Ramsey L. W., Welty A. D., 1999, ApJS, 123, 283
Munari U., Sordo R., Castelli F., Zwitter T., 2005, A&A, 442, 1127 (MUN05)
Nazé Y., Mahy L., Damerdji Y., Kobulnicky H. A., Pittard J. M., Parkin E. R., Absil O., Blomme R., 2012, AA, 546, A37
Neugent K. F., Massey P., 2011, ApJ, 733, 123
Neugent K. F., Massey P., Georgy C., 2012, ApJ, 759, 11
Palacios A., Gebran M., Josselin E., Martins F., Plez B., Belmas M., Lebre A., 2010, A&A, 516, A13
Pascual S., Cardiel N., Picazo-Sánchez P., Castillo-Morales A., Gil de Paz A., 2018, guaix-ucm/megaradrp: v0.8
Prugniel P., Soubiran C., 2001, A&A, 369, 1048
Prugniel P., Soubiran C., 2004, preprint (astro-ph/0409214)
Prugniel P., Vauglin I., Koleva M., 2011, A&A, 531, 165
Rodríguez-Merino L. H., Chavez M., Bertone E., Buzzoni A., 2005, ApJ, 626, 411
Sánchez-Blázquez P. et al., 2006, MNRAS, 371, 703
Simón-Díaz S., Castro N., Herrero A., Puls J., García M., Sabín-Sanjulián C., 2011, Journal of Physics: Conference Series, 328, 012021
Sneden C., Johnson J., Kraft R. P., Smith G. H., Cowan J. J., Bolte M. S., 2000, ApJ, 536, L85
Sobeck J. S. et al., 2011, AJ, 141
Sordo R. et al., 2010, Ap&SS, 328, 331
Sota A., Maiz Apellániz J., Morrell N. I., Barba R. H., Walborn N. R., Gamen R. C., Arias J. I., Alfaro E. J., 2014, ApJSS, 211, 10

Stoehr F. et al., 2008, in Lewis J., Argyle R., Bunclarck P., Evans D., Gonzales-Solares E., eds, ASP Conf. Ser. Vol. 394, Astronomical Data Analysis Software and Systems XVII, Astron. Soc. Pac., San Francisco, CA, p. 505
Teixeira D. C., Sousa S. G., Tsantaki M., Monteiro M. J. P. F. G., Santos N. C., Israelian G., 2017, EPJ Web of Conferences 160, 01013
Valdes F., Gupta R., Rose J. A., Singh H. P., Bell D. J., 2004, ApJS, 152, 251
Vazdekis A., Koleva M., Ricciardelli E., Röck B., Falcón-Barroso J., 2016, MNRAS, 463, 3409
Vidal-García A., Charlot S., Bruzual G., Hubeny I., 2017, MNRAS, 470, 3
Yan R. et al., 2019, ApJ, 883, 175
Yan R., 2019, AAS Meeting 233, id.333.07

## SUPPORTING INFORMATION

Supplementary data are available at *MNRAS* online.

**Appendix A.** M15 Spectra Analysis Summary
**Appendix B.** OT Spectra

Please note: Oxford University Press is not responsible for the content or functionality of any supporting materials supplied by the authors. Any queries (other than missing material) should be directed to the corresponding author for the article.

This paper has been typeset from a TEX/LATEX file prepared by the author.